AFWL-TR-87-115

AFWL-TR-
87-115

STRESS-STRAIN PROPERTIES OF SIFCON IN UNIAXIAL COMPRESSION AND TENSION

J. R. Homrich
A. E. Naaman

University of Michigan
Ann Arbor, Michigan 48109

August 1988

Final Report

Approved for public release; distribution unlimited.

AIR FORCE WEAPONS LABORATORY
Air Force Systems Command
Kirtland Air Force Base, NM 87117-6008

AFWL-TR-87-115

This final report was prepared by the University of Michigan, Ann Arbor, Michigan, under Contract F29601-85-K-0069, Job Order 8809131D, with the Air Force Weapons Laboratory, Kirtland Air Force Base, New Mexico. Captain Susan M. Cheney, AFWL/NTES, was the Laboratory Project Officer-in-Charge.

When Government drawings, specifications, or other data are used for any purpose other than in connection with a definitely Government-related procurement the United States Government incurs no responsibility nor any obligation whatsoever. The fact that the Government may have formulated or in any way supplied the said drawings, specifications, or other data, is not to be regarded by implication or otherwise in any manner construed, as licensing the holder or any other person or corporation; or as conveying any rights or permission to manufacture, use, or sell any patented invention that may in any way be related thereto.

If your address has changed, if you wish to be removed from our mailing list, or if your organization no longer employs the addressee, please notify AFWL/NTES, Kirtland AFB, NM 87117-6008 to help us maintain a current mailing list.

This report has been reviewed and is approved for publication.

Susan M. Cheney

SUSAN M. CHENEY
Capt, USAF
Project Officer

Thomas E Bretz

THOMAS E. BRETZ, JR
Lt Col, USAF
Chief, Applications Branch

FOR THE COMMANDER

Carl L Davidson

CARL L. DAVIDSON
Col, USAF
Chief, Civil Engineering Research Div

DO NOT RETURN COPIES OF THIS REPORT UNLESS CONTRACTUAL OBLIGATIONS OR NOTICE ON A SPECIFIC DOCUMENT REQUIRES THAT IT BE RETURNED.

UNCLASSIFIED
SECURITY CLASSIFICATION OF THIS PAGE

REPORT DOCUMENTATION PAGE

1a. REPORT SECURITY CLASSIFICATION	1b. RESTRICTIVE MARKINGS
2a. SECURITY CLASSIFICATION AUTHORITY	3. DISTRIBUTION/AVAILABILITY OF REPORT: Approved for public release; distribution unlimited.
2b. DECLASSIFICATION/DOWNGRADING SCHEDULE	
4. PERFORMING ORGANIZATION REPORT NUMBER(S)	5. MONITORING ORGANIZATION REPORT NUMBER(S): AFWL-TR-87-115
6a. NAME OF PERFORMING ORGANIZATION: University of Michigan; 6b. OFFICE SYMBOL (If applicable)	7a. NAME OF MONITORING ORGANIZATION: Air Force Weapons Laboratory
6c. ADDRESS (City, State, and ZIP Code): Department of Civil Engineering, Ann Arbor, Michigan 48109	7b. ADDRESS (City, State, and ZIP Code): Kirtland Air Force Base, New Mexico 87117-6008
8a. NAME OF FUNDING/SPONSORING ORGANIZATION; 8b. OFFICE SYMBOL (If applicable)	9. PROCUREMENT INSTRUMENT IDENTIFICATION NUMBER: F29601-85-K-0069
8c. ADDRESS (City, State, and ZIP Code)	10. SOURCE OF FUNDING NUMBERS

PROGRAM ELEMENT NO.	PROJECT NO.	TASK NO.	WORK UNIT ACCESSION NO
62601F	8809	13	1D

11. TITLE (Include Security Classification)
STRESS-STRAIN PROPERTIES OF SIFCON IN UNIAXIAL COMPRESSION AND TENSION

12. PERSONAL AUTHOR(S)
Homrich, Joseph R. and Naaman, Antoine E.

13a. TYPE OF REPORT	13b. TIME COVERED	14. DATE OF REPORT (Year, Month, Day)	15. PAGE COUNT
Final	FROM 29/05/85 TO 30/10/87	1988, August	148

16. SUPPLEMENTARY NOTATION

17. COSATI CODES		
FIELD	GROUP	SUB-GROUP
11	04	

18. SUBJECT TERMS (Continue on reverse if necessary and identify by block number)
SIFCON; Constitutive Modeling; Uniaxial Tension; Fiber Concrete; Mathematical Modeling; Cement Composites; Uniaxial Compression

19. ABSTRACT (Continue on reverse if necessary and identify by block number)

This report presents a comprehensive investigation of the properties of SIFCON composites in both uniaxial compression and uniaxial tension, as well as their stress-displacement response in tension. The importance of the primary reinforcing parameters such as fiber type, fiber orientation, matrix properties, and matrix penetration of the fiber network is highlighted. Test results indicate that very high compressive strengths (up to 20 k/in^2 or 140 MPa) can be achieved and compressive strains of up to 10% can be expected at about half the strength. Similarly, high tensile strengths (up to 4 k/in^2 or 28 MPa) with strains of up to 2% accompanied by extensive multiple cracking were also observed. Surface energies and toughness indexes in tension reached about three orders of magnitude above those known for plain concrete. The toughness of SIFCON in compression computed at 10% strain was up to 50 times that of plain concrete. Analytical models are proposed to predict the stress-strain response of SIFCON in both compression and tension as well as its stress-crack opening response in tension. These models depend on a few variables (over)

20. DISTRIBUTION/AVAILABILITY OF ABSTRACT	21. ABSTRACT SECURITY CLASSIFICATION
☒ UNCLASSIFIED/UNLIMITED ☐ SAME AS RPT ☐ DTIC USERS	Unclassified

22a. NAME OF RESPONSIBLE INDIVIDUAL	22b. TELEPHONE (Include Area Code)	22c. OFFICE SYMBOL
Captain Susan M. Cheney	(505) 846-4656	NTES

DD FORM 1473, 84 MAR — 83 APR edition may be used until exhausted. All other editions are obsolete.

SECURITY CLASSIFICATION OF THIS PAGE
UNCLASSIFIED

19. ABSTRACT (Continued)

that can be determined as function of the fiber reinforcing parameters such as fiber aspect ratio, fiber volume fraction, and fiber type.

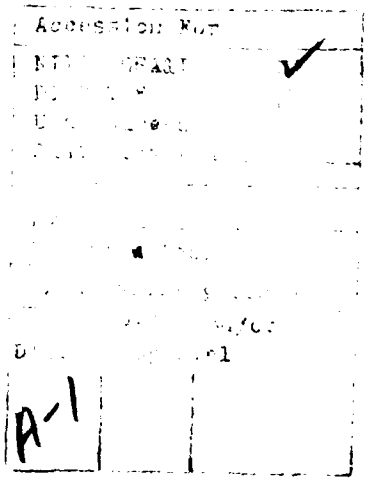

Summary

1. INTRODUCTION

SIFCON (Slurry Infiltrated Fiber Concrete) is a high-performance fiber-reinforced concrete in which formwork molds are filled to capacity with fibers and the resulting fiber network is infiltrated by a cement-based slurry. Infiltration is usually accomplished by gravity flow aided by light vibration or pressure grouting. SIFCON composites exhibit outstanding strength and ductility.

SIFCON is a relatively new construction material. It has already been used successfully in applications such as pavement overlays, bridge repair, blast resistant structures, and safe vaults (Refs. 1-6). However, very little is known about its mechanical properties in either quantitative or qualitative terms.

Although technically a fiber concrete, SIFCON differs substantially from ordinary fiber reinforced concrete in several important respects. First, the fiber volume of conventional fiber reinforced concrete normally varies from only 1% to 3%, whereas with SIFCON the fiber volume may range from 8% to over 20% depending on fiber geometry, specimen preparation procedures, and mold size. Secondly, conventional fiber reinforced concretes are applicable to practically any type of matrix. With SIFCON, a cement-based slurry or fine-grained mortar must be used to ensure infiltration of the tiny spaces between fibers in the molds. Third, the fabrication process of the two materials is very different. With conventional fiber reinforced concrete, the fibers are added directly to the fresh concrete during the mixing process. The high fiber content of SIFCON makes this procedure impossible. For SIFCON composites, a preplaced fiber bed must be infiltrated with a cement slurry or fine mortar. Finally, SIFCON composites introduce a new behavioral phenomenon, that of "fiber interlock." With ordinary fiber concretes, the fiber-to-matrix bond is of greatest importance. Fiber-to-fiber interaction is minimal and has little bearing on the mechanical properties of the concrete. With SIFCON, however, the fibers are subjected to frictional and mechanical interlock. It is believed that this fiber interlock, not just the higher fiber volume, is responsible for SIFCON's outstanding stress-strain properties.

In other respects many of the studies concerning ordinary fiber-reinforced concrete are applicable to the study of SIFCON. These include such topics as the influence of strain rate on composite behavior, cyclic loading response, fiber-to-matrix bond models, and stress-strain behavior.

2. OBJECTIVE AND SCOPE

The main objective of this research is to develop constitutive relations for high-strength

SIFCON in direct uniaxial compression and uniaxial tension. This research should lead to a better understanding of the mechanisms of fiber reinforcement in SIFCON and the variables that control its strength, stress-strain response, toughness, and fracture properties. In particular, this research should clarify the effects of four important parameters; (1) fiber types which vary according to surface characteristics and overall fiber geometry, (2) cement matrices which vary in strengths, water-cement ratio, flowability, and pozzolanic material content (in particular, the effect of microsilica pozzolans on matrix-to-fiber bonding will be studied), (3) specimen preparation procedures with particular emphasis placed upon comparison of responses of cylinders cored from precast blocks and cylinders poured directly into molds, and (4) the anisotropic behavior of SIFCON materials generated by the method and direction of fiber placement with specimen response being studied for fibers placed parallel and normal to the direction of testing.

This study includes an experimental phase and an analytical phase. Results are stated in qualitative and quantitative terms. The basic flowchart of the experimental program (both compression and tension) is shown in Figure S-1, while Figure S-2 describes the specimen notation code used throughout this report. Five major groups of specimens were tested. Each group was composed of four to eleven series, and each series consisted of four specimens. Details for each series are contained within the individual chapters. In the analytical sections, models are proposed for approximating the stress-strain behavior of SIFCON based upon controlling matrix and fiber properties.

This report is divided into four sections: stress-strain response in compression, stress-strain response in tension, stress-crack displacement response in tension, and mathematical modeling. Each section is self-contained, represents a complete study within itself, and includes separate background, experimental setup, and analysis.

3. SUMMARY OF RESULTS

Following is a main summary of the results and conclusions of this investigation. Additional details can be found in the body of this report.

a. The strength characteristics of SIFCON depend on several parameters including: (1) the matrix strength and composition, (2) the fiber orientation and surface properties (smooth, deformed, crimped, hooked), (3) mold edge effects, and (4) proper and complete penetration of the fiber network by the cement slurry.

b. The fiber parameters (length, diameter, aspect ratio) and the extent of vibration during fiber placement and slurry pouring, greatly influence the fiber content (fiber volume fraction) of SIFCON. Volume fractions of up to 23% were achieved in this study; however, corresponding SIFCON composites did not show better performance.

c. Strength in compression of up to 17.5 k/in^2 (122 MPa) were obtained in this investigation for fiber contents of about 12% by volume. Specimens reinforced with fibers with axis normal to the loading direction showed compressive strength up to 30% higher than specimen reinforced with fibers parallel to the loading direction.

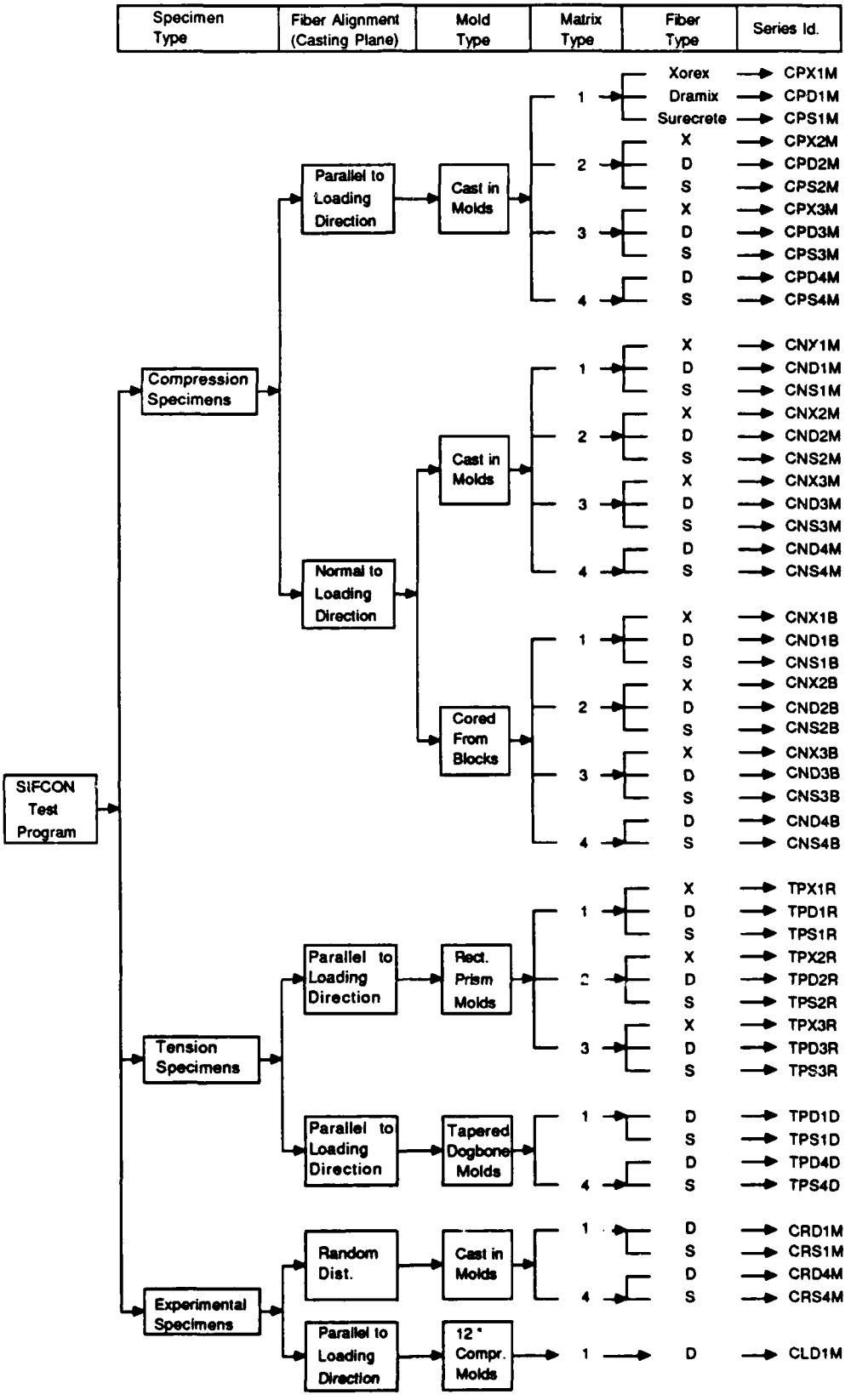

Figure S1. Complete experimental program.

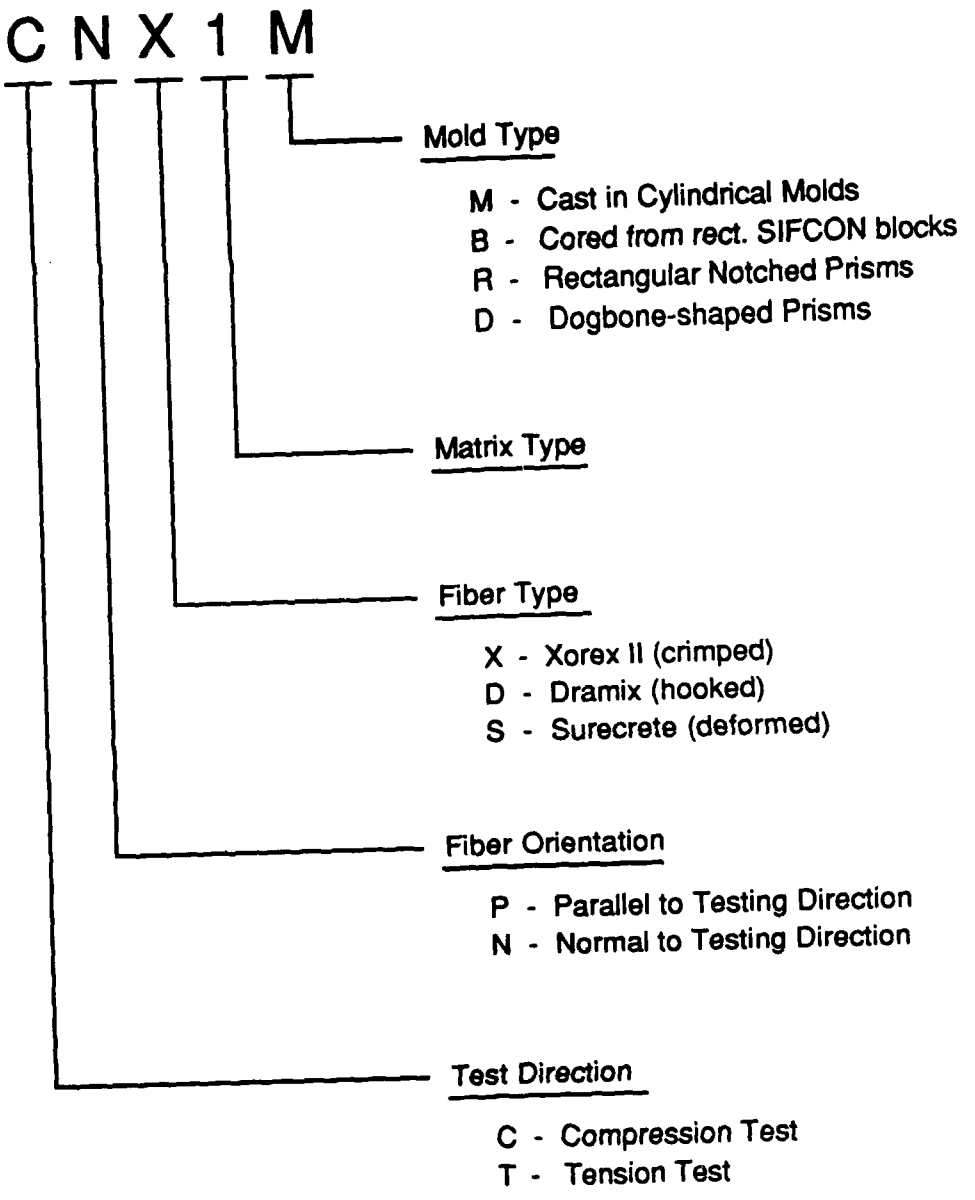

Figure S2. Specimen Notation Code.

d. For specimens reinforced with fibers aligned primarily in the loading direction, average tensile strengths were about 2 k/in^2 (14 MPa) with maximum observed strengths of up to 4 k/in^2 (28 MPa).

e. SIFCON displays outstanding ductility in both compression and tension. Compressive strains of up to 10% with corresponding stresses of between 5 to 11 k/in^2 (35 to 77 MPa) were obtained. The tensile response of SIFCON is linear over a short range of strains up to matrix cracking; increased loading leads to gradual multiple cracking of the matrix accompanied by a gradual non linear response up to the peak stress. Tensile strains of 1 to 2% were maintained at levels of maximum stress.

f. The descending branch of the tensile load elongation response of SIFCON characterizes a single crack and cannot be translated into a stress-strain response. It is specimen and size dependent.

g. Tests on notched prisms to determine the stress versus crack opening response of SIFCON specimens in tension suggest that surface energies of the order of 600 lb-in/in^2 can be achieved. Such a high value is about ten times the average surface energy reported for conventional fiber reinforced concrete and two to three orders of magnitude the surface energy of plain concrete.

h. Internal drying shrinkage cracking of SIFCON composites may lead to a poorer material stress-strain performance resulting in a highly nonlinear response of the ascending portion of the stress-strain curve.

i. Compared to plain concrete the toughness index of SIFCON in compression evaluated at 10% strain can exceed 50.

j. Compared to plain slurry, the toughness index of SIFCON in tension evaluated at 2% strain can exceed 1000.

k. The stress-strain response of SIFCON in both compression and tension, as well as the stress-crack opening response in tension can be properly modeled in terms of the fiber reinforcing parameters and the matrix properties (Section 4).

ACKNOWLEDGMENTS

The authors would like to give special thanks to the following people from the Civil Engineering Department at the University of Michigan, Ann Arbor: David Thompson and Shuenn-Chern Ting for software design and consultation; Rick Burch for tensile grip construction; James Wanzeck and Kevin Schmidt for laboratory assistance; and Duane Otter for his generous and continuous help through every phase of the program.
Special thanks are also due to George Nammur, Jr., Ph.D. candidate in the Civil Engineering Department at the University of Michigan, Ann Arbor, for his invaluable help in editing this document.

Table of Contents

1.0 Stress-Strain Properties of SIFCON in Compression

1.1 BACKGROUND INFORMATION

Although infiltration of fiber mats by cement matrices was undertaken more than a decade ago, Slurry Infiltrated Fiber Concrete (SIFCON) as it is known today was introduced in 1979 by Mr. D. R. Lankard. Lankard pioneered investigations of SIFCON's material properties and published several basic papers concerning the mechanical properties of SIFCON composites, viable slurry mix designs, practical specimen preparation procedures, and the documentation of common problems encountered in SIFCON preparation and testing (Refs. 2-5).

Since SIFCON is a relatively new construction material, very little literature about it exists at the present time. However, a brief review of the existing literature is presented here to give the background information necessary to understand this study.

1.1.1 Fiber Type

By necessity, SIFCON composites must be made with strong, rigid fibers or mesh. To date, SIFCON researchers have been using steel fibers in their studies. Since the fracture strength of steel fibers is much greater than that of the surrounding matrix, failure in SIFCON composites occurs mostly through fiber pullout and fiber-matrix debonding. The most important fiber parameter affecting this behavior is thus the fiber length and geometry.

1.1.2 Fiber Geometry

Surface texture, length-to-diameter (aspect) ratio, length, and shape of the fibers determine the main characteristics of a SIFCON composite's stress-strain response. Surface texture affects the fiber-to-matrix bond. Fiber length and aspect ratio affect the possible volume fraction of fibers that may be placed in molds, and fiber shape controls the degree of mechanical interlock both between fiber and matrix and between the fibers themselves.

A comparison of SIFCON response due to different fiber types or sizes is of current concern especially since the material is new. Recently, Lankard investigated the influence of varying only the aspect ratios of hooked Dramix fibers made by Bekaert Steel Wire Corporation [8]. He found that fibers with a higher aspect ratio resulted in a lower possible volume fraction of fibers that could be successfully placed in the molds and a correspondingly poorer material performance. This lower volume fraction is caused by the high degree of fiber interlock among long, thin fibers which results in the formation of large interstitial voids between the fibers. A detailed investigation of the influence of fiber geometry and fiber surface characteristics on SIFCON performance has yet to be undertaken.

1.1.3 Microsilica Content

Microsilica additives are pozzolans composed almost entirely of fine amorphous silica particles that enable the relatively easy attainment of high strength concrete. The pozzolanic action of microsilica is only partly responsible for the high strengths that it makes possible. Microsilica also contributes to strength by changing the pore structure of concrete. While the overall porosity of concrete made with microsilica is about the same as that for non-microsilica concrete, the pore size distribution is changed with a significant reduction in the maximum pore size and the number of larger capillary pores. This change in the pore structure leads to lower internal stress concentrations, lower permeability, and a change in the bonding properties of the matrix.

The effect of microsilica pozzolans on the behavior of SIFCON flexural specimens has been investigated by Balaguru and Kendzulak (Ref. 1). They have found that specimens made with microsilica slurries show a marked increase in strength and flexural ductility over specimens made without microsilica. Research should continue into the use of high strength slurries in general and microsilica slurries in particular.

1.1.4 Matrix Lumps

Another difficulty encountered in slurry mixtures is that of matrix lumps. Under certain conditions, small lumps of fly ash, microsilica, and cement may form during the mixing process. Lumping is usually a problem with low water-cementitious ratio mixes or mixes containing microsilica. The lumps range in size from that of a coarse sand to lumps over half an inch in diameter. Because these lumps would clog a fiber bed and prevent complete infiltration, they must be removed by fine wire screens placed over the molds during the mixing process. Although the screens effectively eliminate the infiltration problem, another problem arises -- that of an effective raising of the water-cementitious ratio. Because the lumps are primarily solid cementitious particles, their removal from the slurry causes an overall rise in the water-cementitious ratio and a lowering of matrix strength. Strategies to reduce the presence of lumps in slurries are being actively investigated.

1.1.5 Edge Effects

One major difficulty with the testing of SIFCON specimens simply cast in common molds is a phenomenon termed "edge effects." When filling SIFCON molds with fibers, edge effects occur in which the fiber density near the surface of the specimen (edge of the mold) is lower than that of the interior. What's more, some fibers tend to align themselves in the plane of the mold surface when the specimens are filled vertically. These edge effects tend to reduce the effective cross-sectional area of the tested specimen, since the outer edges of the specimen have a lower volume fraction of fibers and correspondingly lower strengths. During tests, the outer surface of the specimen tends to spall off, leaving the central core to sustain most of the loading. This effect is shown in Figure 1. To alleviate this problem, specimens may be cored or cut from precast SIFCON blocks. Cored specimens may show as much as a 30% increase in ultimate strength over specimens cast in molds depending on the relative size between the fibers and the molds. The major drawbacks to coring are the higher cost, the time usually involved, and the difficulty in obtaining good cores.

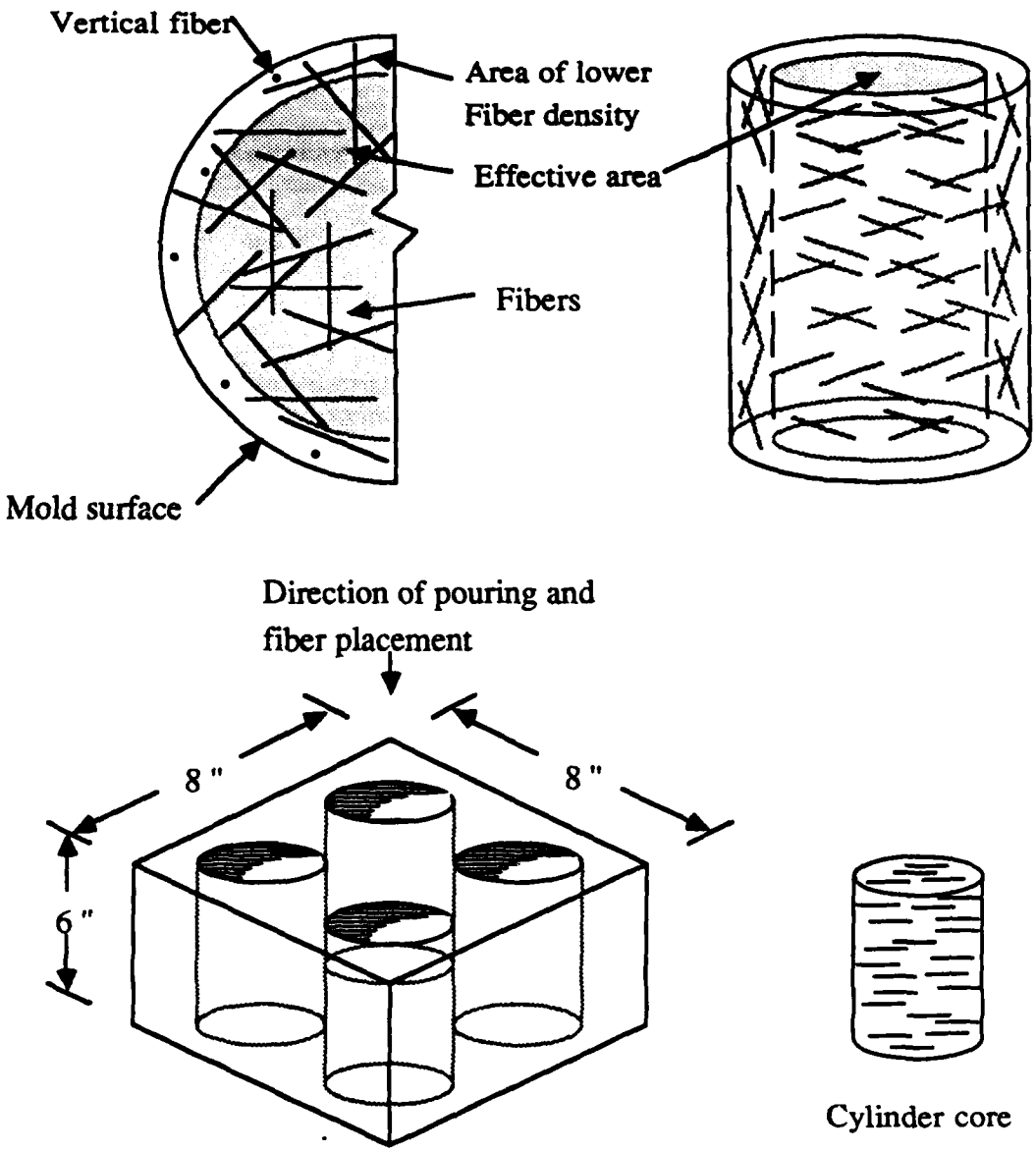

Figure 1. Edge effects and specimen coring.

1.1.6 Anisotropic Behavior

When steel fibers are hand placed and lightly vibrated into molds, a two-dimensional orientation of fibers occurs. Thus, the resultant SIFCON material made from such a fiber placement procedure is non isotropic and the direction in which the material is tested will have a significant effect on its behavioral response. Lankard found that the flexural strength of SIFCON specimens molded as beams (with fiber axes aligned parallel to the longitudinal specimen axis) could be as much as three times higher than that of specimens molded as columns (with fibers aligned normal to the specimen axis) (Ref. 5). Similary, the ultimate compressive strength of SIFCON cylinders is affected by fiber orientation. Lankard found that compression cylinders molded and loaded in the same direction (with fiber axes normal to the direction of loading) exhibited up to twice the compressive strength of specimens having the load applied parallel to the fiber axis (Ref. 5). This effect is shown in Figure 2. These effects are believed due to the efficiency with which certain fiber alignments are able to bridge tension cracks that control the mode of failure in both flexural and compressive cylinder tests.

1.2 EXPERIMENTAL PROGRAM

The experimental program consists of uniaxial compression tests on 3x6-in (75x150-mm) cylinders. Four specimens were poured and tested for each series investigated. The program is summarized in Figure 3. Parameters investigated include slurry mix design, fiber type, fiber orientation, and mold influence on specimen properties. Data from these tests were collected, processed, and analyzed to produce stress-strain relationships and to allow rational comparisons between the various parameters under study.

Referring to Figure 3 and the column headed "Mold Type," it can be observed that the compression specimens may be divided into three major groups according to fiber alignment and testing direction. For the purposes of future discussion, these groups may be listed as:

I. Compression specimens with fibers aligned parallel to the loading direction and cast in cylindrical molds.

II. Compression specimens with fibers aligned normal to the loading direction and cast in cylindrical molds.

III. Compression specimens with fibers aligned normal to the loading direction and cored from precast SIFCON blocks.

1.2.1 Slurry Mixtures

Four slurry mixtures were used in this study; two with microsilica and fly ash pozzolans, and two with fly ash pozzolan only. Corresponding mix compositions are shown in Table 1. All mixes were designed to provide high strength while maintaining flowability.

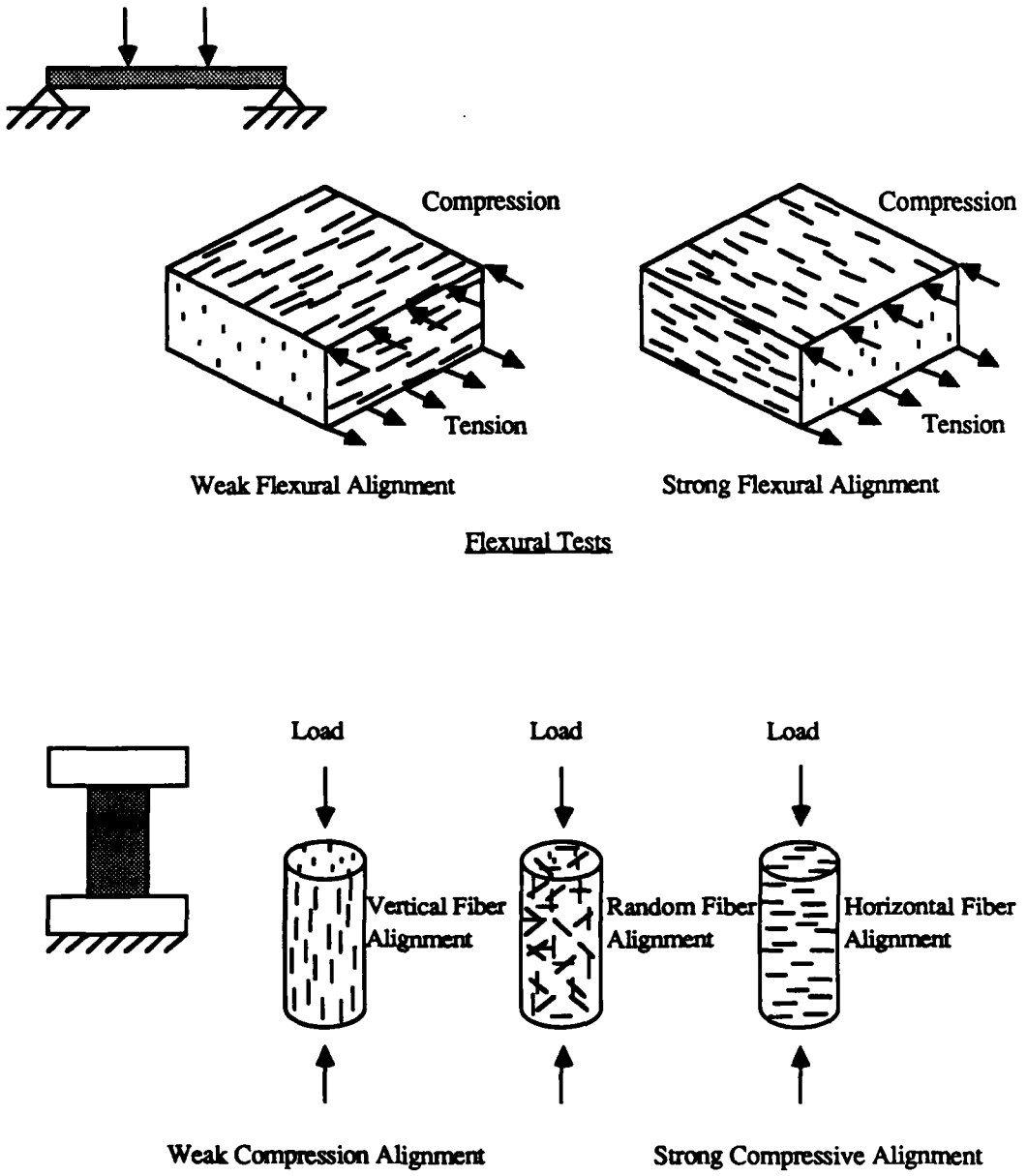

Figure 2. Anisotropic behavior of SIFCON.

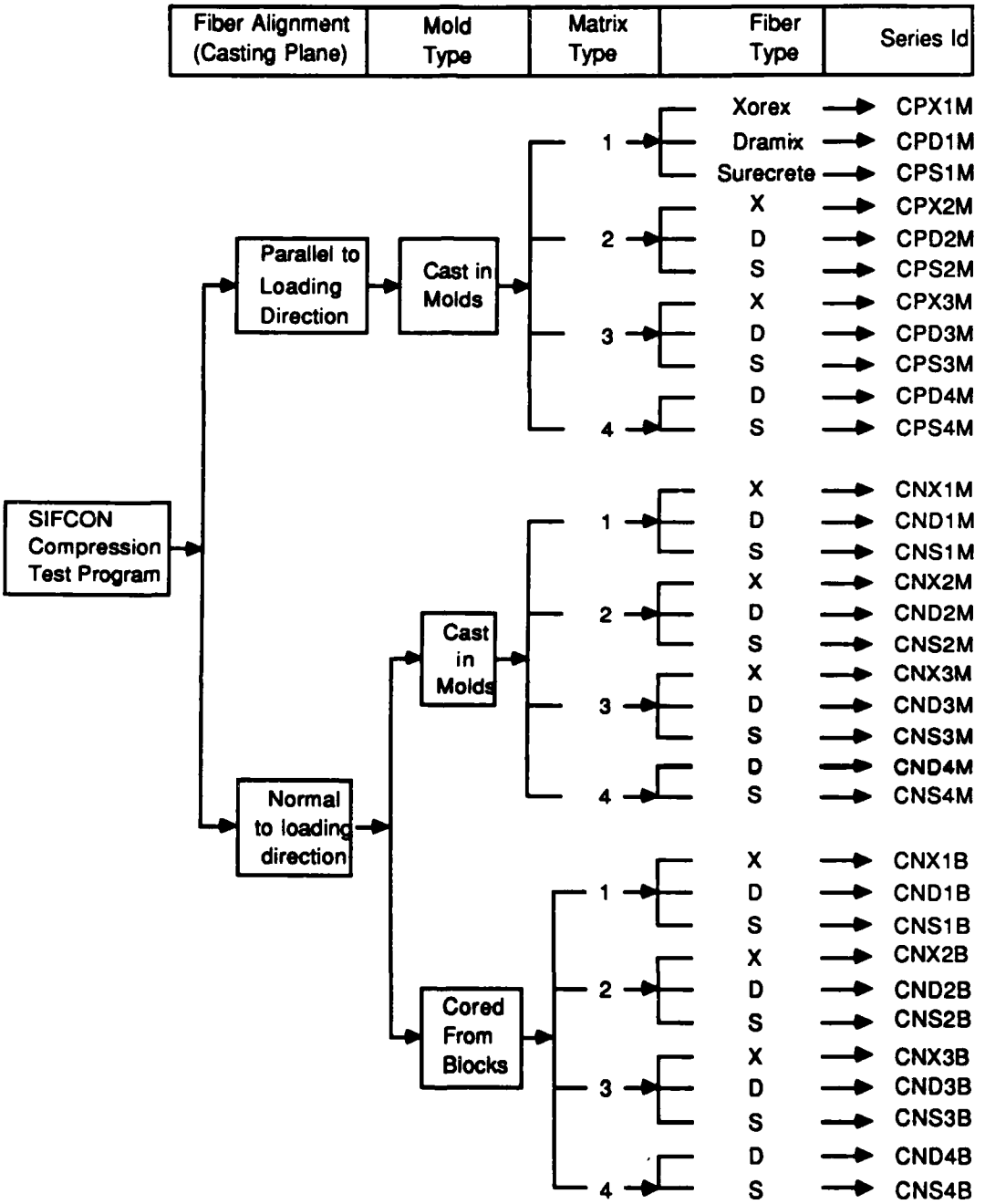

Figure 3. Experimental program for compression tests.

Table 1. Slurry mix designs.

Mix No.	Mix Constituents	Relative Weight of Constituents	Water/Cementitious Ratio	Strength Range (k/in^2)
1	Type I Cement Fly Ash Water Superplasticizer [a]	1.00 0.20 0.36 0.03	$\frac{\text{Water}}{\text{Cement + Fly Ash}} = 0.30$	7.5 to 17.0
2	Type I Cement Fly Ash EMSAC [b] Water Superplasticizer	1.00 0.20 0.20 0.355 0.02	$\frac{\text{Water}}{\text{Cement + Fly Ash + Silica}} = 0.35$	6.0 to 13.5
3	Type I Cement Fly Ash EMSAC Water Superplasticizer	1.00 0.20 0.30 0.255 0.04	$\frac{\text{Water}}{\text{Cement + Fly Ash + Silica}} = 0.30$	6.0 to 12.5
4	Type I Cement Fly Ash Water Superplasticizer	1.00 0.25 0.325 0.04	$\frac{\text{Water}}{\text{Cement + Fly Ash}} = 0.26$	10.0 to 17.5

a Trade name Melment

b Product of ELKEM Chemical Corporation. A slurry of approximately 50 % water and 50 % amorphous silica particles by weight.

Mix One is a conventional slurry similar to that used in previous studies (Ref. 7). It has a fly ash-cement ratio of 0.20, a water-cementitious ratio of 0.30, and a 3% by weight of cement addition of superplasticizer. The result is a very fluid, lump-free matrix with a projected ultimate strength of about 10,000 lb/in^2 (69 MPa).

Because a comparison was sought between slurries containing microsilica and more conventional mixes as well as a desire for very high strength, two microsilica mixes were designed as part of the program.

Mix Two was designed with a fly ash-cement ratio of 0.20, a microsilica-cement ratio of 0.10, a water-cementitious ratio of 0.35, and a 2% by weight of cement addition of superplasticizer. The resultant matrix is very fluid, relatively free of lumps and had a projected ultimate strength of 10,000 lb/in^2 (69 MPa).

Mix Three was designed to achieve the maximum possible strength of the matrices studied. It was designed with a fly ash-cement ratio of 0.20, a microsilica-cement ratio of 0.15, a water-cementitious ratio of 0.30, and a 4% by weight of cement addition of superplasticizer. This slurry is more viscous than mixes one or two, and forms many more lumps, but had a projected ultimate strength of over 15,000 lb/in^2 (104 MPa).

After a number of tests, it was clear that the microsilica slurries were not showing the strengths originally projected. Since mix three (the projected very high strength mix) was already rather viscous, and it was difficult to successfully impregnate the fiber-filled forms with it, pursuit of even lower water-cementitious ratio (higher strength) microsilica slurries was abandoned. Hence mix four was designed as a very high strength conventional slurry mix to fill this role. Mix Four has a fly ash-cement ratio of 0.25, a water-cementitious ratio of 0.26, and a 4% by weight of cement addition of superplasticizer. Mix Four is somewhat viscous but relatively lump-free and workable.

1.2.2 Fibers

Three types of steel fibers were studied; surface-deformed fibers supplied by Surecrete Incorporated, hooked (Dramix) fibers manufactured by Bakaert Steel Wire Corporation, and crimped (Xorex II) fibers manufactured by Ribbon Technology Corporation. A listing of the properties of these fibers is given in Table 2. The fibers differed principally in geometry, surface textures, and aspect ratios. All fibers were made of steel and were approximately the same length.

The hooked and deformed fibers have the same overall dimensions, behave in much the same manner, and allow for approximately the same volume fraction placement. Because of their low aspect ratios and larger diameters, the crimped fibers may be placed with a much higher volume fraction. However, their lower aspect ratio also significantly reduces fiber interlock.

1.2.3 Fiber Orientation

Two fiber axis orientations were studied: parallel and normal to the direction of testing. To study this effect, Groups I and II were poured differing only in fiber alignment: Group I with

load-parallel fiber alignment and Group II with load-normal fiber alignment (i.e., load normal to fiber axis).

Table 2. Fiber properties.

Fiber Type	Supplier	length	diam.	l / d	Tensile Yield Stress (lb/in^2)	Volume Fraction (This Study)
Crimped (Xorex II)	Ribtec[a]	1" (25.4 mm)	0.035"	30	N.A.	20 % to 23 %
Hooked (Dramix)	Bekaert[a]	30 mm	0.5 mm	60	170,000	10 % to 12 %
Deformed (Surecrete)	Surecrete	30 mm	0.5 mm	60	N.A.	10 % to 12 %

a Manufacturer Supplied

1.2.4 Edge Effects

The influence of molds on specimen behavior due to "edge effects" was studied by preparing an additional group of cored cylindrical specimens (Group III) with fiber axes aligned normal to the loading direction. These 2.75x6-in cylinders were cored from 6x8x8-in blocks of SIFCON prepared similarly to Group II.

1.3 SPECIMEN PREPARATION

1.3.1 Molds

The compression cylinder molds are shown in Figure 4, while the test setup is illustrated in Figure 5. Group I cylinders were cast in horizontal Plexiglas molds (Figure 4a). These molds have an open slit on their top to allow for fiber placement and the pouring of slurry.

The horizontal molds were constructed with perfectly flat parallel end faces which eliminated the need for sulfur capping.

Group II cylinders were cast in vertical Plexiglas molds as shown in Figure 4b. A Plexiglas mold cap which fit on the top of the mold, once again ensured flat and parallel end faces. A small hole in the bottom of these molds also allowed for easier form removal through the use of air pressure.

Group III cylinders were cored from precast blocks of SIFCON. The blocks were cast in 6x8x8-in Plexiglas molds. Twenty-four hours later, the blocks were unmolded and cured in water for one week. Following a month of storage in the laboratory environment (70^0F and 70% RH), four cylinders were cored from each block. Since some surface damage occurred to the cylinders during the coring process (usually in the form of chipped edges), all cored cylinders were capped with a high-strength sulfur capping compound (trade name Cylcap) prior to testing.

1.3.2 Fiber Placement

All specimens followed the same general pouring procedure. First, empty Plexiglas molds were weighed on an electronic scale and their weight automatically zeroed. Second, the molds were place on a small vibration table and the table turned on a gentle vibration setting. Third, fibers were carefully hand distributed into the molds until the molds were filled. Fibers were placed one handful at a time while light vibration caused them to settle and ensured sufficient fiber packing. Slow filling of the molds allowed the fibers to essentially fill the molds in layers. Each fiber deviated slightly from horizontal alignment except near the end faces where edge effects occurred. For the normally aligned fiber specimens, these layers were randomly distributed in the two-dimensional horizontal planes but aligned somewhat normal to the vertical direction. For the parallel direction specimens, fibers tended to align themselves in one direction along the principal cylinder axis due to the nature of the molds. Finally, when the molds were filled with fibers, they were weighed to determine fiber content. Then the fiber-filled molds were ready for slurry infiltration.

1.3.3 Mixing

First the slurry components were weighed out. Second, the dry mix ingredients, portland cement and fly ash, were placed in a one cubic foot capacity mixing bowl and mixed together on low speed for about 30 s. Third, with the mixer still on, the liquid components, microsilica and water, were gradually added to the mixing bowl until a paste had been formed. Finally, a measured amount of superplasticizer was added to create a fluid slurry. The slurry was then mixed for an additional minute on high speed to ensure fluidity and to help remove existing lumps. The slurry was then ready for infiltration of the fiber bed.

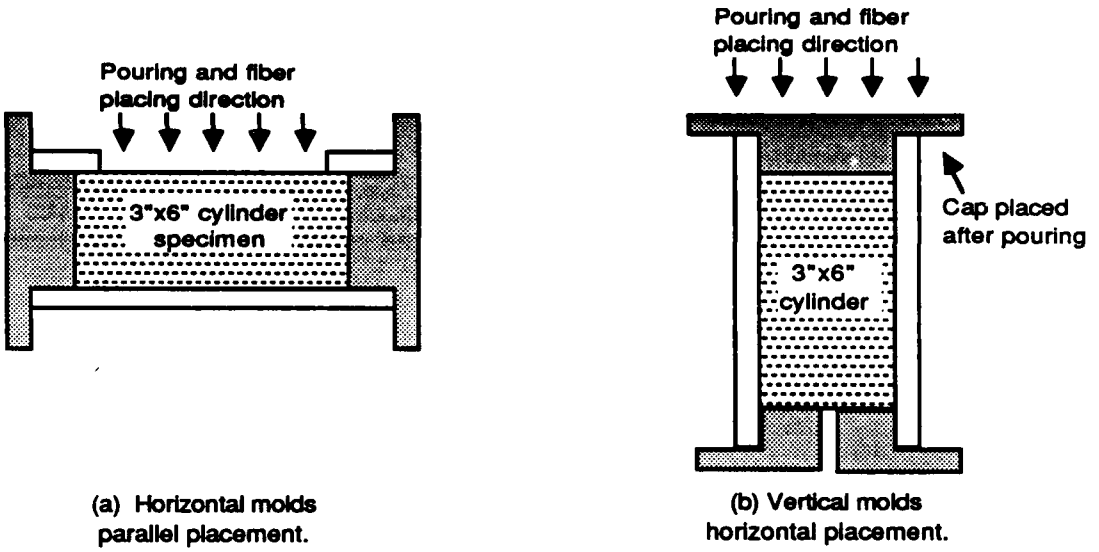

Figure 4. Compression molds.

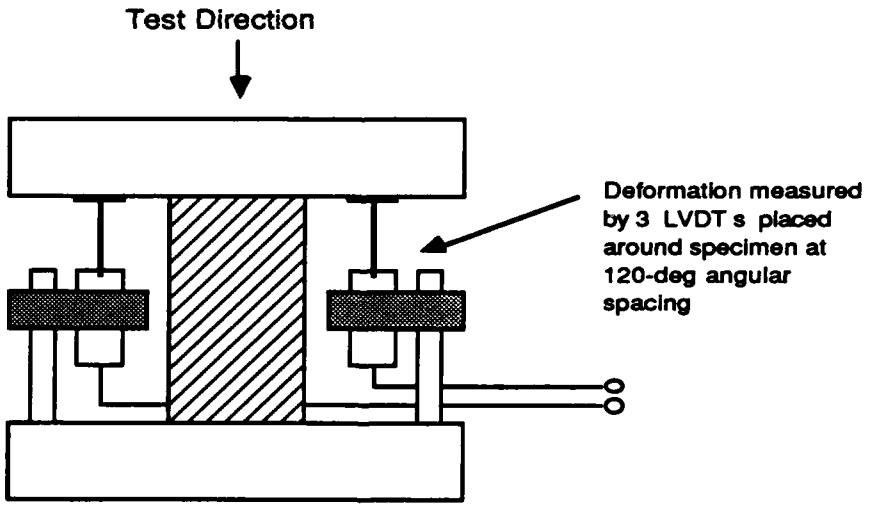

Figure 5. Compression test setup.

1.3.4 Pouring

To ready the forms for slurry infiltration, a fine wire mesh was placed on top of the mold opening. This mesh served to remove any lumps in the slurry which would have clogged the spaces between fibers and made complete infiltration more difficult. Then the molds were placed once again on the vibration table. Slurry was scooped up in a plastic cup and poured through the wire screen into the molds. Infiltration was assisted by vibration. When the molds were filled with slurry, the specimens were removed from the vibration table. The specimens were then covered with plastic sheeting to aid in specimen curing. The specimens were left to cure overnight in the molds. The next day the specimens were unmolded, labeled, and placed under water for one week. They were then removed from the water and stored in the laboratory environment (about 70^0F and 70% RH) until tested.

1.4. TESTING

1.4.1 Instrumentation

The testing system used consisted of a computer-controlled, closed-loop, servohydraulic universal testing machine (Instron System 8000 with a 200 kip frame) and a high-speed data acquisition system capable of taking up to 1000 readings per second. The testing system is also equipped with a Hewlett-Packard x-y recorder to help monitor ongoing tests.

During the tests, load and deformation data were recorded and stored by the data acquisition system. A flowchart of the data acquisition process is shown in Figure 6. The load level was read as an analog signal directly from the testing machine's control computer into the data acquisition unit's analog to digital (A/D) converter. The deformation of the tested specimen, however, could not be taken directly from the testing machine's control computer, since the measurement of the hydraulic actuator's piston displacement included the deformation of the loading frame and loading devices as well as the deformation of the specimen. This quantity was recorded, however, on the x-y recorder of the testing machine. To obtain a more accurate reading, the deformation of the specimen was measured by linearly variable differential transformers (LVDTs). The LVDTs were placed so as to measure the actual specimen deformation excluding the deformation of the loading frame. The signal from these LVDTs was processed by a signal conditioner which converted the readings to the standard analog output range of -10 V to +10 V.

Once the signals were converted to digital values by the A/D unit, they were read by a microcomputer. The computer utilized a specially tailored high-speed data acquisition program to accomplish this task. This microcomputer is also equipped with a graphics terminal, so that initial results could be inspected immediately after testing. The data were collected in the form of load versus time and deflection versus time, and were stored on floppy disks.

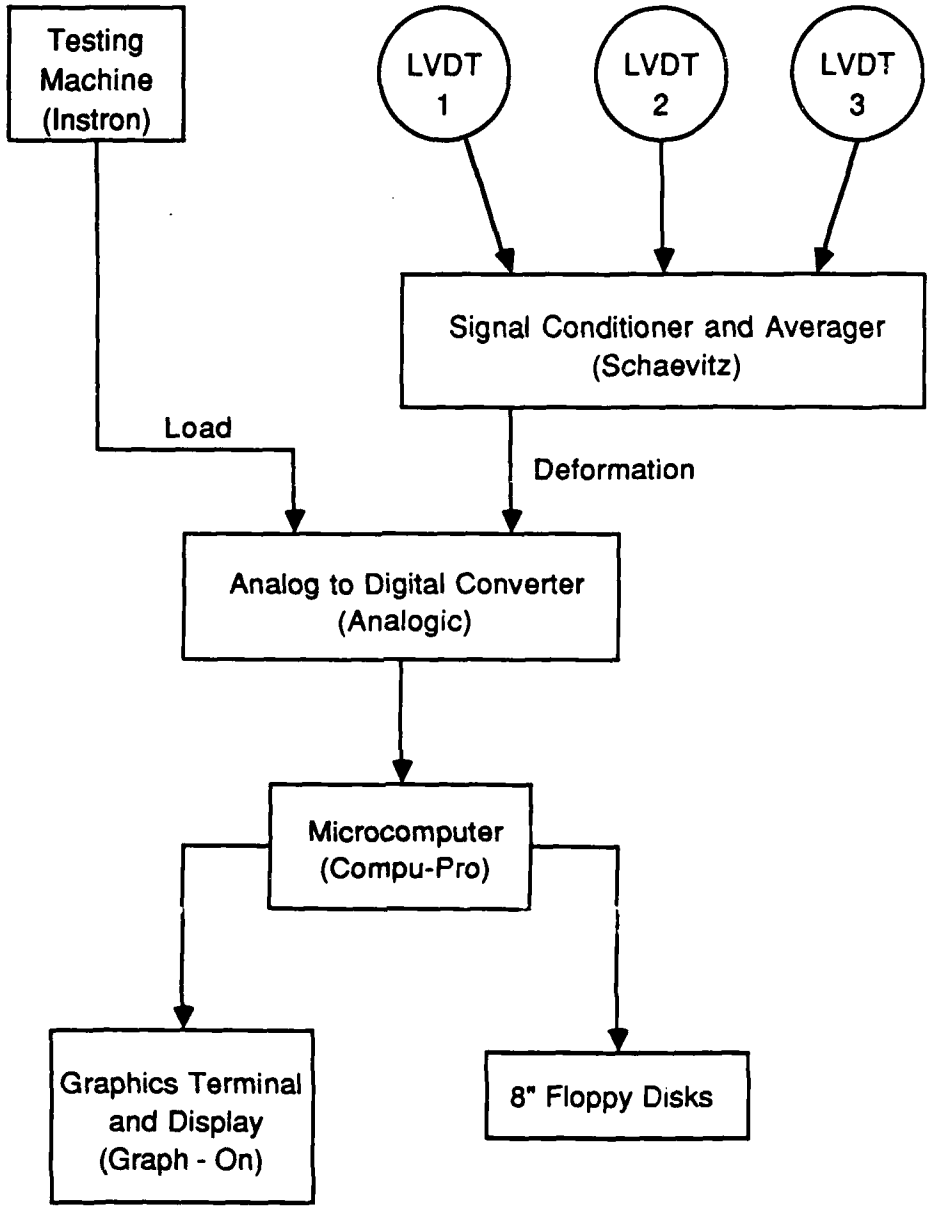

Figure 6. Data Acquisition.

1.4.2 Compression Tests

The test setup for the compression cylinder specimens is shown in Figure 5. Three LVDTs were placed in a horizontal arrangement around the specimen at 120-deg spacings, and were positioned vertically between the two platens of the testing machine. The signal from these LVDTs was averaged by a signal conditioner and the averaged signal sent to the A/D converter as specimen deformation data. Load signal was taken directly from the Instron control computer. After about two months of air curing in the laboratory environment, all specimens were tested in uniaxial compression. The compression tests were run on stroke control at a constant rate of 0.001 in/s (166 μstrains/s). All compression cylinders were tested in this manner.

1.4.3 Data Processing

After data were obtained, they were processed into a useful form for analysis. For this study, the processing of data was done on an IBM PC/XT to free the data acquisition system's computer for testing purposes. The data transfer from one computer to the other was accomplished through the use of a data transfer program named Kermit. Kermit is a file transfer program which allows communication and error-free data transmission between two computers. By sending packets of information and comparing the received packets to the transmitted packets, Kermit discovers any errors in information transfer and resends the erroneous data until transfer is completed correctly.

After file transfer was accomplished, a series of programs were employed to produce stress-strain plots of the specimens. The first step involved the reading of data into a useful format so that calculations could be more readily performed. Second, the load and deformation were converted into stress and strain values. A third program prepared the data in a format suitable for plotting, and a fourth program performed the plotting and provided for graphical output of the data. Figure 7 summarizes the data processing procedure.

1.5. RESULTS, DISCUSSION AND ANALYSIS

1.5.1 Core Survival

Due to poor infiltration and a lack of technical expertise on the part of the crew performing the coring operation, very few of the microsilica mix cylinders survived the coring process without substantial damage. Because of this, the microsilica series (Groups II and III) will have to be repoured and retested at a future date. Of the specimens that did survive, many had significant end surface damage and had to be capped with sulfur before testing.

1.5.2 Failure Mode

Figures 8a and 8b show the failure mode of tested cylinders, while Figures 9a through 9d show the complete failure sequence of an individual compression cylinder. It may be readily

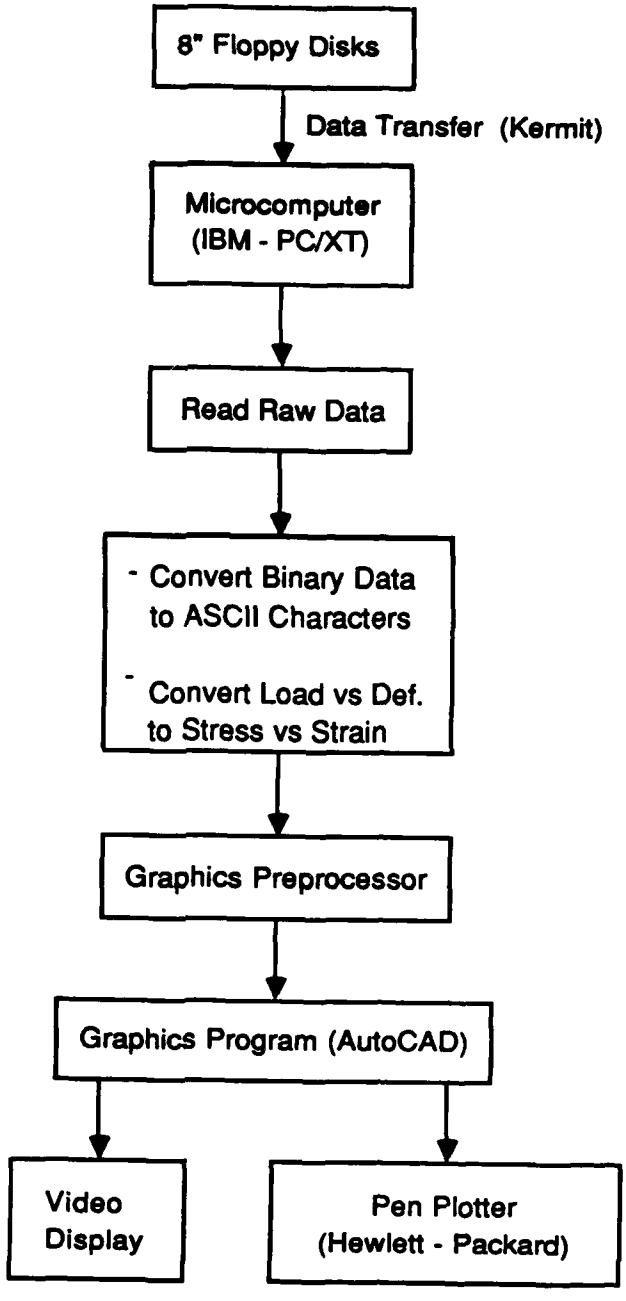

Figure 7. Data processing.

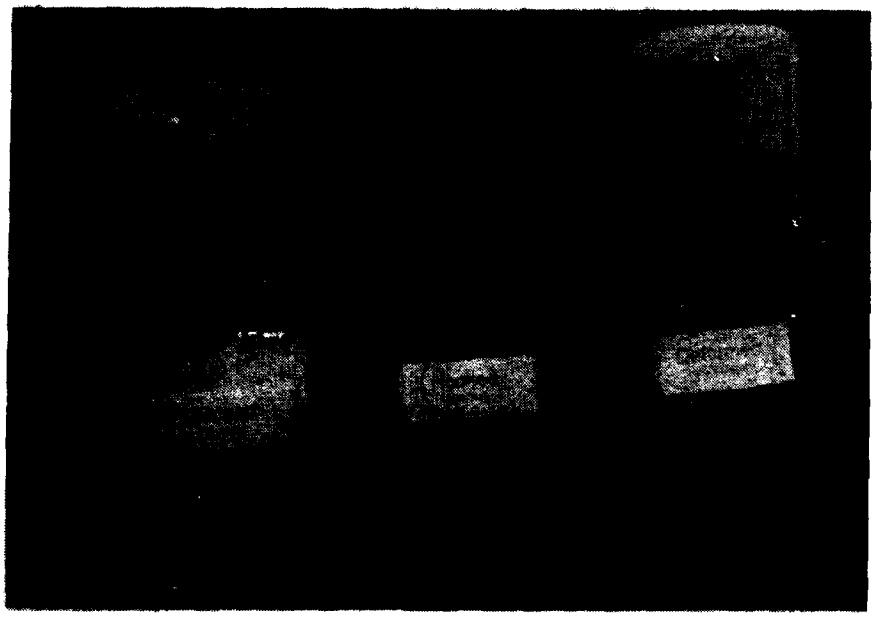

(a)

(b)

Figure 8. Tested compression specimens showing consistent shear type failure.

a. Molded specimens.
b. Cored specimens.

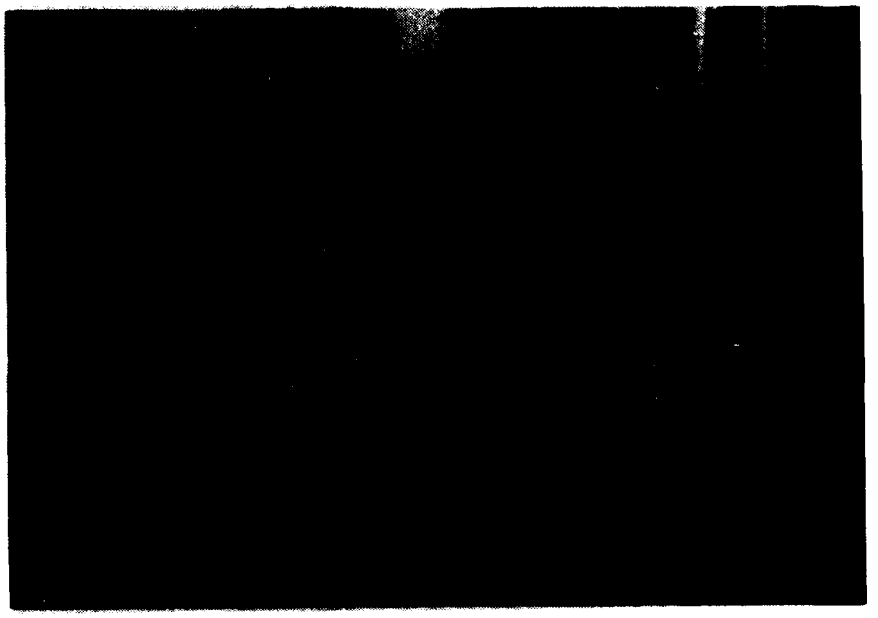

(a)

(b)

Figure 9. Compression test in progress.

a. Before load application.
b. Spalling of outer layer of slurry.

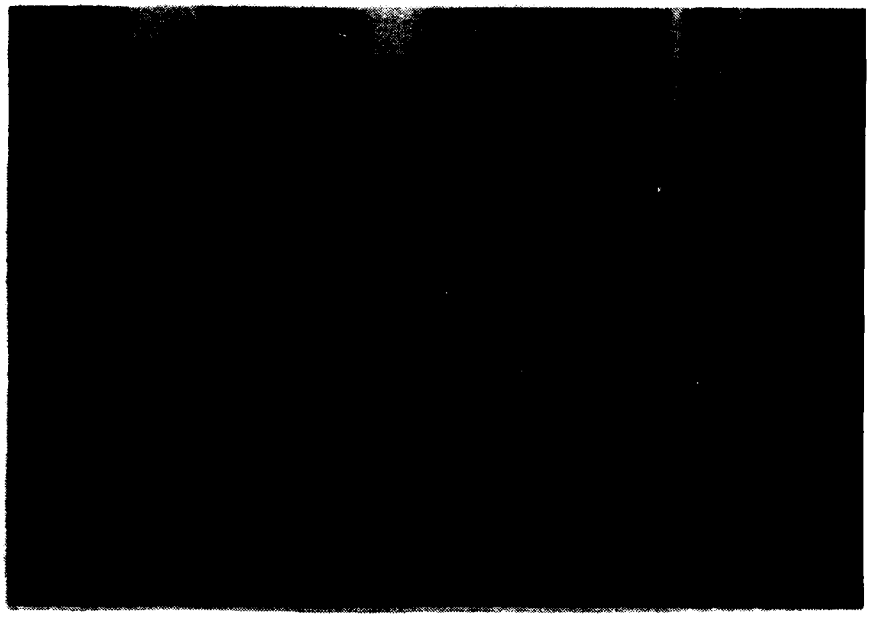

(c)

(d)

Figure 9. Compression test in progress.

c. Progressive deterioration.
d. Formation of diagonal shearing plane.

observed that failure occurs through the formation of a large diagonal shear crack in the cylinder. Figure 8a also shows the effect of edge spalling on molded specimens. During the spalling process, damage appears to be more localized near the surface for specimens containing hooked or deformed fibers than for specimens containing crimped fibers.

A typical stress-strain curve is shown in Figure 10. By examining the shape of this curve, three regions may be identified and the effect of shear failure more readily observed.

Ascending Branch This portion of the curve is very similar to that of conventional fiber reinforced mortar. It is initially linear with gradual loss of linearity as the maximum load approaches and major cracks develop.

Descending Branch After the peak load, the load drops off gradually as a shearing crack develops. It then asymptotically approaches a limiting shear stress plateau.

Plateau As the test progresses, the two specimen halves slide across each other along the shear crack. This results in a constant shearing strain test and a horizontal stress plateau.

The development of this shear crack was surprisingly consistent. It occurred during almost every test. The angle of the crack was also consistent. The cracking plane usually deviates by 55-60 deg from the horizontal when hooked and deformed fibers are used, and by 30-45 deg from the horizontal when crimped fibers are used.

The shear crack usually develops near an end face of the specimen. For the cored and molded specimens with fiber axis normal to the axis of the cylinder, the shear crack started primarily near the end face representing the surface of the specimen. Since the specimens have a length-to-diameter ratio of only 2, it is not known whether shear cracking represents the true failure mode of the material or whether the confining effects of the loading machine platens cause the development of the shear crack.

In order to investigate whether shear cracking is a true material behavior, a number of 12-in -long (and 3-in -diam) cylindrical specimens with fiber axis parallel to the axis of the cylinders were poured and tested. These specimens duplicated those of series CPX1M, CPD1M, and CPS1M described in Figure 3. In all cases failure occurred by a major shear crack and did not initiate near an end face (Figure 11).

1.5.3 Fiber Type

Tables 3,4, and 5 list the important results of the compression tests in tabular form for test groups I, II, and III respectively. The results listed are the average results for the four cylinders in each series.

1.5.3.1 Parallel Alignment . Figure 12a gives a comparison of typical stress-strain curves of SIFCON specimens reinforced with fibers aligned parallel to the loading direction. It can be observed that specimens reinforced with hooked and deformed fibers behave in a comparable manner and show a consistently higher strength than do those reinforced with crimped fibers.

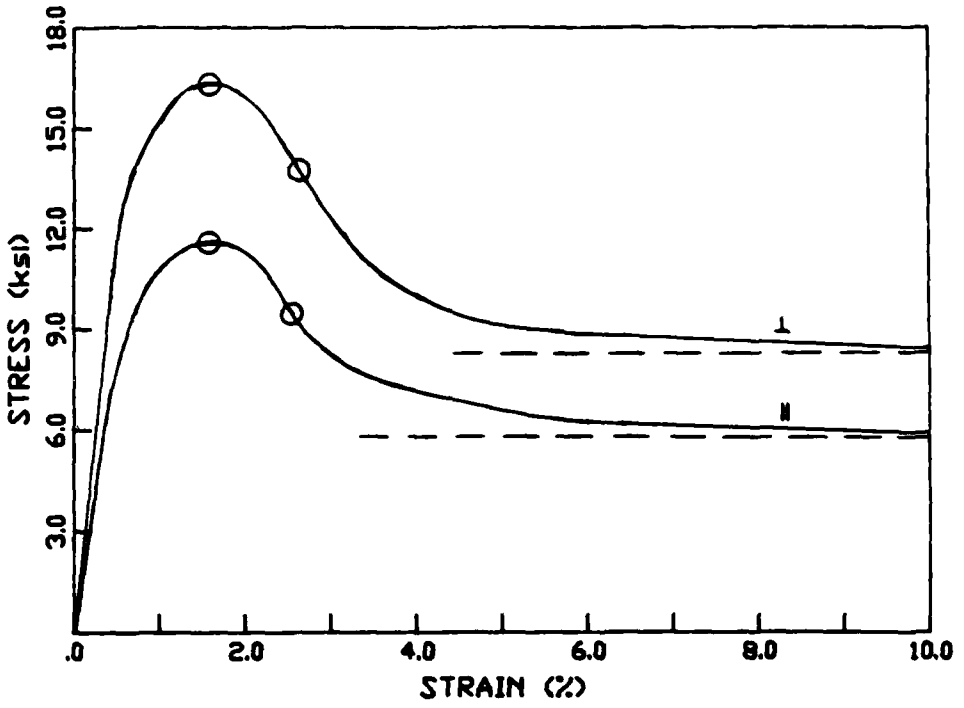

Figure 10. Typical Stress-Stain Curve of SIFCON in Compression.

Figure 11. Failure Mode of 12" x 3" SIFCON Compression Cylinders.

Table 3. Test results of poured cylinders with parallel fiber alignment.

Series Code	Matrix Type	Fiber Type	Fiber Volume Fraction (%)	Average Properties						
				Elastic Modulus, E[a] 10^6 (lb/in^2)	Peak Point strain	Peak Point stress (k/in^2)	Post-Peak Plateau, f_p (k/in^2)	Inflection Point strain	Inflection Point stress (k/in^2)	Toughness Index[b]
CPX1M	1	Xorex II	22.9	1.12	0.009	7.6	4.3	0.018	6.0	41.7
CPD1M	1	Dramix	12.9	1.43	0.010	10.6	7.2	0.026	8.6	47.4
CPS1M	1	Surecrete	12.7	1.25	0.010	9.6	7.0	0.025	8.3	48.0
CPX2M	2	Xorex II	23.1	1.58	0.008	6.4	2.7	0.013	4.8	31.4
CPD2M	2	Dramix	12.0	1.43	0.010	8.7	6.3	0.019	7.3	49.2
CPS2M	2	Surecrete	12.4	1.25	0.010	9.7	5.9	0.020	7.8	43.1
CPX3M	3	Xorex II	22.2	0.83	0.009	5.9	1.8	0.015	4.0	25.3
CPD3M	3	Dramix	11.9	0.87	0.015	10.6	7.0	0.021	8.5	46.0
CPS3M	3	Surecrete	12.2	0.80	0.015	9.3	6.4	0.026	8.0	47.8
CPD4M	4	Dramix	12.2	1.43	0.010	10.0	6.1	0.022	8.1	43.5
CPS4M	4	Surecrete	12.2	1.25	0.010	10.4	5.2	0.019	7.8	37.1

a Secant Modulus measured from origin of stress-strain curve to 45% of ultimate strength using average strain between platens.

b Area under stress-strain curve of SIFCON up to 10% strain divided by area under stress-strain curve of ordinary concrete of same ultimate strength to failure strain.

Table 4. Test results of cored cylinders with normal fiber alignment.

Series Code	Matrix Type	Fiber Type	Fiber Volume Fraction (%)	Average Properties						
				Elastic Modulus, E^a 10^6 (lb/in^2)	Peak Point strain	Peak Point stress (k/in^2)	Post-Peak Plateau, f_p (k/in^2)	Inflection Point strain	Inflection Point stress (k/in^2)	Toughness Index ^{b}
CNX1B	1	Xorex II	22.8	0.90	0.020	13.4	8.6	.066	11.2	55.4
CND1B	1	Dramix	12.1	1.26	0.020	15.4	5.1	.038	10.7	35.6
CNS1B	1	Surecrete	12.1	1.23	0.022	14.9	6.6	.041	10.1	41.6
CNX2B	2	Xorex II	22.7	N.A.	N.A.	N.A.	N.A.	N.A.	N.A.	N.A.
CND2B	2	Dramix	11.6	1.05	.019	13.1	10.0	.032	11.5	53.1
CPS2B	2	Surecrete	12.1	N.A.	N.A.	N.A.	N.A.	N.A.	N.A.	N.A.
CNX3B	3	Xorex II	22.7	0.75	.019	10.0	6.6	.022	8.0	46.1
CND3B	3	Dramix	11.8	N.A.	N.A.	N.A.	N.A.	N.A.	N.A.	N.A.
CNS3B	3	Surecrete	12.0	N.A.	N.A.	N.A.	N.A.	N.A.	N.A.	N.A.
CND4B	4	Dramix	12.1	1.33	.022	16.0	11.1	.043	13.4	51.7
CNS4B	4	Surecrete	12.0	1.41	.022	16.7	10.0	.029	12.9	43.8

N.A. (Not Available). These series were damaged by the coring process.

a Secant Modulus measured from origin of stress-strain curve to 45% of ultimate strength using average strain between platens.

b Area under stress-strain curve of SIFCON up to 10% strain divided by area under stress-strain curve of ordinary concrete of same ultimate strength to failure strain.

Table 5. Test results of poured cylinders with normal fiber alignment.

Series Code	Matrix Type	Fiber Type	Fiber Volume Fraction (%)	Average Properties						
				Elastic Modulus, E [a] 10^6 (psi)	PeakPoint strain	PeakPoint stress (k/in^2)	Post-Peak Plateau, f_{pl} (k/in^2)	Inflection Point strain	Inflection Point stress (k/in^2)	Toughness Index [b]
CNX1M	1	Xorex II	21.7	1.29	.016	11.7	8.7	.061	10.0	56.7
CND1M	1	Dramix	10.2	1.50	.037	13.6	6.0	.071	10.0	52.5
CNS1M	1	Surecrete	9.9	1.06	.018	11.0	5.0	.031	7.9	38.2
CNX2M	2	Xorex II	21.3	1.06	.018	10.5	8.1	.022	9.5	51.8
CND2M	2	Dramix	10.1	1.13	.019	11.5	7.3	.050	9.1	51.2
CNS2M	2	Surecrete	10.0	1.20	.019	11.3	6.7	.033	8.8	44.1
CNX3M	3	Xorex II	21.3	0.91	.018	10.7	8.2	.022	9.5	51.6
CND3M	3	Dramix	10.1	1.13	.018	12.2	5.8	.028	9.4	37.8
CNS3M	3	Surecrete	10.1	1.20	.018	11.7	5.6	.036	8.3	40.0

a Secant Modulus measured from origin of stress-strain curve to 45% of ultimate strength using average strain between platens.

b Area under stress-strain curve of SIFCON up to 10% strain divided by area under stress-strain curve of ordinary concrete of same ultimate strength to failure strain.

Using slurry mix No. 2 (Table 1) as a comparison, the average strength of specimens reinforced with each type of fiber was 8.7 k/in^2 (60 MPa), 9.7 k/in^2 (67 MPa), and 6.4 k/in^2 (45 MPa), respectively. Thus the use of hooked and deformed fibers led on the average to a 36% and 50% higher strength than did the use of crimped fibers. A similar trend was observed when SIFCON specimens made with the three other slurry matrices of Table 3 were tested.

It is noted that while the volume fraction of crimped fibers in the test specimens is almost twice that of hooked or deformed fibers, their aspect ratio is about half. This implies that the three test groups of Figure 3 have about the same reinforcing index ($V_f l / d$). Hence, for a given slurry matrix, the observed stress-strain behavior cannot be solely explained in terms of the reinforcing index alone.

Significant increases (up to 50%) in compressive strength due to steel fiber additions (up to 3% by volume) have been observed in conventional low strength (4 k/in^2 (28 MPa)) fiber-reinforced concrete where fiber interlock is unimportant (Ref. 7). This increase probably results from the arresting of microcrack growth by the fibers and is significantly influenced by the fiber-to-matrix bond. It seems likely, therefore, that the superior performance of hooked and deformed fibers as compared to crimped fibers, is a result of better fiber-to-matrix bonding properties and perhaps a greater degree of fiber interlock among those fibers.

In the post peak region of the compressive stress-strain curve (Figure 10), a shear crack becomes dominant and the response of the material is dependent upon the parameters that affect the movement of the shearing material: fiber-to-matrix bonding, fiber volume fraction, dowel action, and the alignment of fibers across the shear crack.

Here, too, composites reinforced with the hooked and deformed fibers outperform those reinforced with the crimped fibers. The average post peak plateau stress for these composites was 6.3 k/in^2 (44 MPa), 5.9 k/in^2 (41 MPa), and 2.7 k/in^2 (19 MPa), respectively. These trends were also consistent when other slurry mixes were used. Overall, the plateau stress for specimens reinforced with hooked and deformed fibers averaged respectively 133% and 118% higher than the plateau stress of corresponding specimens reinforced with crimped fibers.

Once again, since the various test specimens had about the same reinforcing index ($V_f l / d$), material performance cannot be explained in terms of the reinforcing index alone.

It seems probable, therefore, that fiber pullout, fiber-to-matrix bond, and fiber interlock also have a significant influence on the postcracking behavior in compression of SIFCON composites.

1.5.3.2 Normal Alignment. Figure 12b shows a typical comparison of compressive stress-strain curves for specimens reinforced with fibers aligned normal to the loading direction. In this case, composites reinforced with crimped fibers show a compressive strength only 15% smaller than that observed when hooked and deformed fibers are used, but the corresponding plateau stress on the descending branch is substantially higher. Using cored cylinders with slurry mix No. 1 as a comparison, the average post peak stress plateau

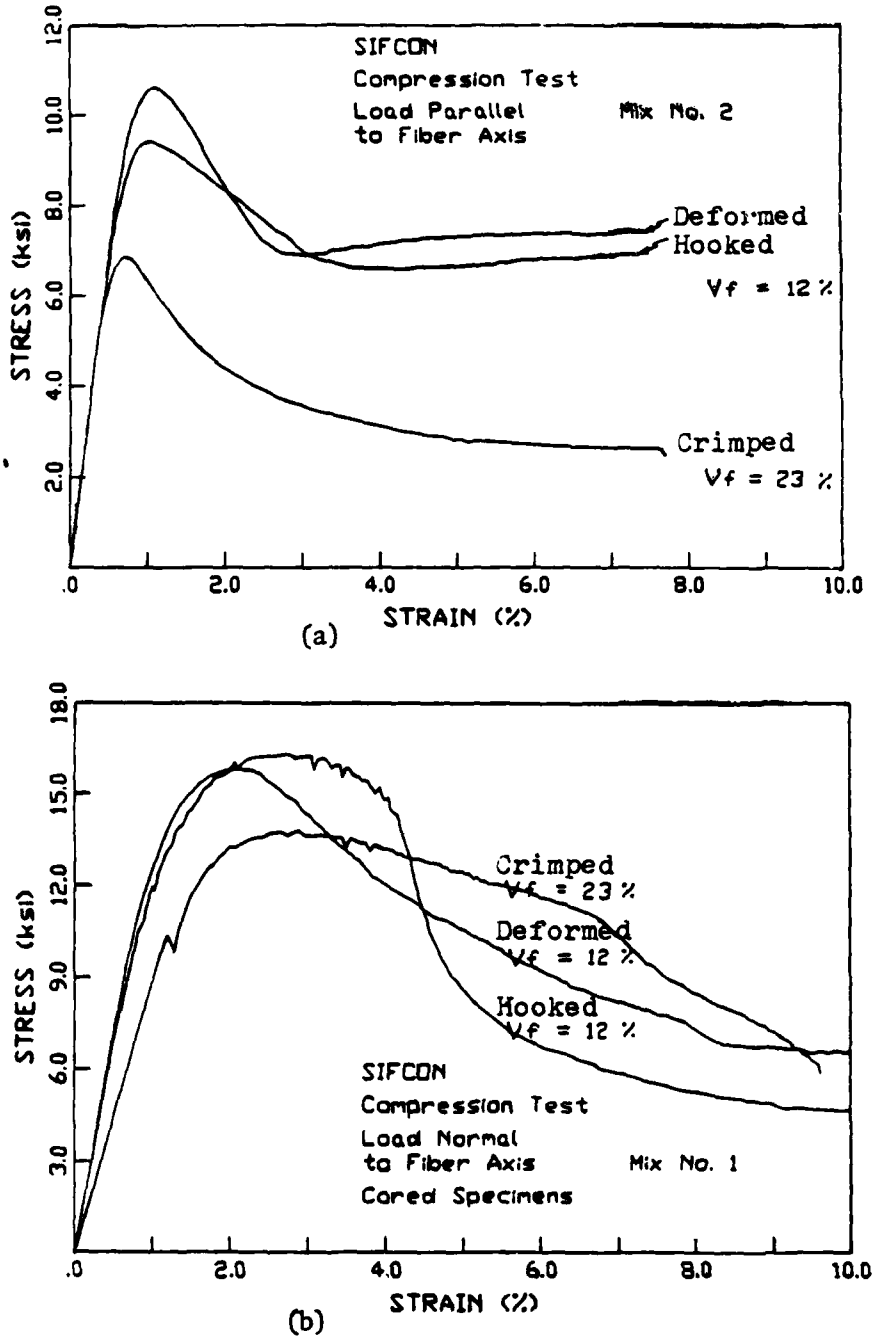

Figure 12. Typical Effects of Fiber Type on the Stress-Strain Curve. of SIFCON in Compression:
a. Loading Parallel to Fiber Axis
b. Loading Normal to Fiber Axis

of specimens reinforced with crimped, deformed, and hooked fibers was 5.1 k/in^2 (35 MPa), 6.6 k/in^2 (46 MPa), and 8.6 k/in^2 (59 MPa), respectively. Overall, for all test series, the stress plateau value obtained with crimped fibers was 10% to 68% higher than that observed with hooked or deformed fibers. Two additional effects are present in normal fiber alignment that may help to explain this behavior: more reinforcement of vertical tensile cracks by crimped fibers since their volume fraction was larger, and the contribution of fiber-to-fiber compression.

First, the failure mode of high-strength concrete is usually that of numerous splitting cracks parallel to the loading direction. During testing, small vertical microcracks develop in the matrix. The higher volume fraction of crimped fibers means a greater area of tensile reinforcement across these cracks and probably improved resistance in the postcracking range.

Second, the higher volume fraction of crimped fibers, as compared to hooked or deformed fibers, probably causes a much greater incidence of direct fiber-to-fiber compression along the fiber's strongest compression alignment (normal to the applied load). In essence the fibers aligned normal to the loading direction act as contacting beams whereas fibers aligned parallel to the loading direction act as individual columns.

The combination of fiber-to-fiber compression and high volume fraction may thus explain the higher post peak stress plateau of composites reinforced with crimped fibers when the fibers are aligned normal to the applied load.

1.5.4 Slurry Mixes

Figure 13 shows a typical comparison of compressive stress-strain curves for SIFCON specimens reinforced with crimped fibers and using the four slurry mixes of Table 1. These specimens were poured directly into molds with the fiber axis aligned primarily normal to the loading direction. Overall, mix four led to the highest strength followed by mixes one, three, and two respectively. Among cylinders reinforced with deformed fibers parallel to the loading direction, mixes one, two, three, and four showed an average compressive strength of 9.6 k/in^2 (66 MPa), 9.7 k/in^2 (67 MPa), 9.3 k/in^2 (64 MPa), and 10.4 k/in^2 (72 MPa), respectively. Among cylinders reinforced with crimped fibers normal to the loading direction, mixes one, two, and three showed an average compressive strength of 13.6 k/in^2 (94 MPa), 11.5 k/in^2 (79 MPa), and 12.2 k/in^2 (84 MPa), respectively.

The slurry mixes using microsilica (Nos. 2 and 3) gave poorer strengths than expected. Three reasons may be given for this poor performance: (1) there was a significant loss of cementitious material due to matrix lumps in the microsilica mixes, (2) microsilica slurries tend to be more viscous because of the ultrafine nature of the silica particles which may have resulted in incomplete infiltration of the fibers, and (3) the microsilica particles may have competed with the fly ash for a limited supply of cementitious calcium hydroxide reactants and resulted in an incomplete hydration of both pozzolans. In the future, microsilica mixes without fly ash additive may be used to help eliminate the latter problem.

1.5.5 Coring and Fiber Alignment

Figure 14 shows a typical comparison of the compressive stress-strain curves of SIFCON specimens, illustrating the differences between the three test groups of Figure 3. It can be observed that the behavior of SIFCON is highly dependent on fiber alignment and quite sensitive to mold edge effect. In the case of cylinders poured with slurry mix one and filled with crimped fibers, the strength of the parallel aligned (Group I), normally aligned molded (Group II), and normally aligned cored (Group III) cylinders was 10.6 k/in^2 (73 MPa), 13.6 k/in^2 (94 MPa), and 15.4 k/in^2 (106 MPa), respectively. For other series, the results were of the same order. Normally aligned cored specimens showed a 15% to 35% increase in strength over parallel aligned specimens cast in molds. The post peak plateau stress also showed similar relative results.

The superior performance of specimens reinforced with fibers aligned normally to the applied load over those reinforced with fibers parallel to the applied load may be due to the effects of fiber-to-fiber compression and tensile crack reinforcement as described earlier.

The superior performance of cored versus molded specimens is most likely due to the elimination of edge effects in the cored cylinders since this is the only real difference in fiber placement and specimen preparation.

The above hypothesis may be readily tested by pouring and coring larger specimens with shorter fibers. This would minimize the edge effects difference between specimens and should result in a smaller discrepancy in material stress-strain performance.

1.6. MODELING

Although the purpose of this paper is not a detailed mathematical modeling of test results, some mention will be made of one method of modelling the stress-strain curve of SIFCON in compression, which is currently under consideration by the authors.

Previously, Fanella and Naaman used a fractional equation for fitting the stress-strain curve of fiber-reinforced mortar in compression (Ref. 8). By applying basic boundary conditions, the equation parameters were readily evaluated, leading to accurate prediction of the stress-strain curve.

In a recent study, Absi and Naaman proposed the use of a curve to model the exponentially decaying nature of SIFCON in the post peak region (Ref. 9). The corresponding relationship is given by:

$$\sigma = a\, e^{-b(\varepsilon-\varepsilon_0)^m} + c$$

where a and c are given input data and b and m are parameters to be determined from boundary conditions. These boundary conditions may be present in the form of: (1) the

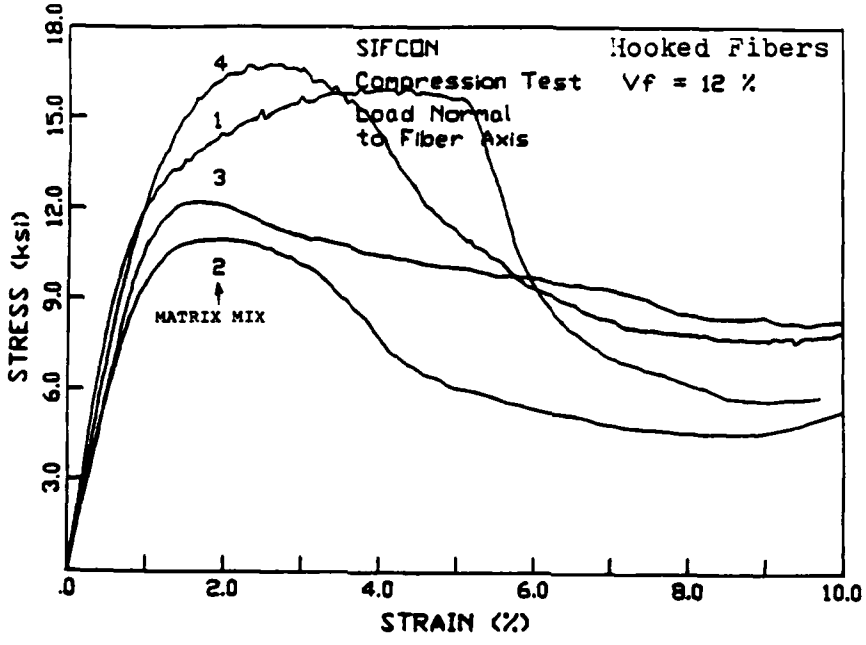

Figure 13. Typical Stress-Strain Curves of SIFCON in Compression for Different Matrix Strengths.

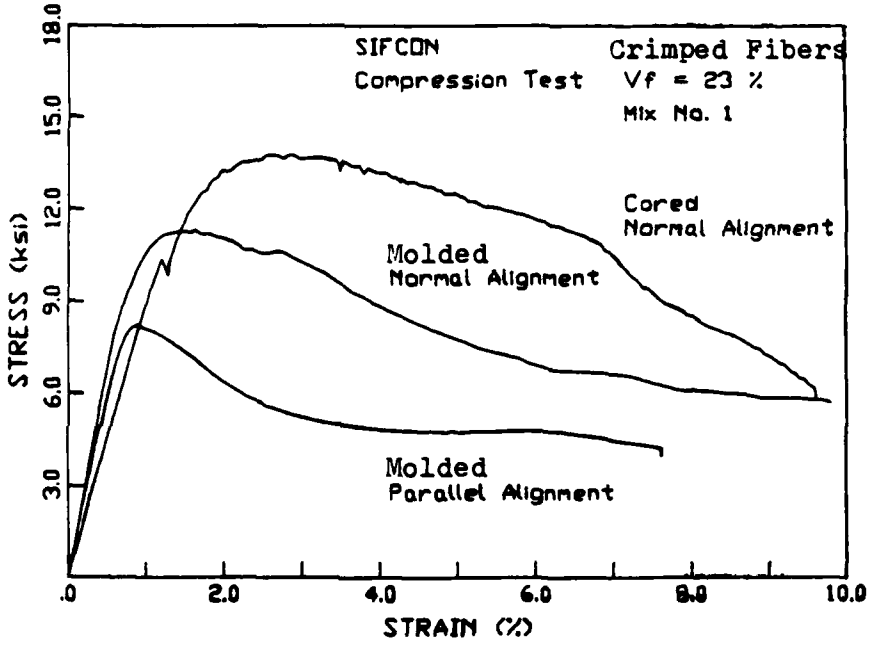

Figure 14. Typical Stress-Strain Curves of Molded and Cored SIFCON Specimens in Compression.

inflection point in the curve, (2) two points along the descending branch of the curve, or (3) a series of points along the descending branch through which a least squares fitting may be passed.

An example of this technique is shown in Figure 15. Using knowledge of the inflection point's location, the characteristic curve parameters may be determined according to:

(ε_0,σ_0)	coordinate of the peak point	(.0175,11 k/in^2)
c	asymptote	(6.4 k/in^2)
a	σ - c	(4.6 k/in^2)
(ε_f,σ_f)	coordinate of the inflection point	(.028,8.5 k/in^2)

Assuming the curve passes through the inflection point leads to:

$$m = \frac{1}{1 + Ln[(\sigma_f - c)/a]} = 4.63$$

$$b = [(m - 1) / m] * (\varepsilon_f - \varepsilon_0)^{-m} = 1.15 \times 10^9$$

The fitted curve is plotted in Figure 15a and shows a good agreement with the experimental curve. Figure 15b shows the fit of a more irregular curve to illustrate possible deviation between observed and predicted curves. It also illustrates the case where the descending branch of the curve is forced to pass through two prescribed points instead of through the inflection point.

1.7. CONCLUSIONS

The following conclusions may be drawn from the compression tests of SIFCON specimens. Since only three types of fibers were used in this study and since for each type many varieties exist (i.e., different lengths, yielding properties, etc.), conclusions should be limited to the fibers described in Table 2 and may not apply at large.

1.7.1 For composites made with fibers aligned parallel to the loading direction, specimens made with hooked and deformed fibers show a better composite material performance than specimens made with crimped fibers all along the stress-strain curve. The specimens made with hooked and deformed fibers averaged a 30% to 50% higher strength than those made with crimped fibers and a 50% to 250% higher post peak plateau stress.

1.7.2 For composites made with fibers aligned normal to the loading direction, specimens made with hooked and deformed fibers showed a higher ultimate stress

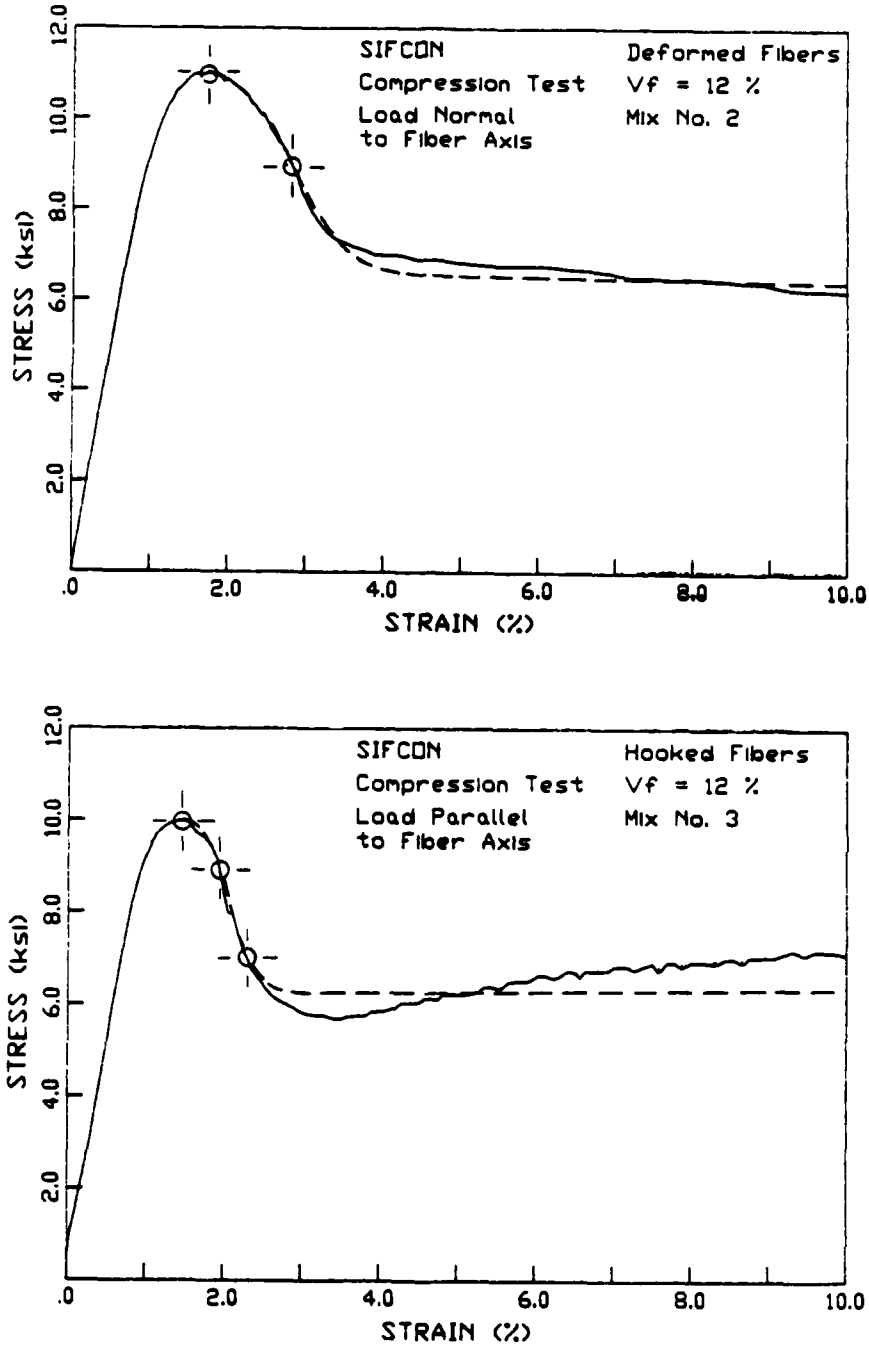

Figure 15 Typical Comparison Between Predicted and Observed Stress-Strain Curves:
a. Using the Inflection Point
b. Using two points

than those made with crimped fibers but a lower post peak plateau stress. The specimens with crimped fibers averaged a 10% to 68% higher post peak plateau stress than specimens with hooked or deformed fibers of the same matrix.

1.7.3 In this study the use of slurry mix No. 4 (Table 1) which contained 25% fly ash, a water-cementitious ratio of 0.26, and 4% superplasticizer by weight of cement led to the highest strength among the four mixes tried. The compressive strength of SIFCON composites using slurry mix No. 4 ranged from 10.0 k/in^2 to 17.5 k/in^2 (70 to 121 MPa).

1.7.4 The stress-strain curve of SIFCON is highly dependent on fiber alignment. SIFCON specimens cast with fiber axis normal to the loading direction may show up to 45% and 75% higher strength and post peak plateau stress, respectively, than specimens cast with fibers aligned parallel to the loading direction.

1.7.5 For the size of specimens and fibers used in this investigation, cored specimens showed a 15% to 30% higher compressive strength and post peak stress than molded specimens using the same matrix and fiber type. This is most probably due to the elimination of mold edge effects during the coring process.

1.7.6 The post peak branch of the stress-strain curve of SIFCON in compression may be accurately modeled through the use of an exponentially decaying fitted curve.

1.7.7 Compared to plain slurry, the toughness index in compression of SIFCON evaluated at 10% strain can exceed 50.

2.0 Stress-Strain Properties of SIFCON in Tension

2.1 INTRODUCTION

To date most studies of SIFCON have dealt with its compressive behavior [see references in Section 1], and although flexural tests have been performed (Refs. 1 and 10), no report of uniaxial tensile response of SIFCON is known to the writers of this report. However, results of flexural tests indicate that SIFCON's performance may be as impressive in tension as it is in compression.

SIFCON composites differ from conventional fiber reinforced concrete (FRC) in at least two aspects: they contain a much larger volume fraction of fibers and they use a very fine matrix slurry instead of concrete. From the behavioral viewpoint, fibers in SIFCON are subjected to frictional and mechanical interlock between fibers, in addition to the usual bond with the matrix. In SIFCON the matrix plays the role, not only of transferring forces between fibers by shear (as in FRC), but also of acting as a bearing to keep the fibers interlocked.

2.2 OBJECTIVE AND SCOPE

The main objective of this chapter is to qualitatively and quantitatively describe the stress-strain response of high-strength SIFCON in direct uniaxial tension. In particular, this chapter examines the effects of two important parameters: (1) fiber type where length, aspect ratio, surface characteristics, and overall fiber geometry vary, and (2) matrix strength. This research should provide a better understanding of the mechanisms of fiber reinforcement in SIFCON and the variables that control its tensile strength, stress-strain response, and toughness. This study includes experimental results and analytical modeling.

2.3 EXPERIMENTAL PROGRAM

The experimental program consists of uniaxial tensile tests on 18-inch (457 mm) dogbone-shaped prism specimens with a 3x1.5-in (76x38-mm) testing area. Four specimens were poured and tested for each of the four series investigated. Two fiber types (Dramix and Surecrete of Table 1) and for each fiber type two slurry mixes (Mix One and Mix Four of Table 2) are investigated. The program is summarized in Figure 16. Complete information about mix compositions and fiber properties are available in Section 1 (Ref. 9). Data from the tests were collected, processed, and analyzed to produce stress-strain relationships and to allow rational comparisons between the various parameters under study.

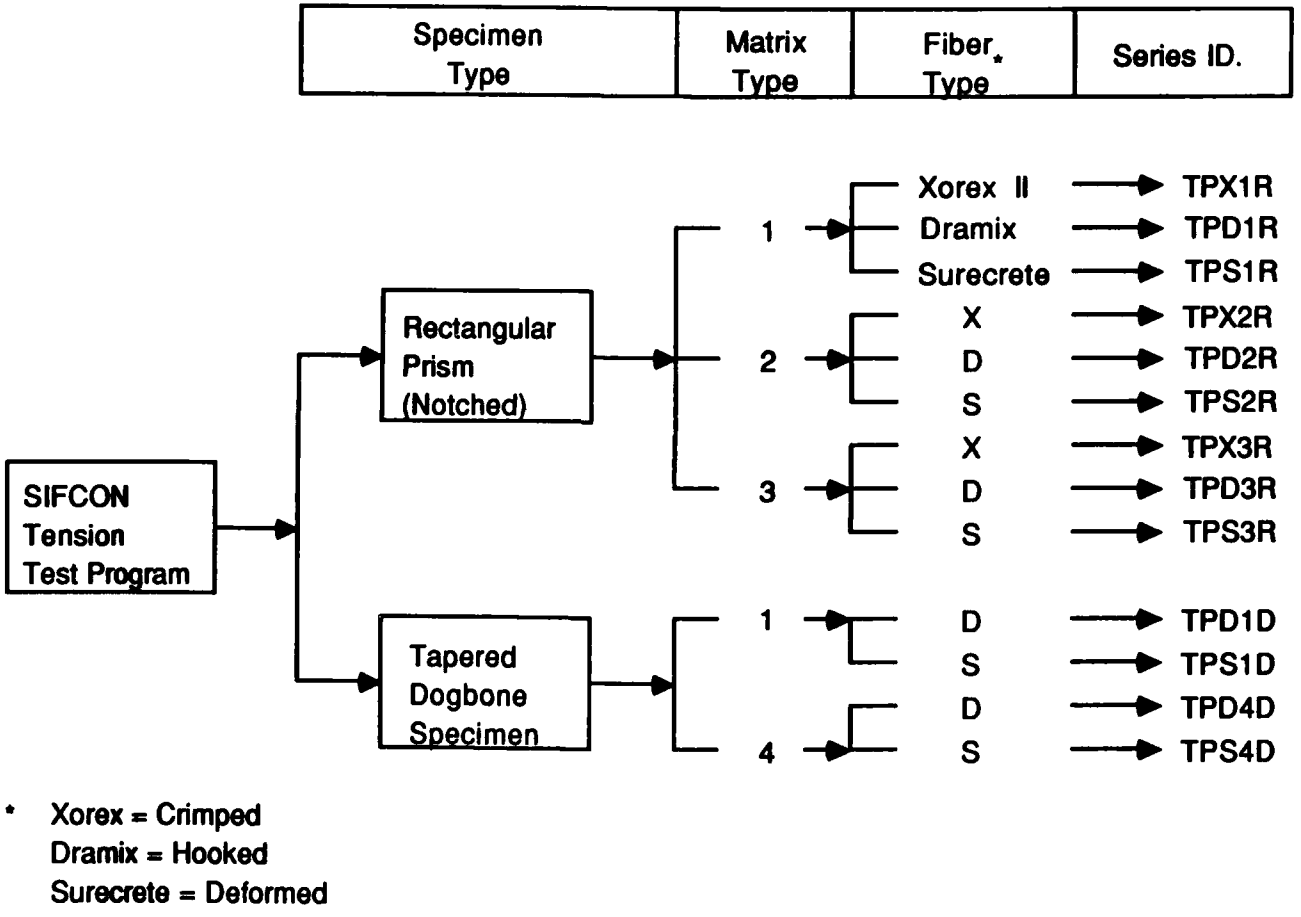

Figure 16. Experimental program.

2.4 SPECIMEN PREPARATION

2.4.1 Molds

Dogbone-shaped Plexiglas molds were especially built for the tensile specimens. The molds assemble and disassemble easily to facilitate specimen removal, mold cleaning, and surface oiling.

2.4.2 Mixing, Pouring, and Curing

The procedures for fiber placement, slurry mixing, pouring, and specimen curing were the same as those described for the compression specimens in Section 1.5. The fibers were hand distributed into the molds which were placed on a vibrating table and subjected to light vibration. The fibers were aligned predominantly along the longitudinal (testing) axis of the specimens. Alignment was more effective in the narrow testing region of the molds. After one week of immersed curing in water followed by about two months of air curing in the laboratory environment at approximately 70 °F, all sixteen specimens were tested in uniaxial tension.The experimental program consists of uniaxial tensile tests on 18-in (457-mm) dogbone-shaped prism specimens with a 3x1.5-in (76x38-mm) testing area. Four specimens were poured and tested for each of the four series investigated. Two fiber types (Dramix and Surecrete of Table 1) and for each fiber type two slurry mixes (mix one and mix four of Table 2) are investigated.

2.5 TESTING

2.5.1 Instrumentation, Data Collection, and Processing

The testing system consisted of a computer controlled, closed loop, servohydraulic universal testing machine (Instron System 8000), tensile friction grips, and a high-speed data acquisition system. The tensile friction grips and the fixture attachement to the specimen are shown in Figure 17. The grips consisted of self-clamping steel plates and a universal joint connection to the loading machine which allowed freedom of rotation along both coordinate axes and eliminated the possibility of inducing end moments in the specimens. During the tests, load and deformation data were recorded and stored by the data acquisition system and later processed for analysis. The data collection and processing procedures are described in detail in Section 1 (Ref. 9).

2.5.2 Tensile Test Setup

A schematic representation of the test setup for the tensile dogbone specimens is shown in Figure 18. Two LVDTs were placed on opposite sides of the specimen at a predetermined gauge spacing of 6 in. The signal from each LVDT was conditioned and recorded by an analog to digital converter as specimen deformation data. The load signal was taken directly from the Instron control computer.

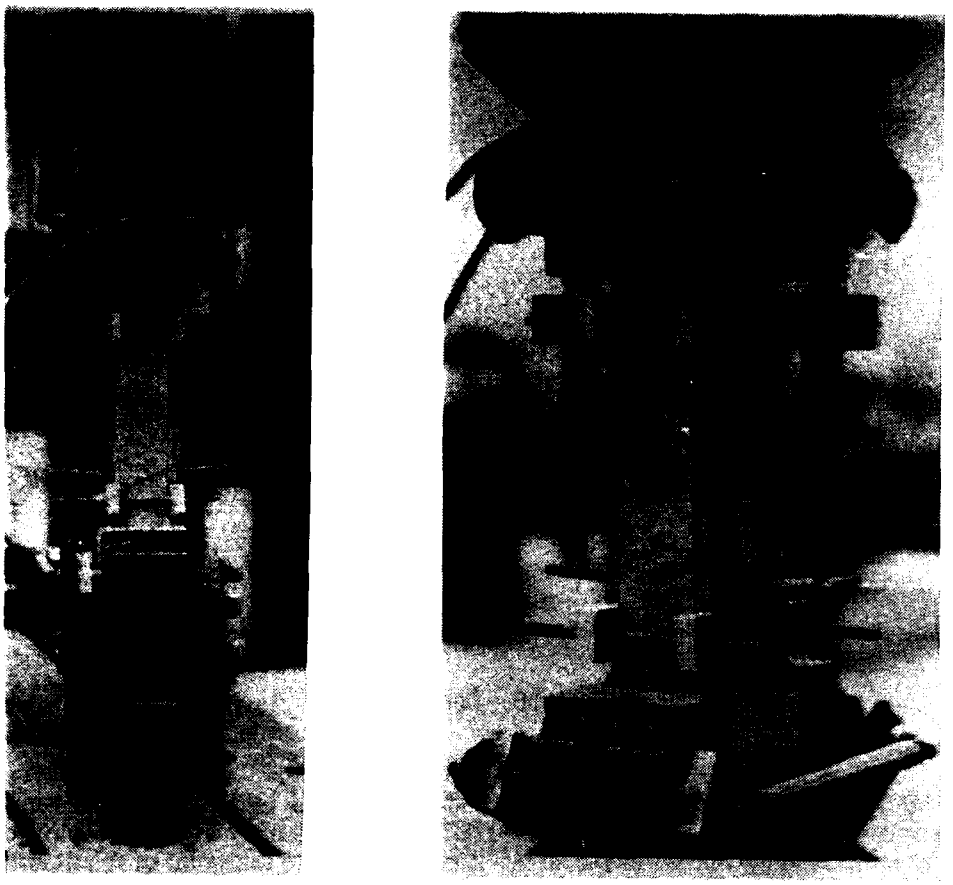

Figure 17. Friction grips in action.

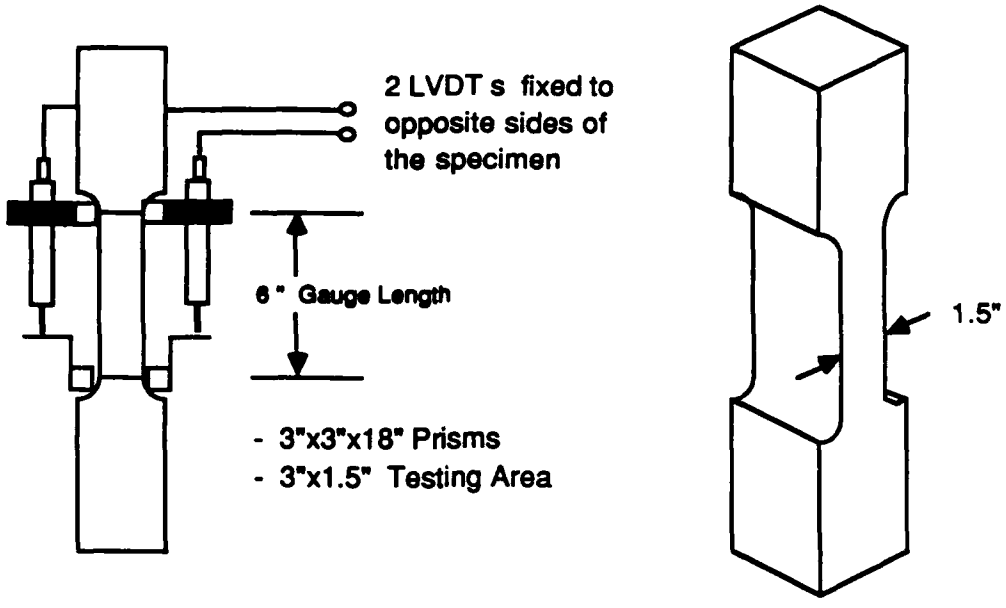

Test Setup - Dogbone Specimens

Figure 18. Tensile setup.

After curing, the specimens were tested in tension. The tension tests were run using stroke control at a variable rate. A rate of 0.001 in/s (166 μstrains/s) was employed during the initial ascending branch of the stress-strain curve up to the point of maximum stress. As failure proceeded, the stroke rate was reduced in an attempt to record a significant part of the descending branch of the stress-strain curve. The stroke rate was often reduced to 10^{-6} in/s (0.166 μstrains/s) before complete specimen failure occurred.

2.6 RESULTS, DISCUSSION, AND ANALYSIS

2.6.1 Stress-Strain Response

Figure 19 shows a typical tensile load-elongation response up to complete separation as recorded from the data. For the purpose of discussion, the curve may be divided into two parts: an ascending branch up to the peak load, and a descending branch from the elongation at the peak load to complete separation. The elongations up to the peak load can be translated into tensile strains (i.e., strain = elongation divided by gage length); the

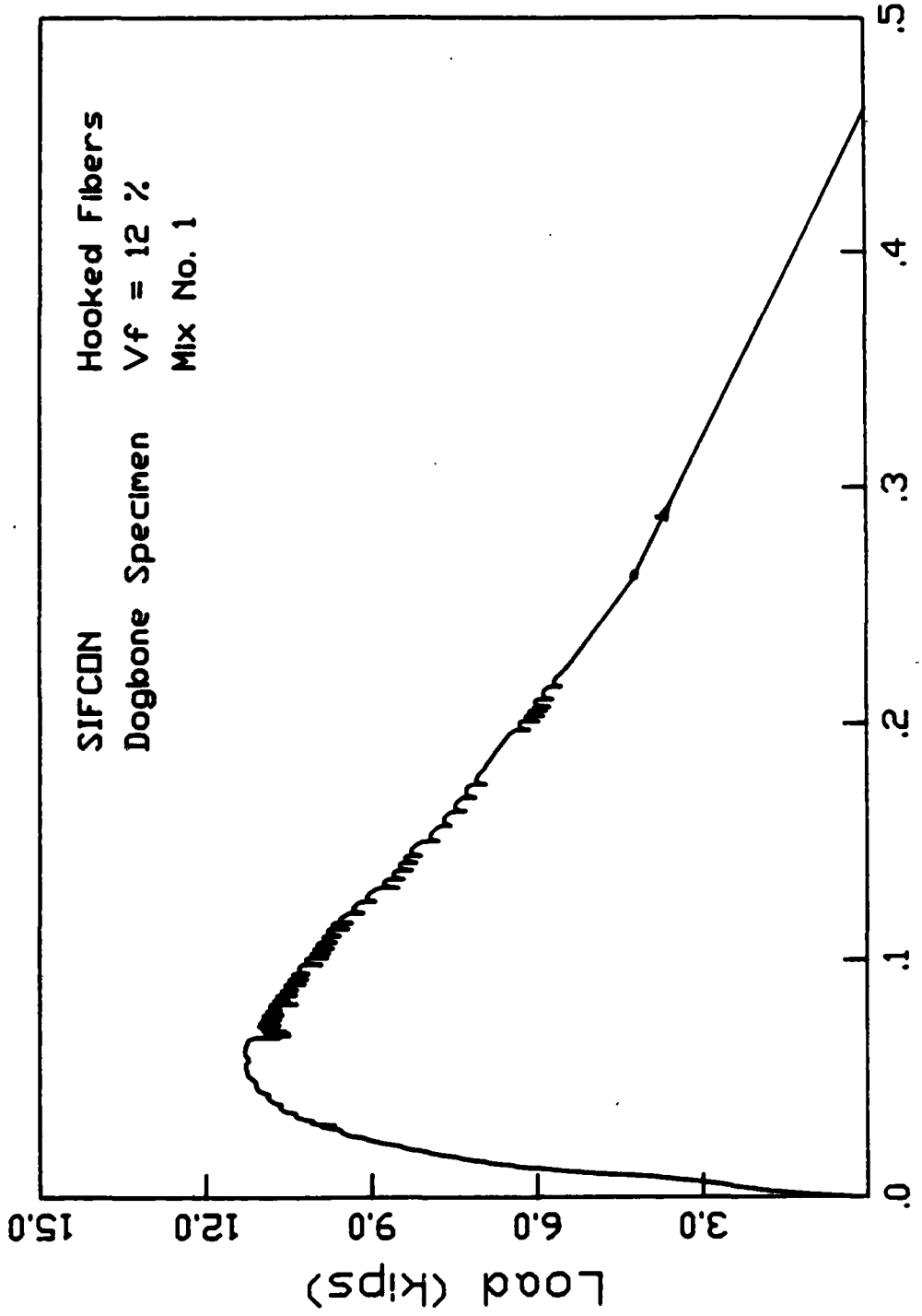

Figure 19. Typical load-elongation curve of SIFCON in tension.

elongation beyond the peak load represents primarily the opening of a critical crack and cannot be directly used as a strain. Figures 20 and 21 show the graphical results of the tensile tests where the strains are plotted up to an equivalent value of 2%. Figure 22 illustrates a typical comparison between the stress-strain response of the four series of tests. Two immediate observations can be made: the ascending branch of the stress-strain curve is nonlinear, and the strains to the peak load and to failure are very high. Additional observations are reported next.

2.6.1.1 Ascending Branch As testing begins, the curve is linear over a small portion, then gradually becomes nonlinear as the maximum load is approached. It is believed that the nonlinearity of the curve is caused by multiple cracking in the testing zone. These cracks are usually small but clearly visible during testing and tend to be evenly distributed across the testing zone; however, they are not "through" cracks as in reinforced concrete prisms. The ascending branch region up to the peak stress represents the true stress-strain response of the composite. In the final stages of this region, failure mode and location are determined as one of the many small tensile cracks in the testing zone begins opening to become the failure zone. A peak point could be determined from each curve, but often a flat plateau can better describe the behavior near the peak. This is why Figures 20 to 22 all have a maximum strain scale of 2%.

2.6.1.2 Descending Branch After the peak stress is attained, the failure proceeds as a single crack opening with fibers debonding on either side of the crack area. The opening of one large failure crack is accompanied by the release of strain energy in the testing system and the closing of microcracks in the testing zone. Typical cracking and failure modes are shown in Figures 23 and 24. As the failure crack opens, recoverable stress-strain response is lost and the observed curve becomes instead a representation of load versus crack opening response. This response cannot be considered very useful, since the failure crack is never truly planar nor perpendicular to the testing direction. Since this paper concerns the stress-strain response of SIFCON, this portion of the curve is not investigated here. A comprehensive investigation of the stress-displacement response of a planar crack is described in Section 3.

2.6.2 Average Properties

Table 6 lists the average results of the tensile tests of SIFCON specimens for the four series investigated. The table lists important parameters including the elastic modulus up to 45% of peak stress, the composite strength, and the toughness index in comparison with normal strength concrete in tension. Since only a narrow spectrum of variables was involved in this study, comparisons are difficult to make. Table 6 shows that the combinations of the two fibers and two matrices examined in this study resulted in composites with very similar stress-strain behavior. This is predictable since the matrices had similar strengths and the fibers had the same reinforcing index (Vfl/d).

The performance of the SIFCON in tension is impressive. The highest strength obtained in this study was 3000 lb/in^2 (21 MPa), an order of magnitude greater than would be expected of unreinforced normal concrete. The strains obtained (up to 1% with some recoverable elastic strain) are about two orders of magnitude greater than that of the unreinforced matrix. If the energy absorption capacity of a material is defined as the area under the stress-strain

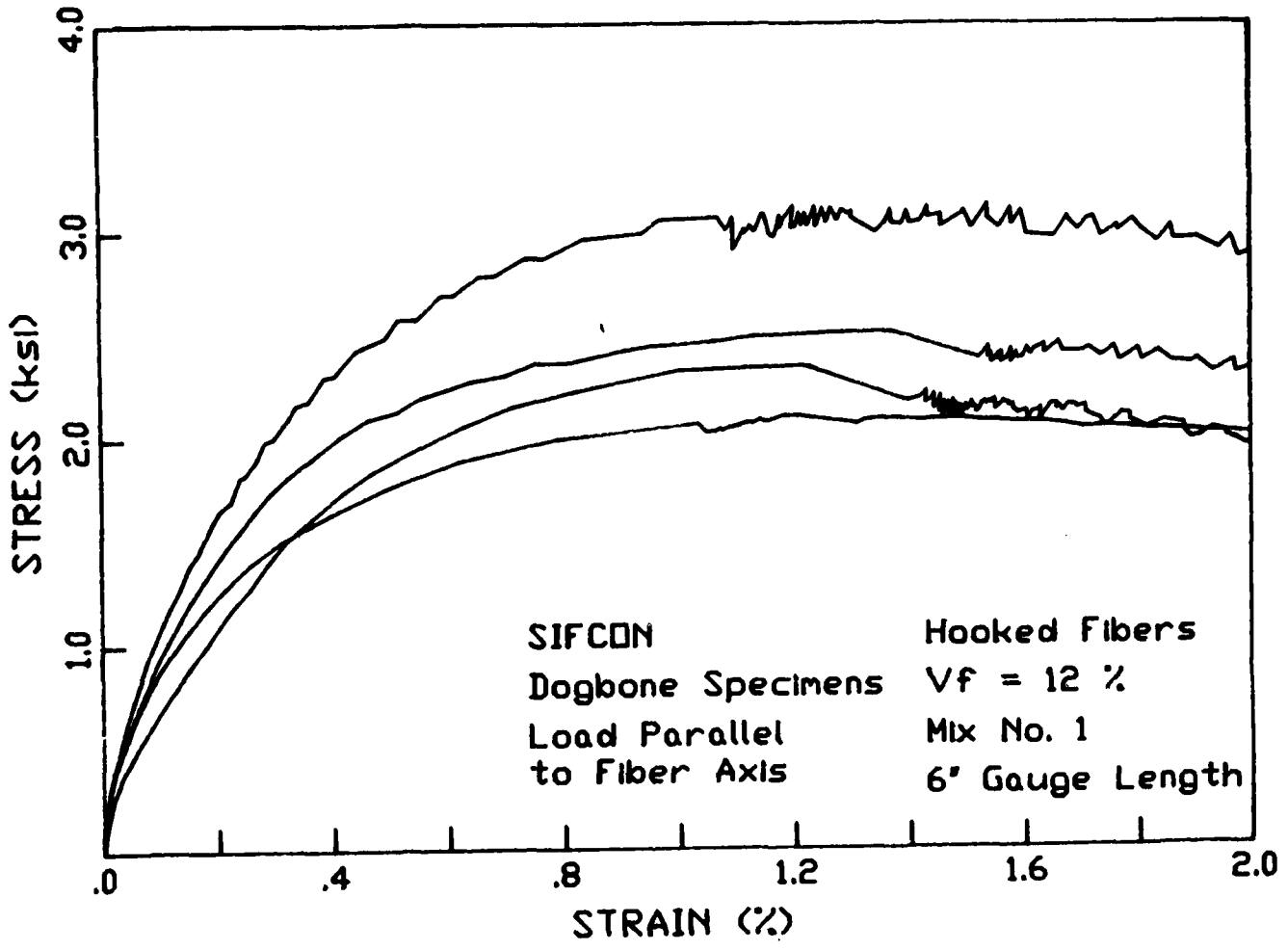

Figure 20a. Tensile stress-strain response of hooked fiber composites using Mix One.

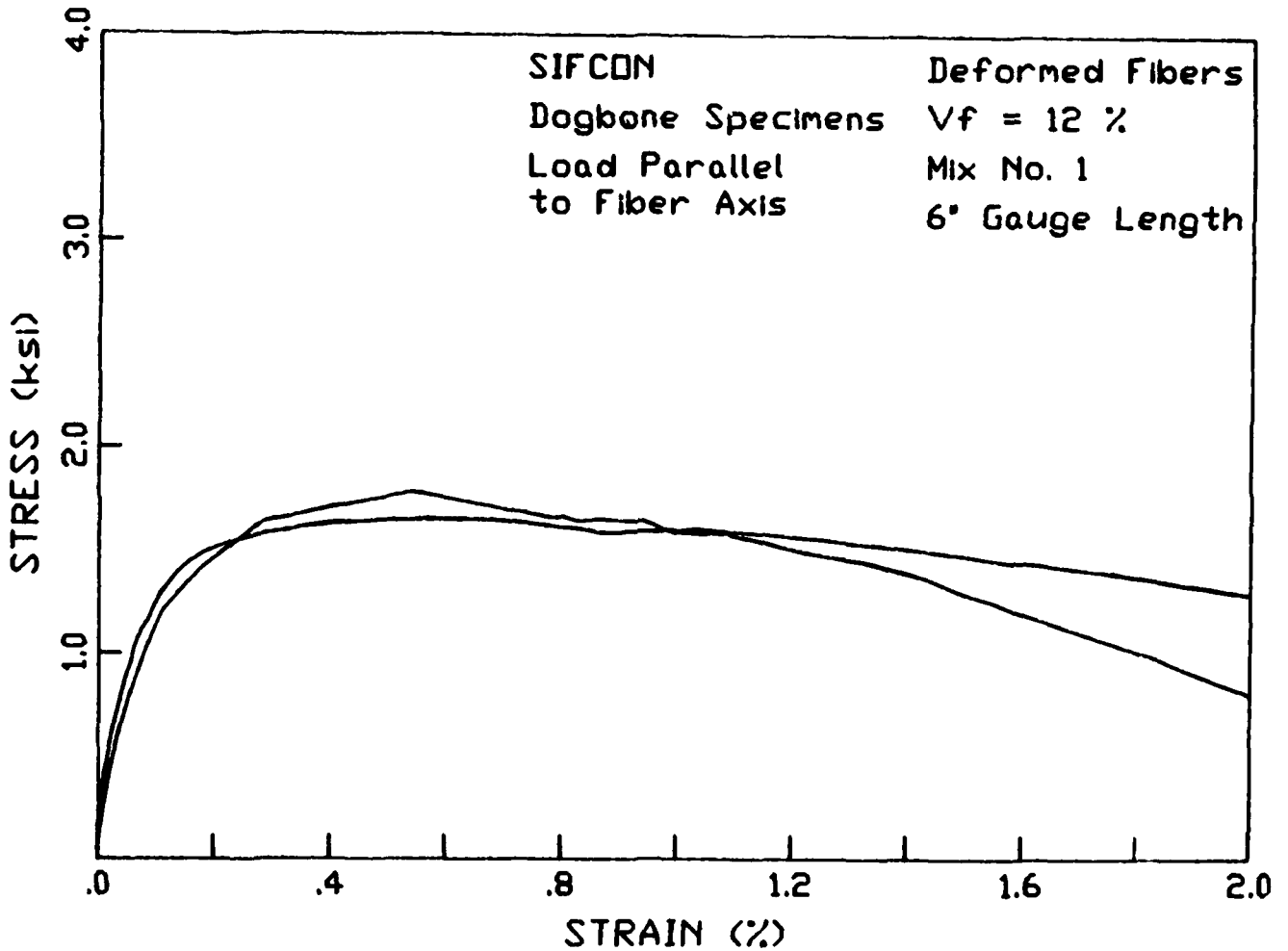

Figure 20b. Tensile stress-strain response of deformed fiber composites using Mix One.

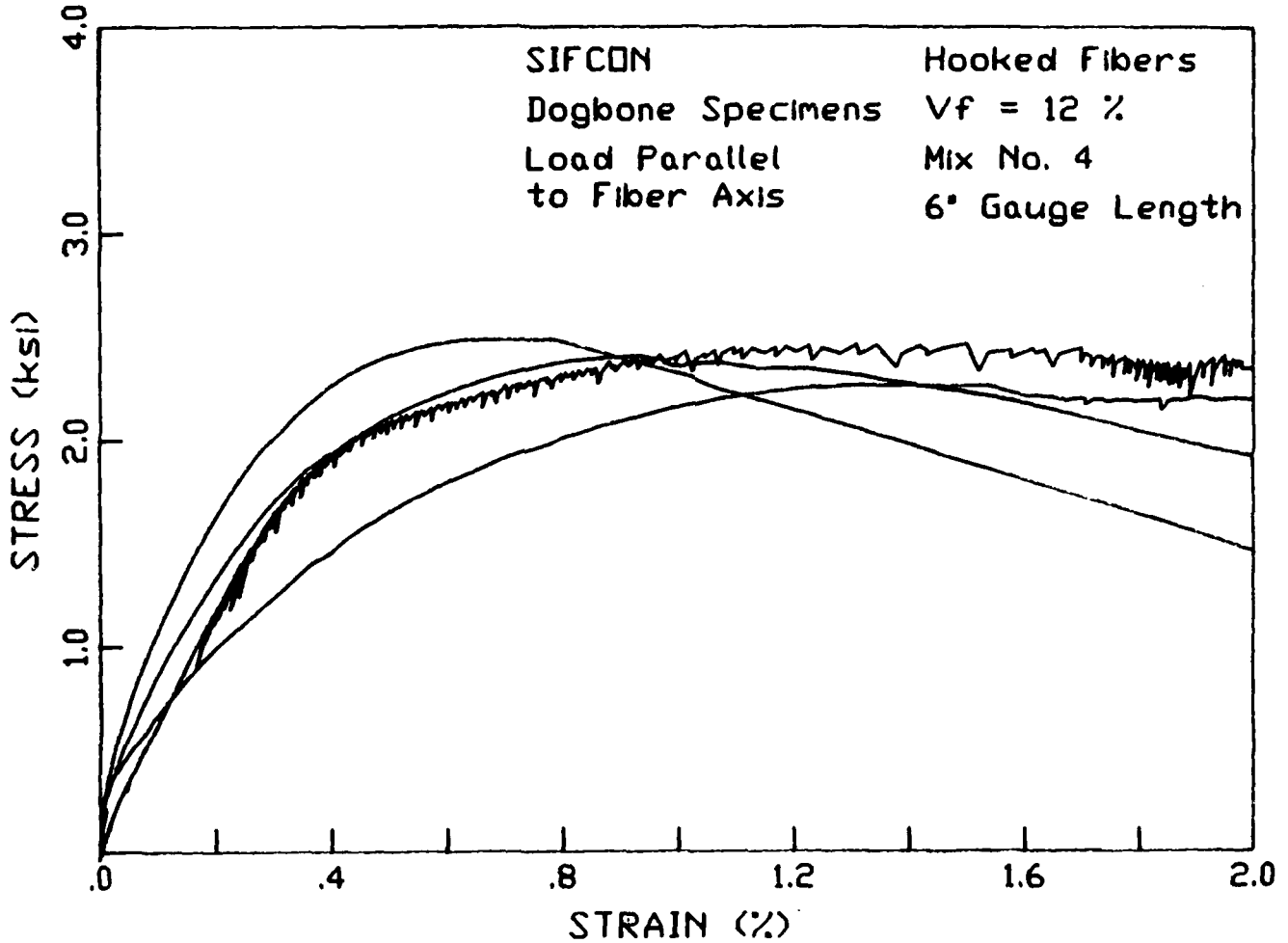

Figure 21a. Tensile stress-strain response of hooked fiber composites using Mix Four.

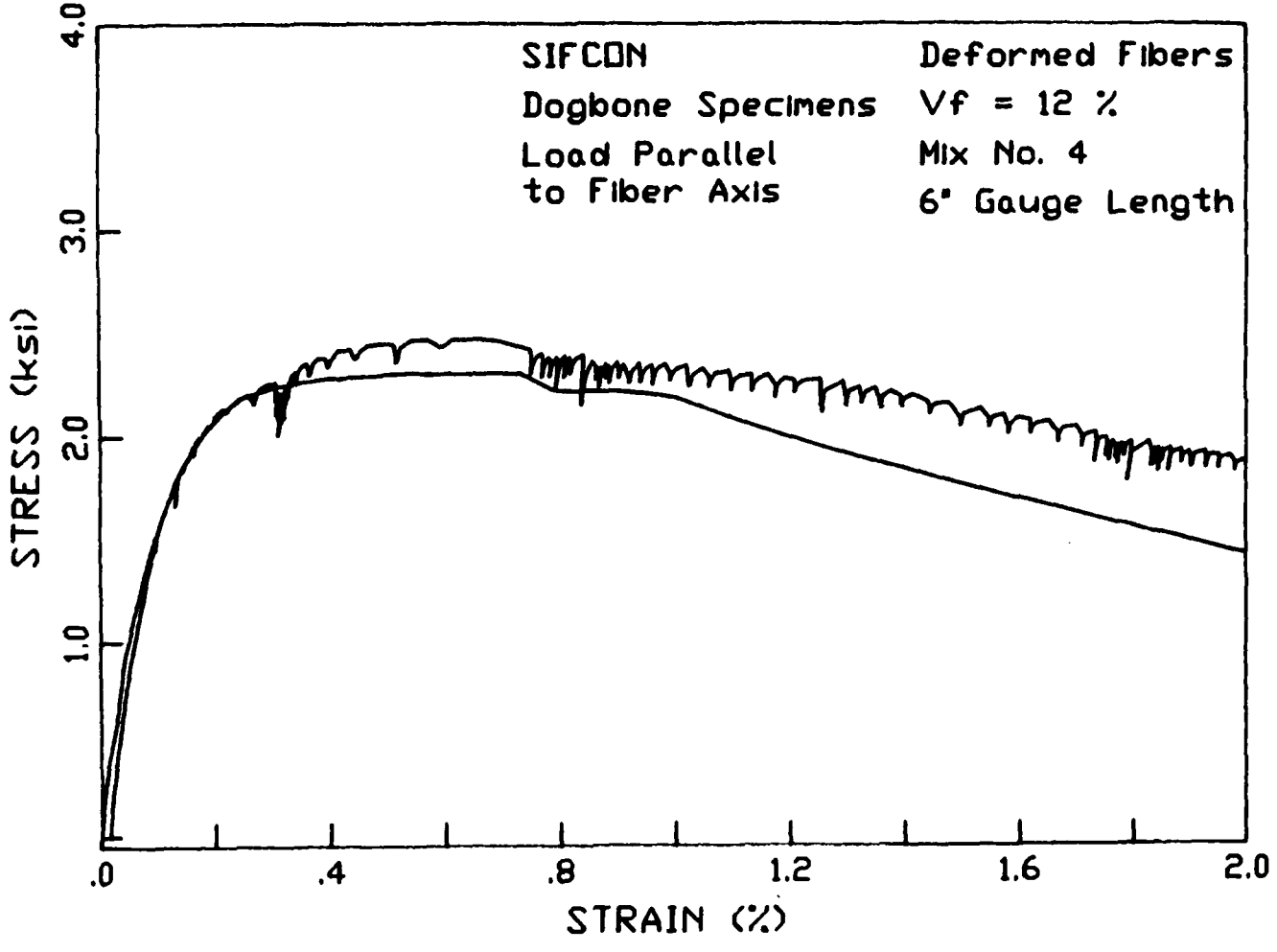

Figure 21b. Tensile stress-strain response of deformed fiber composites using Mix Four.

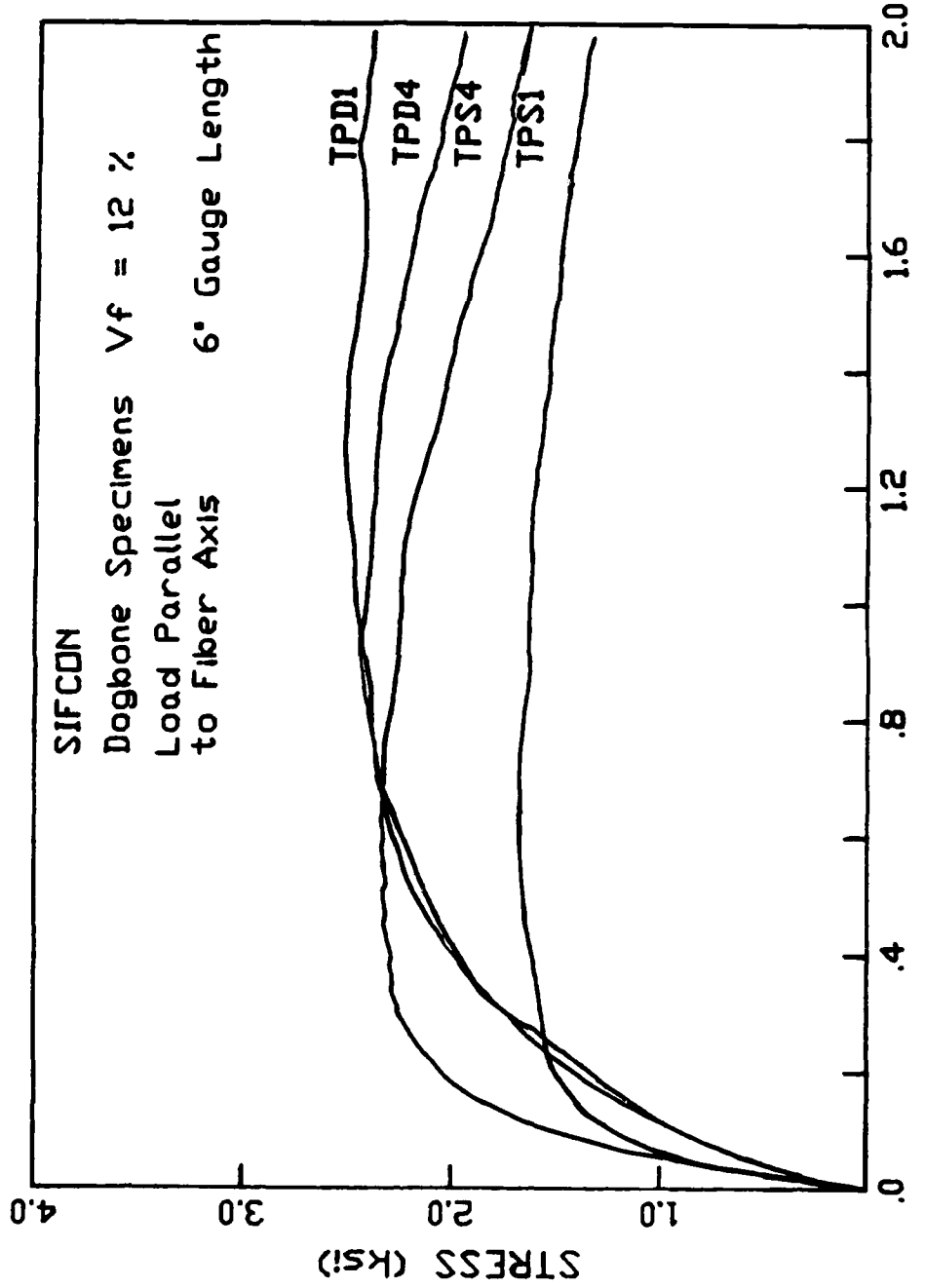

Figure 22. Typical comparison between tensile test series.

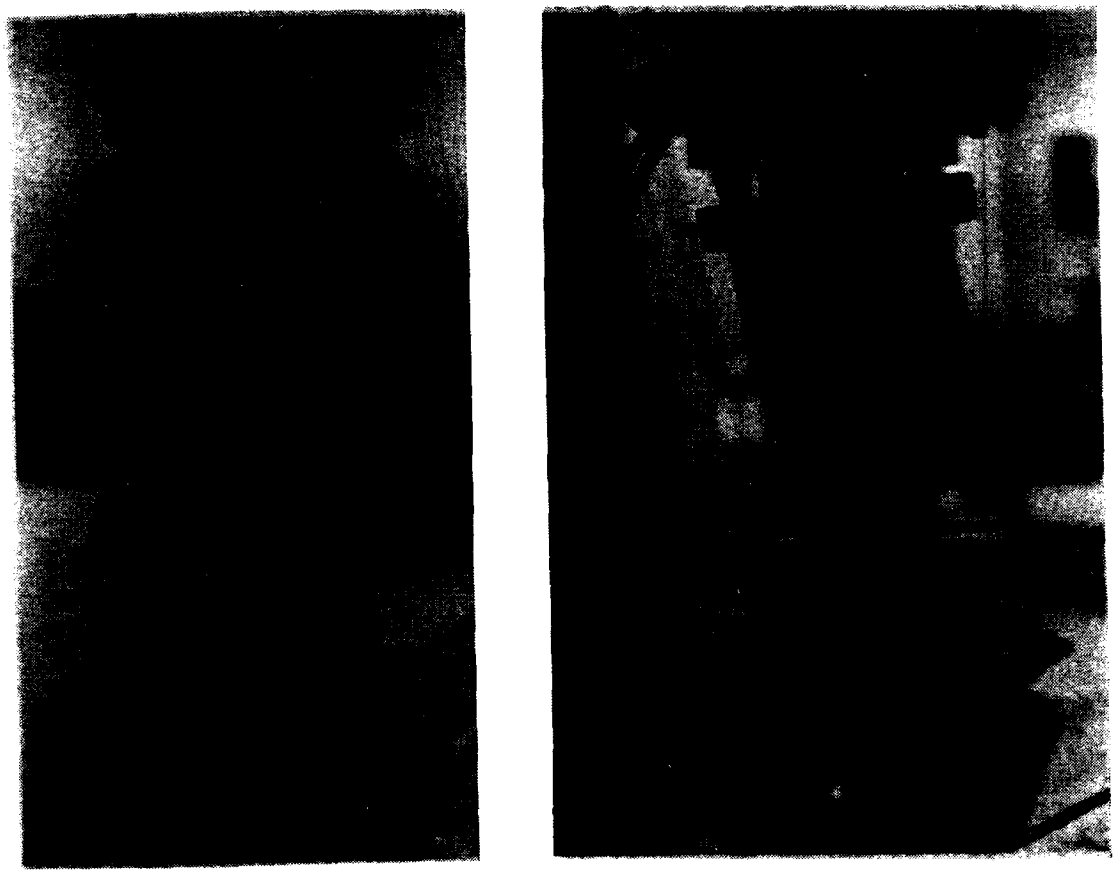

Figure 23. Tensile SIFCON specimens at failure.

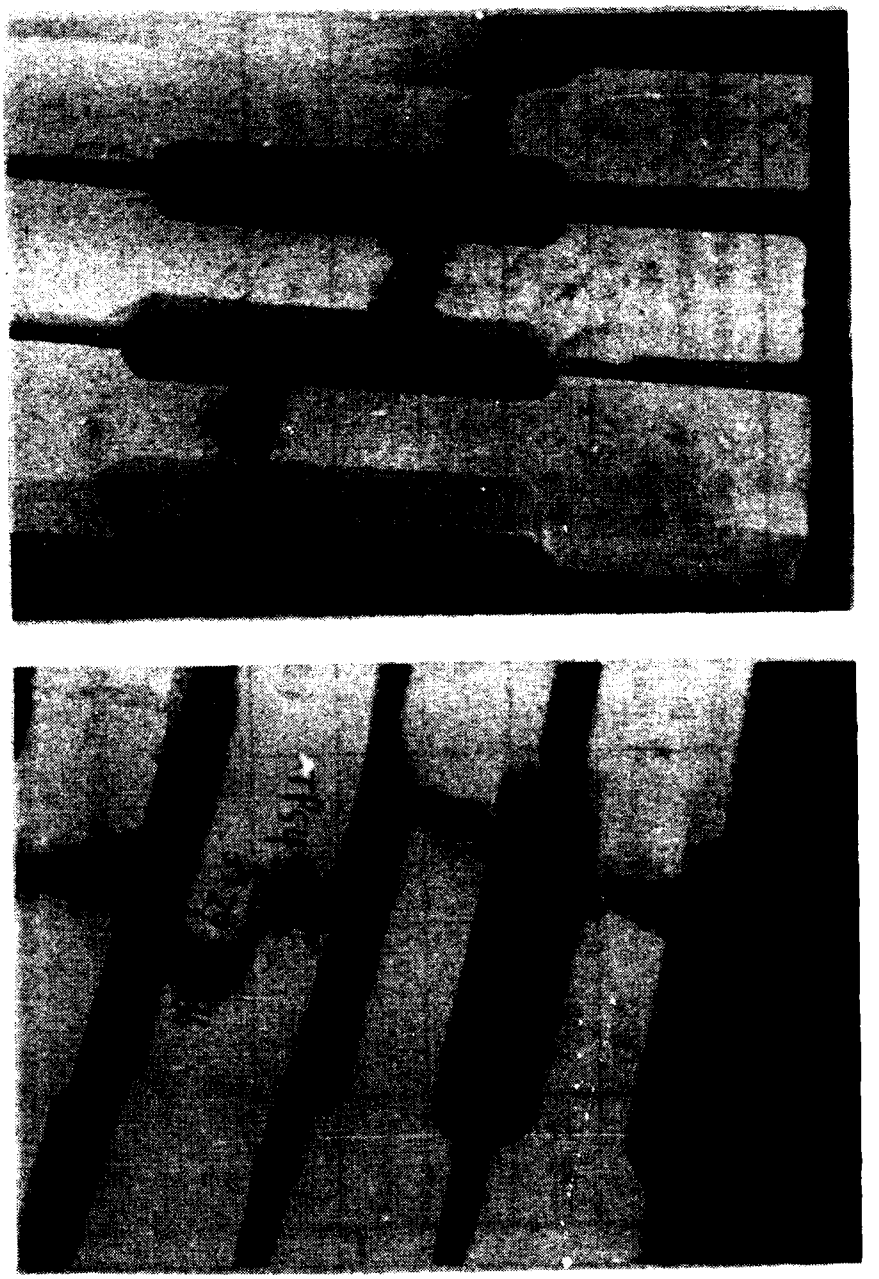

Figure 24. Typical failure cracks.

Table 6. Average tension tests results.

Series ID.	Fiber Volume (%)	Elastic Modulus[a] 10^3 (k/in^2)	Maximum Stress (k/in^2)	Strain at Maximum Stress (%)	Stress at 2% Equivalent Strain (k/in^2)	Toughness Index[b]
TPD1D	11.7	0.665	2.26	1.29	2.24	770
TPS1D	12.6	1.48	1.58	0.61	1.19	570
TPD4D	12.1	0.665	2.28	1.21	1.98	770
TPS4D	13.8	2.01	2.34	0.68	1.68	800

a Secant Modulus measured from origin to 45% of peak stress.

b Toughness Index measured as area under stress-strain/load-deflection curve of SIFCON up to 2% strain divided by area under stress-strain curve of normal strength, (5000 psi compressive strength) concrete up to peak stress.

curve, then the energy absorption capacity of SIFCON is up to three orders of magnitude greater than that of the unreinforced matrix. Table 6 presents this information in the form of a toughness index. The toughness index is defined in this report as the area under the stress-strain curve of SIFCON up to 2% strain, divided by the area under the stress-strain curve of normal strength concrete up to peak tensile stress. The toughness index of the series investigated in this study ranges from approximately 570 to 800.

2.6.3 Effect of Fiber Type

Like SIFCON in compression, failure of SIFCON in tension takes place mostly through fiber pullout, fiber-matrix debonding, and loss of fiber-to-fiber interlock. Thus, the length and geometry of the fibers used in the composite have a significant influence on the composite's stress-strain behavior. Fiber surface texture, length-to-diameter (aspect) ratio, length, and fiber shape determine the degree of fiber-to-matrix bonding, fiber interlock, and the optimum volume fraction of fibers that may be placed in the composite.

The similarity in stress-strain behavior of the fibers and matrices examined in this study was pointed out previously. However, a major difference was observed in the initial elastic modulus of the composites. Specimens made with deformed (Surecrete) fibers showed an elastic modulus more than twice the elastic modulus of specimens made using hooked (Dramix) fibers (Table 6). Specimens made with Mix One and deformed fibers yielded an average elastic modulus of 1.48×10^3 k/in^2 (10,200 MPa). Specimens made with Mix Four and deformed fibers yielded an average elastic modulus of 2.01×10^3 k/in^2 (13,860 MPa); while specimens made with Mix One or Four and hooked fibers yielded an average elastic modulus of only 0.66×10^3 k/in^2 (4550 MPa). Two things may be responsible for this behavior. First, the smooth surface of the Dramix fibers may not restrain internal shrinkage cracking as well as the deformed surface of the Surecrete fibers. This leads to greater internal cracking and a material with lower stiffness. Second, because of their surface texture, Surecrete fibers may have a better matrix-to-fiber and fiber-to-fiber bond than the Dramix fibers and result in a stiffer composite at small strains.

2.6.4 Comparison Between Tensile and Compressive Response

Figures 25 and 26 show typical comparisons of the stress-strain response of SIFCON composites in tension and compression. For the compression tests two curves are plotted, one corresponding to the case where the fibers are normal to the loading axis and the other where the fibers are parallel to the loading axis. Like SIFCON in compression, specimens made with Dramix and Surecrete fibers had very similar stress-strain responses. The ultimate strengths obtained with the two types of fibers were close, as was the overall shape of the stress-strain curves. This may imply that many of the variables responsible for SIFCON's stress-strain behavior in compression are also responsible for its stress-strain behavior in tension, and that a fiber's performance in compression will be indicative of its performance in tension. Unfortunately, no specimens were made using the crimped Xorex fibers of Section 1 in order to test this theory more completely. The curves of Figures 25 and 26 suggest that the tensile strength of SIFCON ranges from about 15% to 25% of the compressive strength, depending on the orientation of the fiber axis to the axis of loading.

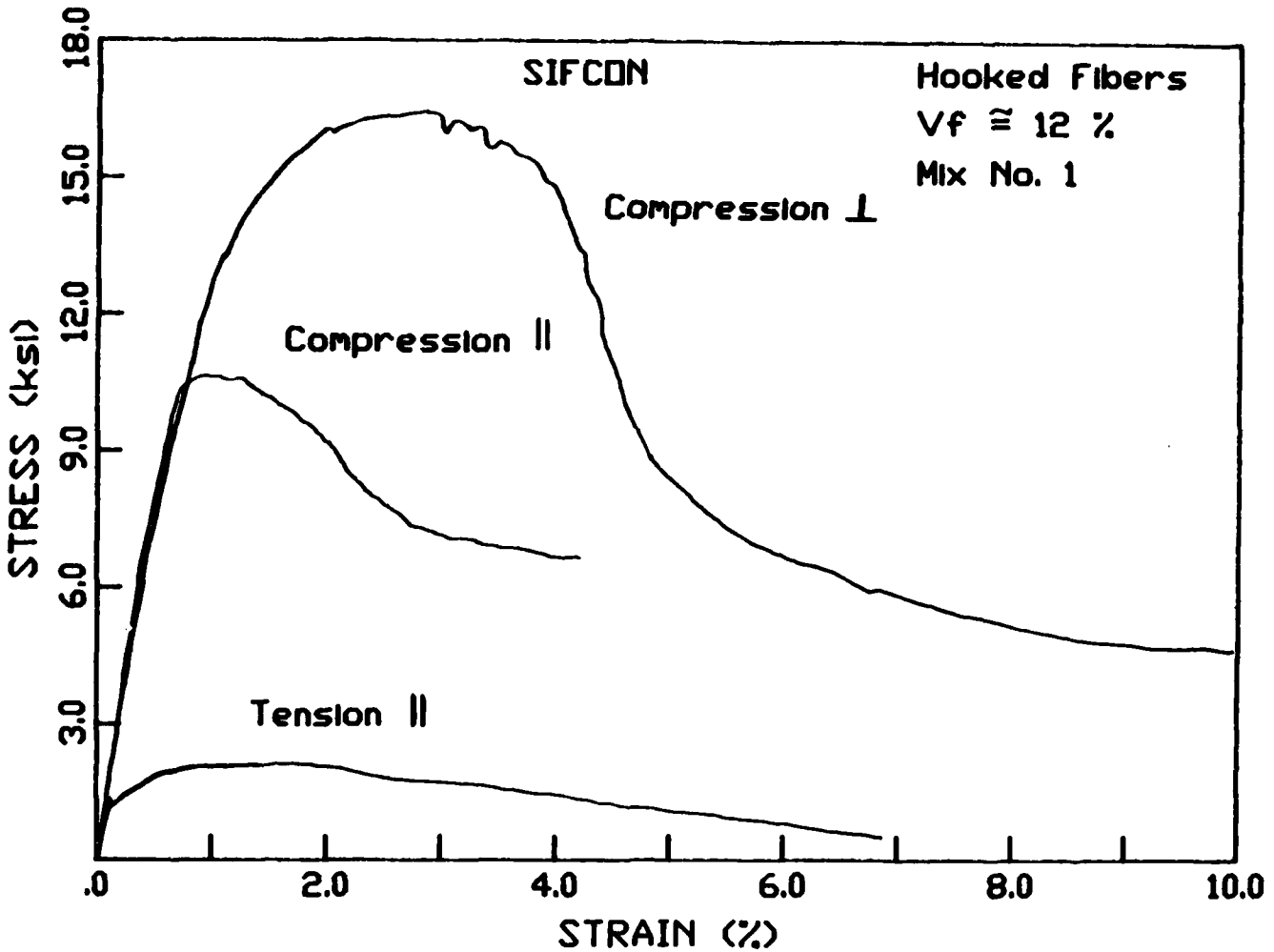

Figure 25a. Comparison between compression and tension response of SIFCON.

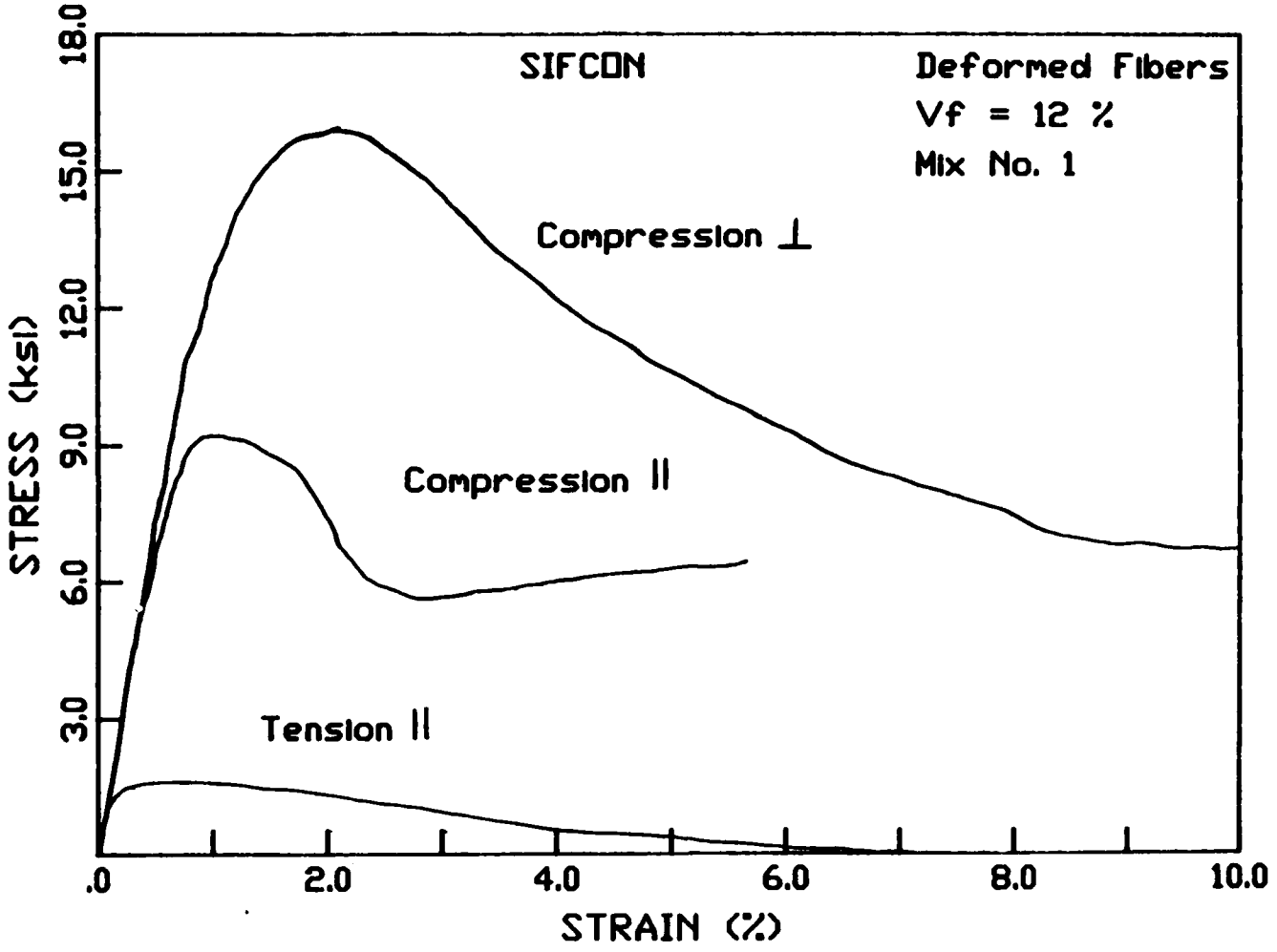

Figure 25b. Comparison between compression and tension response of SIFCON.

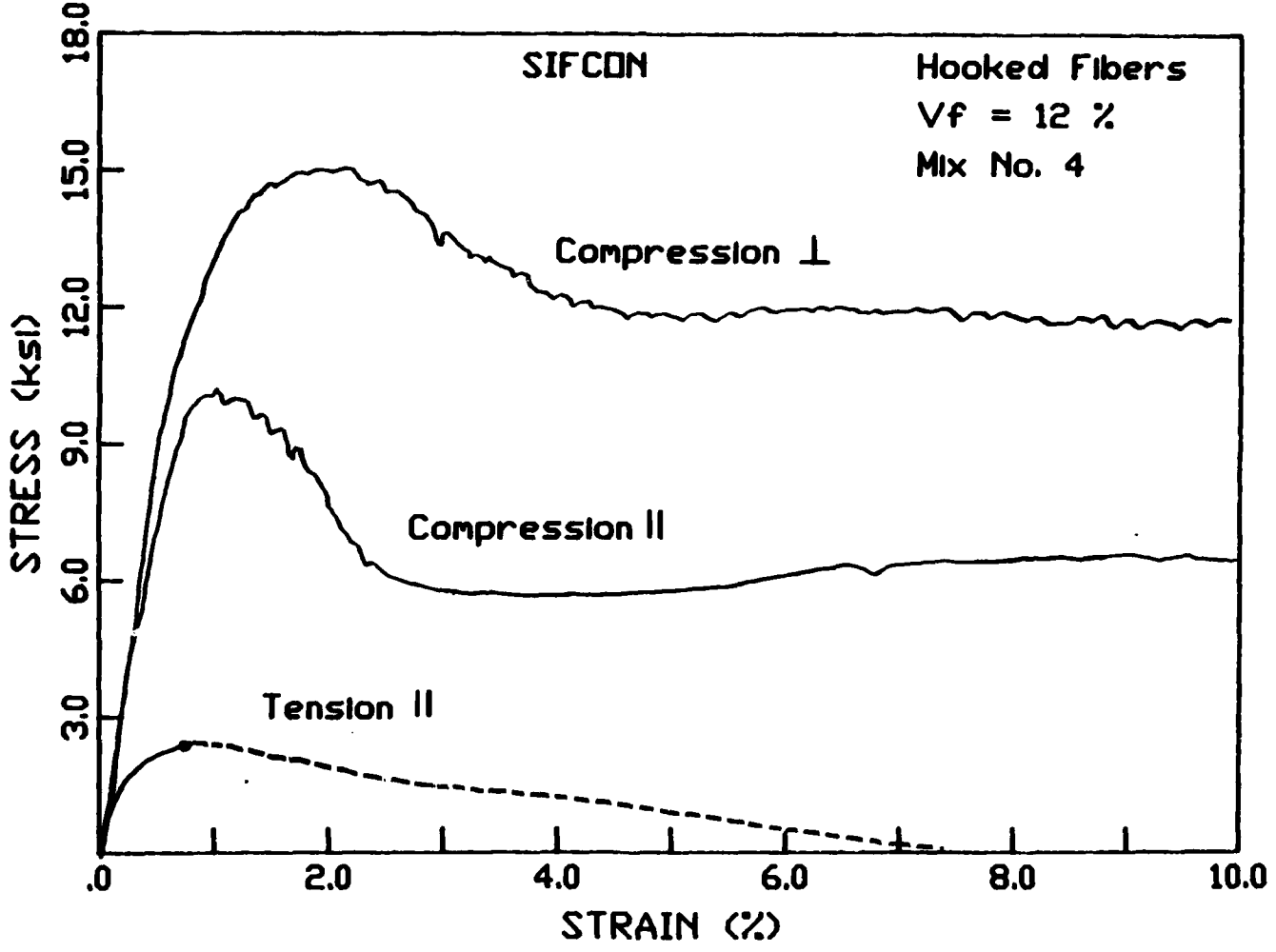

Figure 26a. Comparison between compression and tension response of SIFCON.

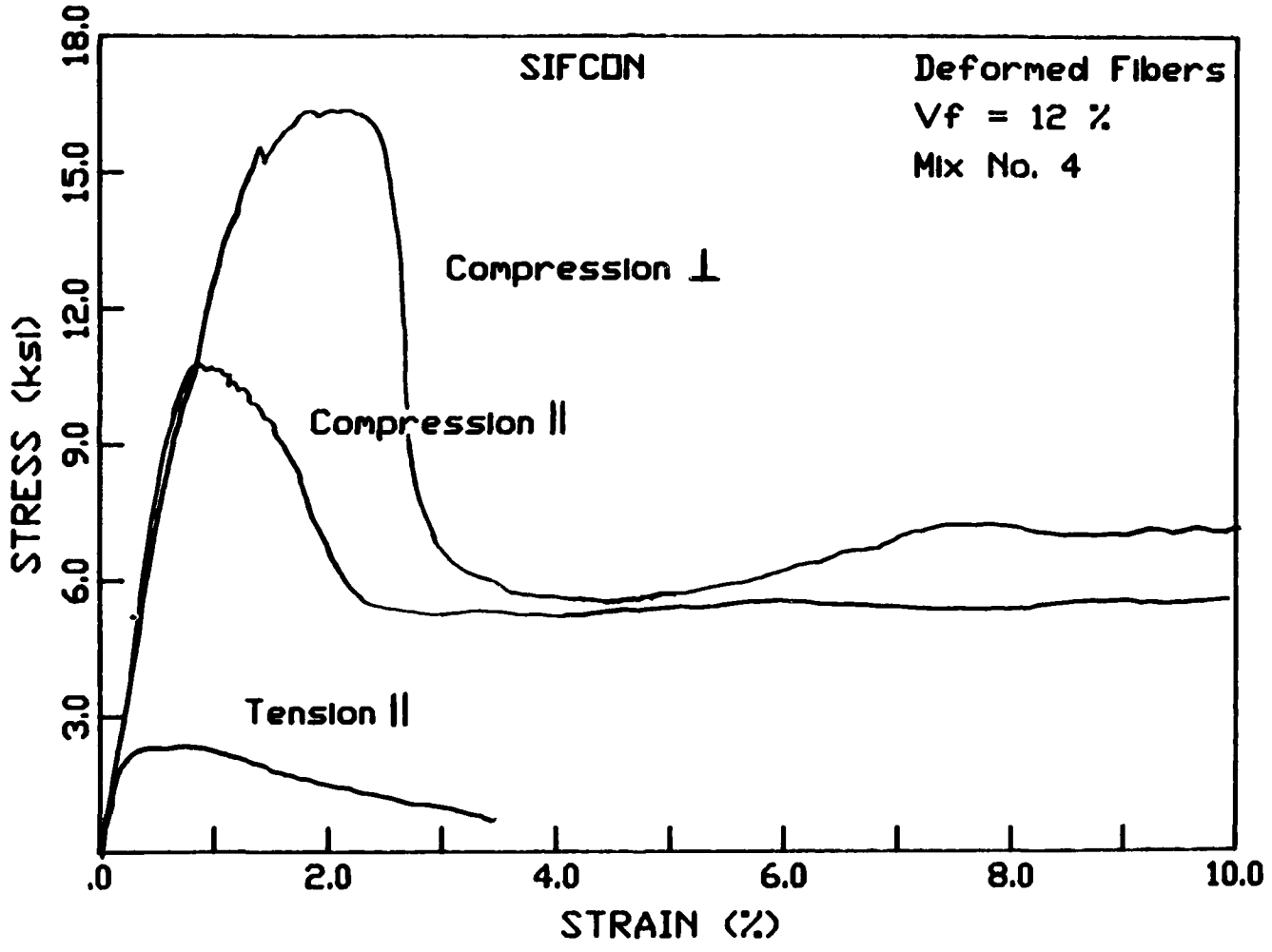

Figure 26b. Comparison between compression and tension response of SIFCON.

2.6.5 Composite Strength

Table 6 lists the average composite strengths attained in this study. Since the two matrices studied in the tests were similar in design and composition, it is not suprising that similar strengths were obtained by all specimens. Thus, no conclusions may be drawn on the issue of how matrix strengths influence the composite behavior without additional testing using other matrices. However, since the main function of the matrix in SIFCON composites in tension is to restrain fiber net movement through bond and compressive clamping action, it seems likely that the tensile strength of the composite will increase with an increase in the compressive strength of the cementitious matrix.

2.6.6 Testing Difficulties

2.6.6.1 Shrinkage Cracking. One difficulty encountered during specimen curing was that of surface shrinkage cracks. The influence of fiber edge effects made it difficult to fill the molds with the same fiber density near the top of the molds as near the bottom. Moreover, the fiber density near the surface of the molds was smaller than in the core, providing a differential restraint against shrinkage and leading to the development of tiny shrinkage cracks on the surface of the specimens. These shrinkage cracks appeared on all specimens during air curing in the laboratory environment. Because of this precracked condition, extensive specimen cracking and the development of the failure crack always appeared first in the low fiber density region of the specimens during testing.

A low water-cementitious ratio slurry and a high dosage of lignosulfonate-based superplasticizer are probably responsible for the development of cracking. Because the water-cementitious ratio is quite low, the cement particles may not be able to completely react. All available water is drawn from the surrounding matrix pore structure, resulting in differential shrinkage and cracking of the unreinforced matrix. The high dosage of superplasticizer necessary to pour SIFCON slurries may also cause a problem. All major superplasticizers increase drying shrinkage when added at high dosages. Some, such as sodium melamine sulfonate and sodium lignosulfonate, increase shrinkage even when added at a normal dosage (Ref. 11).

The cracking problem appears attributable to drying shrinkage, since cracking appears in specimens only during air curing. The extensiveness and severity of the cracking observed in test specimens suggests that this phenomenon has the potential for being a real durability problem. Further research into the problem of drying-shrinkage cracking of low water-cementitious ratio composites is desirable.

2.6.6.2 Specimen Bending. To eliminate the possibility of inducing any end moments in the specimens, the friction grips used in testing were designed with a universal joint attachment to the loading machine. This joint served the intended function but also caused unwanted specimen bending during the tensile tests. Since the fiber density near the top face of the specimens was lower, failure was always initiated on that side of the specimen. As the composite began to fail more rapidly on the weakened side, specimen bending began, and since the grips allowed freedom of specimen rotation, there was nothing in the testing system to hinder this bending.

To correct this problem in future tests, new testing grips with fixed end connections should be constructed. This will eliminate the problem of specimen bending, but will also make the requirement of perfect uniaxial specimen alignment more critical if unintentional end moments are to be avoided.

2.6.7 Stress-Strain Curve Nonlinearity

The nonlinearity of the majority of the stress-strain curves even at small fractions of the ultimate load is apparent from observation of the stress-strain curves of Figures 20-22. This nonlinear shape is due to the immediate opening of cracks and possible debonding of fibers during testing. Since the matrices involved are very strong, it is unlikely that load-induced cracking is responsible for the initial nonlinearity of the curve. The observed nonlinearity must exist due to the presence of cracks already in the matrix before testing. Cracks are probably induced by drying-shrinkage cracking as explained above.

A special series of specimens will be prepared at a future date; the specimens will be kept immersed in water until time of testing in order to check the drying shrinkage hypothesis. If correct, then the immersed specimens should show a more linear early stress-strain response than those examined in this study.

2.7. BACKGROUND AND CORRELATION

As part of a comparative study of the flexural properties of microsilica and nonmicrosilica slurry mixes, Balaguru and Kendzulak performed flexural tests on SIFCON slabs reinforced with hooked Dramix fibers made by Bekaert Wire Corporation (Ref. 1). A brief summary of their results and observations is given below along with comparisons to the results of this investigation.

Like the tensile stress-strain curve, the flexural stress-strain curve of SIFCON was nonlinear for all but a very small initial portion of the curve. This behavior was explained in terms of continuous cracking of the matrix and debonding of the fibers throughout the test duration. This explanation is similar to that for SIFCON in tension.

The flexural strength of SIFCON is about an order of magnitude higher than that of ordinary FRC. The maximum apparent flexural strength of SIFCON beams tested in Reference 1 was over 13,000 lb/in^2 with 10% fiber volume (calculated from simple homogeneous section bending theory).

Flexural specimens made with microsilica mixes showed higher flexural strength than those made without microsilica, and the increase in flexural strength was directly proportional to the increase in compressive strength of the unreinforced matrix. An increase in matrix compressive strength led to a proportional increase in composite flexural strength. Since failure in bending occurs due to a tensile failure, this implies that a proportional increase in direct tensile strength is also expected. Because there was very little variability of composite strengths examined in this study no correlation could be made with the flexural tests.

Baggott and Sarandily performed tests on high fiber volume fraction autoclaved mortars (Ref. 10). The results of their work is summarized below.

Baggott and Sarandily noted high strains at failure in their test specimens. They explained the substantial increase in strain to failure in high volume fraction composites in terms of fine-scale multiple cracking, despite the fact that they were not able to find any direct physical evidence of this cracking. Instead, they assumed that the microcracks were so small that they were able to effectively close up after testing and removal of load and thus avoid visual detection. Their observations are partly confirmed in this investigation since specimen cracks were clearly visible during testing of SIFCON specimens and the relationship to composite nonlinearity was more readily observable.

Baggott and Sarandily explain the stress-strain behavior of high-fiber-volume composites in terms of increased fiber-to-fiber contact and fiber-to-matrix bond in a model which relates well to the behavior of SIFCON. According to Baggott and Sarandily, the essential feature of high-fiber-volume composites is the existence of direct fiber-to-fiber contact within the hardened structure. The number of contact points increases with increasing fiber volume, and matrix infiltration is less effective in separating the fibers. At lower fiber volumes, the role of the cement matrix is the conventional one of transferring stress from fiber to fiber via a shear stress. At higher fiber volumes, the function of the cement matrix is to prevent any displacement of contact points by the sliding of fibers. At these higher volumes, the major stresses in the matrix are due to a "clamping" action between fibers and are compressive. Thus, although eventual matrix failure will be due to a shear/tensile process, higher loads can be supported than in the direct shear mode.

It follows that the fiber-to-matrix bond is of less importance to composite strength since there is predominantly a compressive fiber-to-matrix interfacial stress. Baggott and Sarandily also used this mechanism to explain their observation of high strengths in specimens with significant air voids. Since only sufficient matrix is required to ensure that the fiber network is locked together, the occasional air void is not harmful to composite behavior. This model would tend to support the assumption that the tensile strength of a high volume fraction fiber composite is directly related to the compressive strength of its matrix.

2.8 CONCLUSIONS

The following conclusions may be drawn from the tension tests of SIFCON specimens:

2.8.1 SIFCON possesses outstanding tensile strength. In this study, the use of slurry mixes one and four with hooked and deformed fibers led to average tensile strengths of 1.6 to 2.3 k/in^2 (11 to 16 MPa) with a maximum observed strength of 3.0 k/in^2 (21 MPa).

2.8.2 SIFCON possesses outstanding tensile ductility. SIFCON specimens are able to reliably sustain tensile stresses of about 2 k/in^2 (14 MPa) at tensile strains ranging from 1% to 2%.

2.8.3 Internal drying-shrinkage cracking of SIFCON composites may lead to a poorer

material stress-strain performance, resulting in a highly nonlinear ascending portion of the stress-strain response.

2.8.4 The early nonlinearity of SIFCON's stress-strain response is less pronounced with deformed fibers than with hooked fibers. This is probably the result of better fiber-to-matrix and fiber-to-fiber bonding with deformed fibers at small strains.

2.8.5 SIFCON composites exhibit multiple tensile cracking at low and intermediate load levels. Final failure occurs through the opening of a single large tensile crack.

2.8.6 Compared to plain slurry, the toughness index of SIFCON in tension evaluated at 2% strain can exceed 1000.

3.0 Stress-Displacement Properties of SIFCON in Tension

3.1 INTRODUCTION

To date most studies of SIFCON have dealt with its compressive behavior [see references in Section 1], and although flexural tests have been performed, no report of uniaxial tensile response or tensile stress-displacement response of SIFCON is known to the writers of this report. However, the high volume fraction of fibers would seem to predict impressive postcracking preformance in tension.

The postcracking response of SIFCON in direct uniaxial tension will be controlled by many of the same factors that control the response of conventional fiber-reinforced concrete (FRC) in tension since the failure of both materials involves the pullout of fibers from a cementitious matrix. However, the materials will differ in many other respects and in the parameters affecting fiber pullout. Primarily, the materials may differ in matrix composition and fiber volume fraction. The fibers in conventional FRC are subjected to frictional contact with large aggregate particles, while SIFCON fibers must be embedded in a fine slurry and are subject to contact with other fibers. The high volume fraction of fibers in SIFCON also modifies the parameters controlling postcracking response. From a behavioral viewpoint, fibers in SIFCON are subjected to frictional and mechanical interlock between fibers, in addition to the usual bond with the matrix. In SIFCON the matrix plays the role, not only of transferring forces between fibers by shear (as in FRC), but also of acting as a bearing to keep the fibers interlocked. In SIFCON composites, there is a large amount of fiber-to-fiber interference which is not important to the study of FRC.

3.2 OBJECTIVE AND SCOPE

The main objective of this chapter is to qualitatively and quantitatively describe the stress-crack opening response of high strength, slurry infiltrated fiber concrete (SIFCON) in direct uniaxial tension. In particular, this chapter examines the effects of two important parameters: (1) fiber type where length, aspect ratio, surface characteristics, and overall fiber geometry vary, and (2) matrix strength. This research should provide a better understanding of the mechanisms of fiber reinforcement in SIFCON and the variables that control its tensile strength, stress-displacent response, and toughness.

The complete study includes an experimental phase and an analytical phase. This section describes the experimental investigation.

3.3 EXPERIMENTAL PROGRAM

The experimental program consists of uniaxial tensile tests on 18-in (457-mm) rectangular prism specimens with notched midspan section having a 2.5x2.5-in (64x64-mm) testing area. Four specimens were poured and tested for each of the nine series investigated. Three fiber types (Dramix, Surecrete, and Xorex II of Table 1), and for each fiber type three slurry mixes (Mix One, Mix Two, and Mix Three of Table 2) are investigated. The program is summarized in Figure 27. Complete information about mix compositions and fiber properties are available in Section 1 (Ref. 9). Data from the tests were collected, processed, and analyzed to produce stress-displacement relationships and to allow rational comparisons between the various parameters under study.

3.4 SPECIMEN PREPARATION

3.4.1 Molds

Rectangular Plexiglas molds were especially built for the tensile specimens. The molds assemble and disassemble easily to facilitate specimen removal, mold cleaning, and surface oiling.

3.4.2 Mixing, Pouring, and Curing

The procedures for fiber placement, slurry mixing, pouring, and specimen curing were the same as those described for the compression specimens in Section 1.5. The fibers were hand distributed into the molds which were placed on a vibrating table and subjected to light vibration. The fibers were aligned randomly in a two-dimensional mat along the longitudinal (testing) axis of the specimens. Specimens were poured, removed from their molds after 24 h, cured in water for 1 wk, then cured in the laboratory environment for about 5 mo at approximately 70 °F (21 °C). Prior to testing, a diamond saw was used to cut a 1/4-in notch around the midlength of the specimens. The notched specimens were then tested in uniaxial tension at an age of 5 mo.

3.5 TESTING

3.5.1 Tensile Test Setup

After notching and curing, the specimens were tested in uniaxial tension. A schematic representation of the test setup for the notched tensile specimens is shown in Figure 28. Figure 29 shows a specimen with jaw grips attached to the specimen by threaded bolts, and Figure 30 shows the specimen in the loading machine prior to testing. Two LVDTs were placed on opposite sides of the specimen at a predetermined gauge spacing of 1.5-in. The

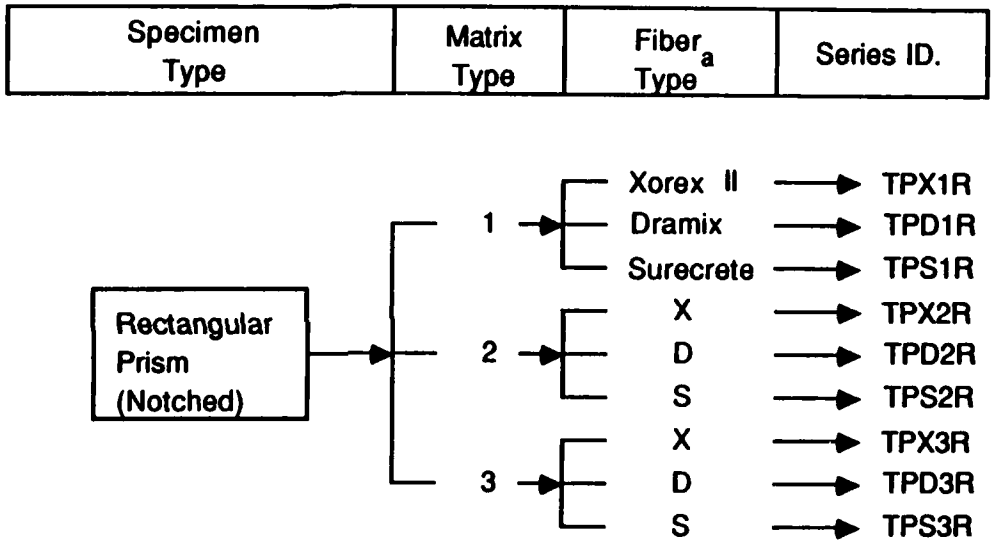

a Xorex = Crimped
Dramix = Hooked
Surecrete = Deformed

Figure 27. Experimental program stress-crack displacement.

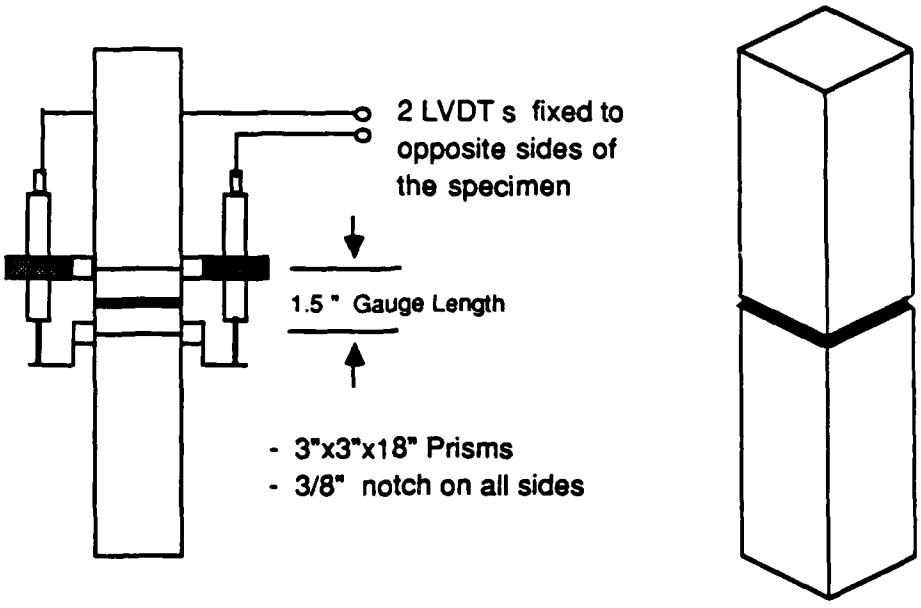

Test Setup - Notched Rectangular Prism Specimens

Figure 28. Tensile setup.

signals from each LVDT were conditioned, averaged, and recorded by an A/D converter as specimen deformation data. The load signal was taken directly from the Instron control computer.

The tension tests were run using stroke control. A stroke rate of 0.001 in/s was used during the initial ascending branch of the stress-elongation curve up to the point of maximum stress. The stroke rate was reduced to 0.0001 in/s to record the descending branch of the stress-elongation curve. The large stiffness of the grips relative to that of the specimens and the slow testing rate helped to virtually eliminate the influence of machine strain energy release on the ductile descending branch of the stress-elongation curve.

3.5.2 Instrumentation, Data Collection, and Processing

The testing system consisted of a computer controlled, closed loop, servohydraulic universal testing machine (Instron System 8000), tensile friction grips, and a high-speed data acquisition system. The friction grips are shown schematically in Figure 31. The grips consisted of rigid, self-clamping steel plates and a rigid connection to the loading machine

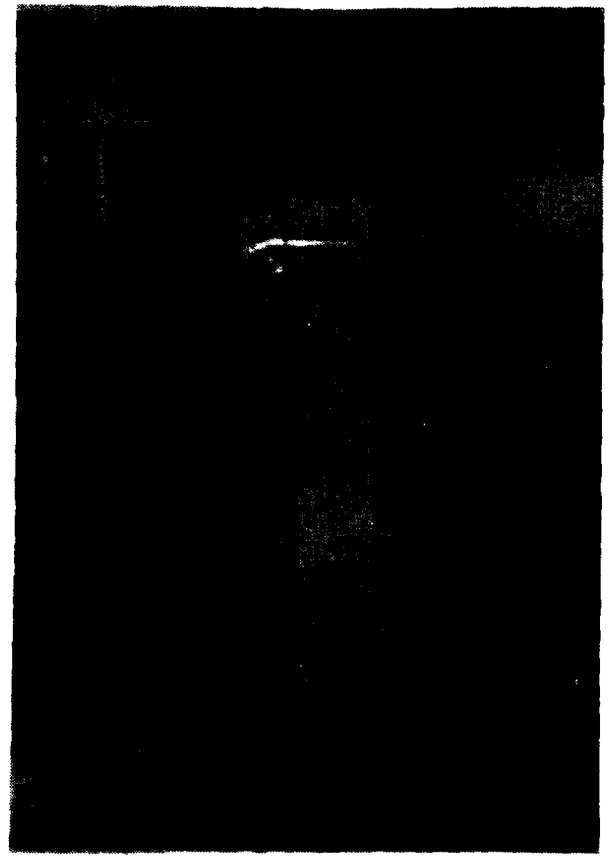

Figure 29. Tensile specimen with attached grips.

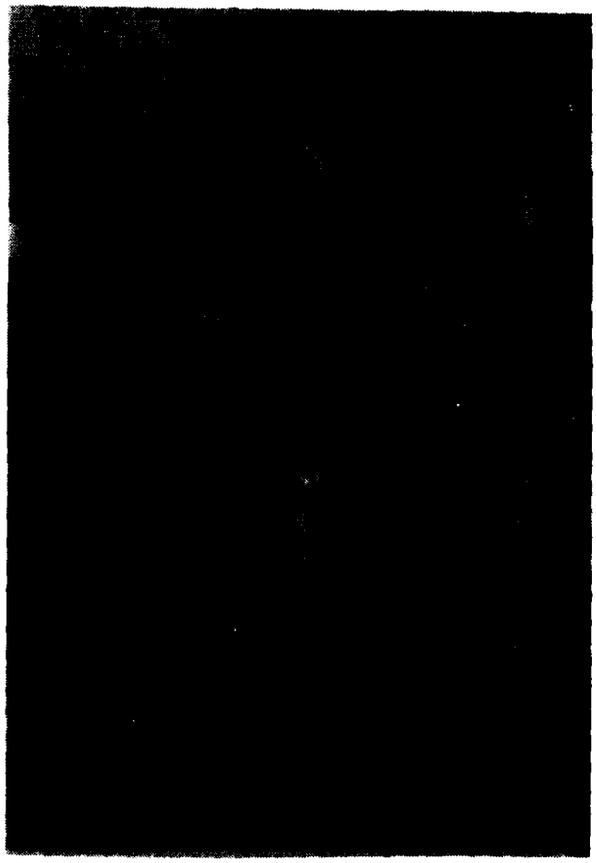

Figure 30. Specimen in loading machine.

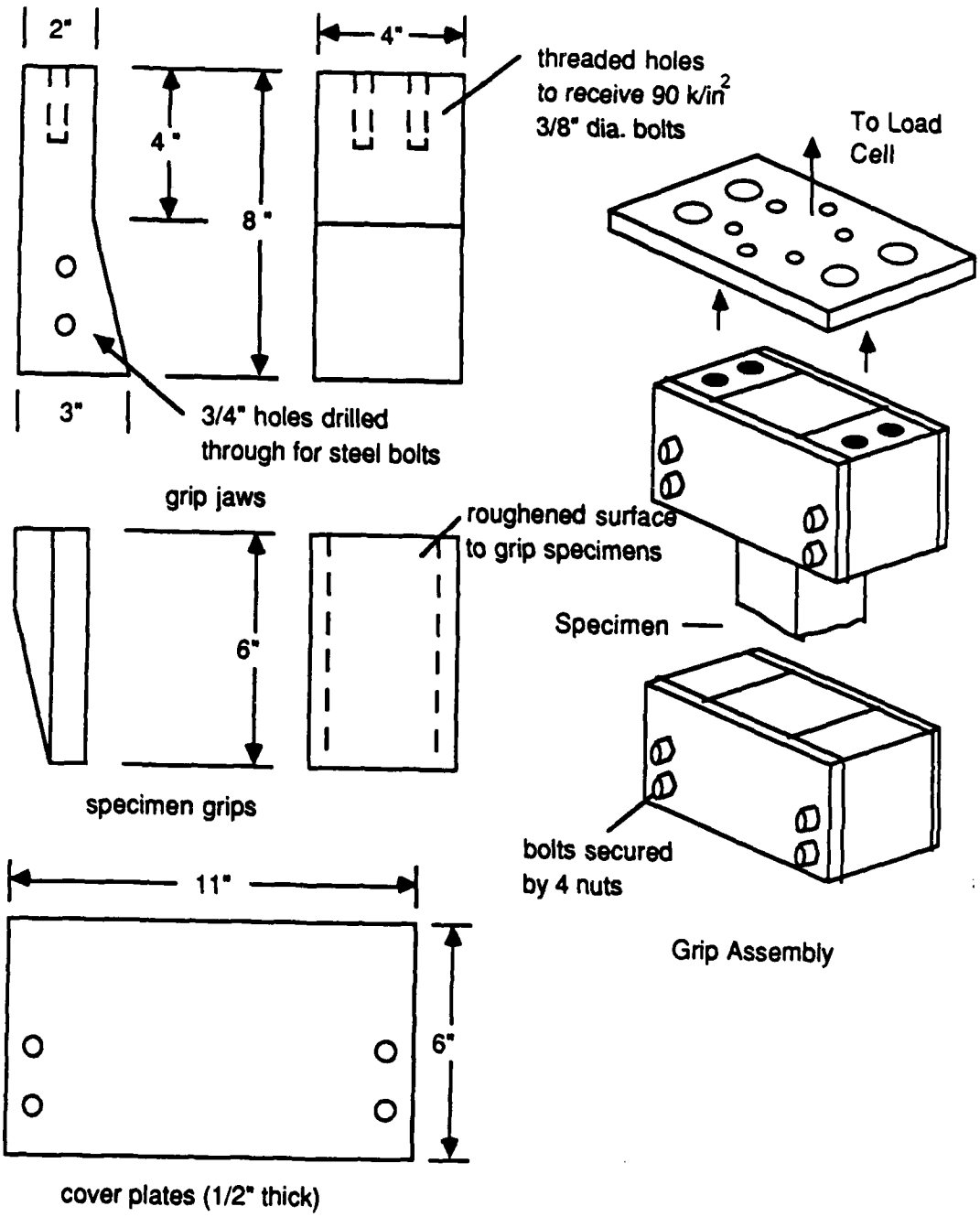

Figure 31. Tension grips.

which prevented any specimen bending or out-of-plane crack development during testing. Specimen bending had been a problem with previous tensile specimens (see Section 2). During the tests, load and deformation data were recorded and stored by the data acquisition system and later processed for analysis. The data collection and processing procedures are described in detail in Section 1 (Ref. 9).

3.6 RESULTS, DISCUSSION, AND ANALYSIS

In spite of the peripheral notch which reduced the cross-sectional area of the specimens by 30%, a significant number of tensile specimens were lost due to failure outside of the notched testing zone. Some digital data were also lost due to problems with the data acquistion system (the X-Y recorder plots were saved, however). Despite these difficulties, the tested specimens did yield useful and interesting data which is analyzed in this chapter.

3.6.1 Stress-Elongation Response

Figures 32a through 32f show the tensile stress-elongation curves of the specimens tested in this study. Figures 33a through 33f show the stress-crack displacement curves of the tested specimens and are plotted from the point of maximum stress to the point of complete separation of specimen halves. Finally, Figures 34a through 34f show the initial stress-strain response of tested specimens up to 1.5% strain. In these figures, the strain was obtained by dividing the elongation by a gauge length of 1.5 in. The stress was obtained from the load divided by the area of the notched section (6.25 in).

Examination of Figures 32a through 32f illustrates typical specimen response. The ascending branch, which yields a stress-strain response, is briefly linear prior to matrix cracking (Figures 33a through 33f). After matrix cracking, linearity is gradually lost as the peak load is approached. This stage corresponds to the development of multiple cracking. Finally the failure crack opens and the stress-strain response is lost as the curve becomes a respresentation of stress versus crack-opening displacement (Figures 34a through 34f).

Several interesting points may be noted about the shape of the stress-elongation curve. The ascending branch is nonlinear after matrix cracking and levels off to the peak stress. As the failure crack opens, microcracks in the testing zone tend to close, the curve levels off and reaches a peak stress. The failure crack then opens in a gradual debonding process in which fibers pull out of the cementitious matrix and become disentangled from each other and the surrounding matrix. In the descending branch, the shape of the stress-displacement curve is very similar to the descending branch of the compressive stress-strain curve. This is unlike conventional fiber-reinforced concrete where the stress follows an exponentially decaying curve and the drop in stress is abrupt, not a gradual decline. Like ordinary fiber-reinforced concrete, the stress descends to zero when crack separation reaches approximately half of the fiber length (about 0.5 in in this case). A comparison of tensile stress-elongation response of SIFCON and ordinary fiber reinforced concrete is given in Figure 35. With ordinary fiber-reinforced concrete, the cracking of the cementitious matrix is signaled by an abrupt change in the stress-strain curve where the volume fraction of fibers is below 2%. With SIFCON, the stress-elongation response shows a more gradual change and also exhibits

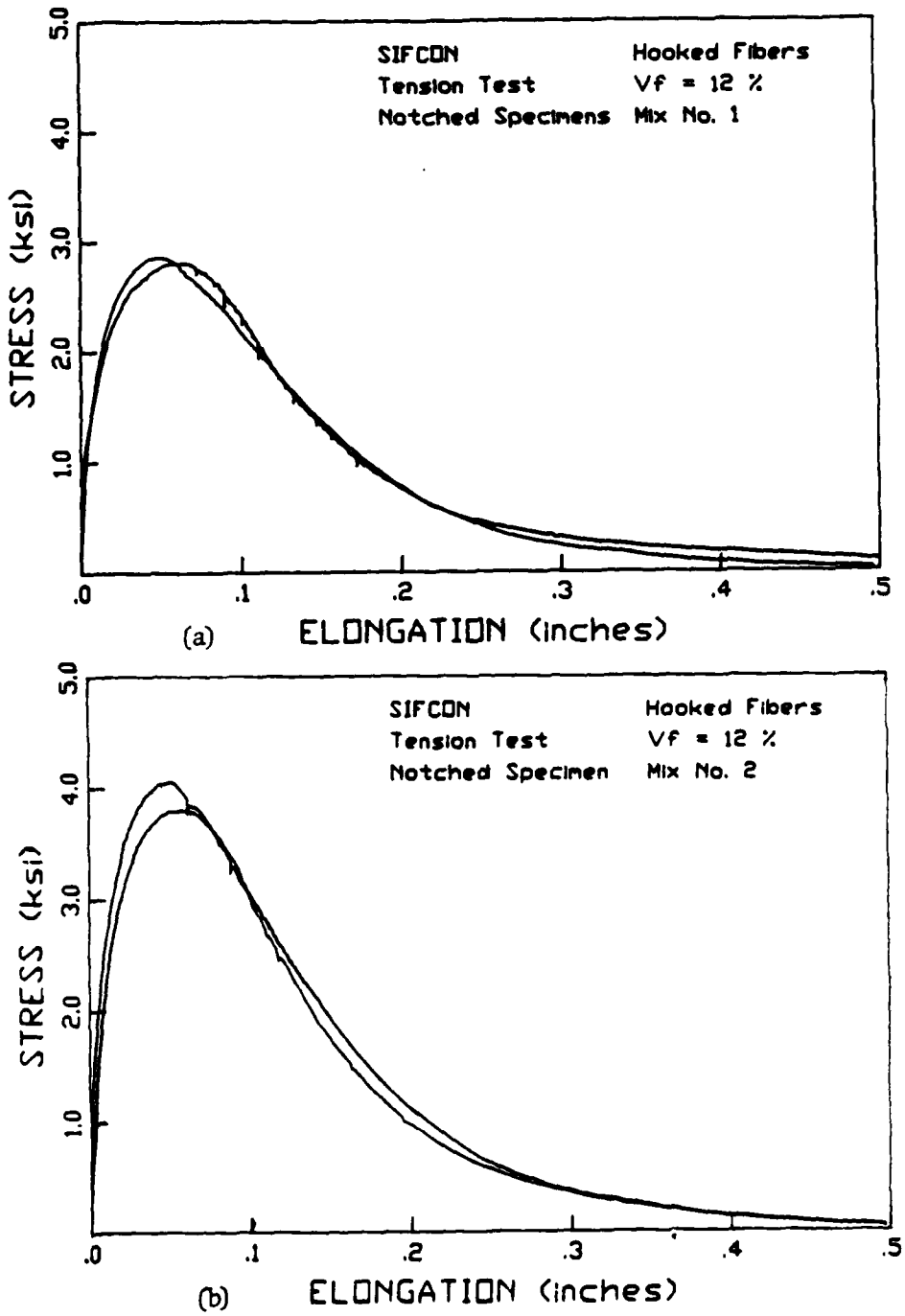

Figure 32. Stress-elongation response.
a. Hooked fibers. Mix One.
b. Hooked fibers. Mix Two.

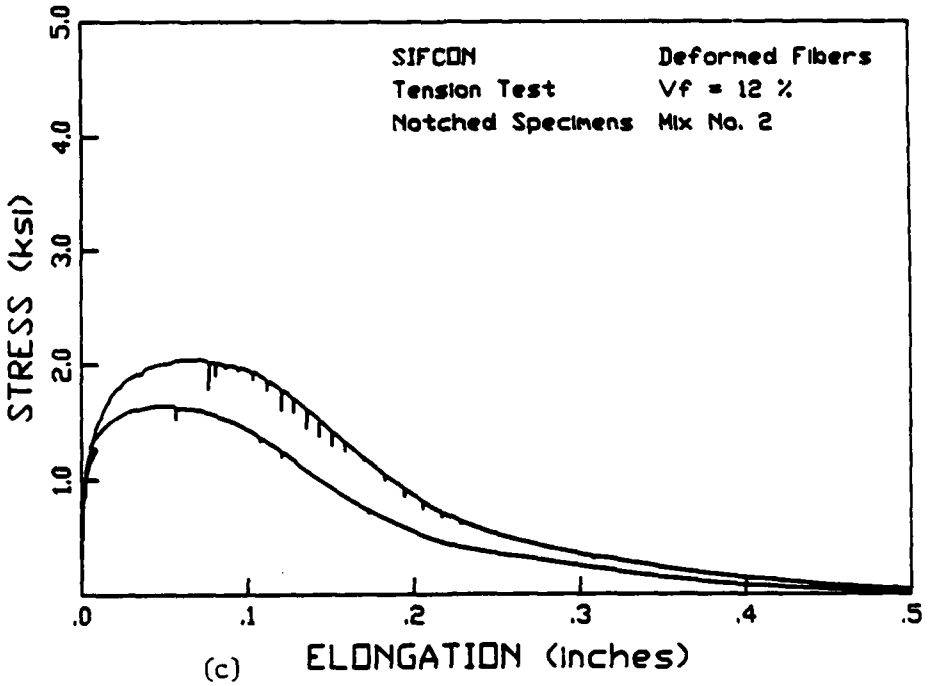

(c)

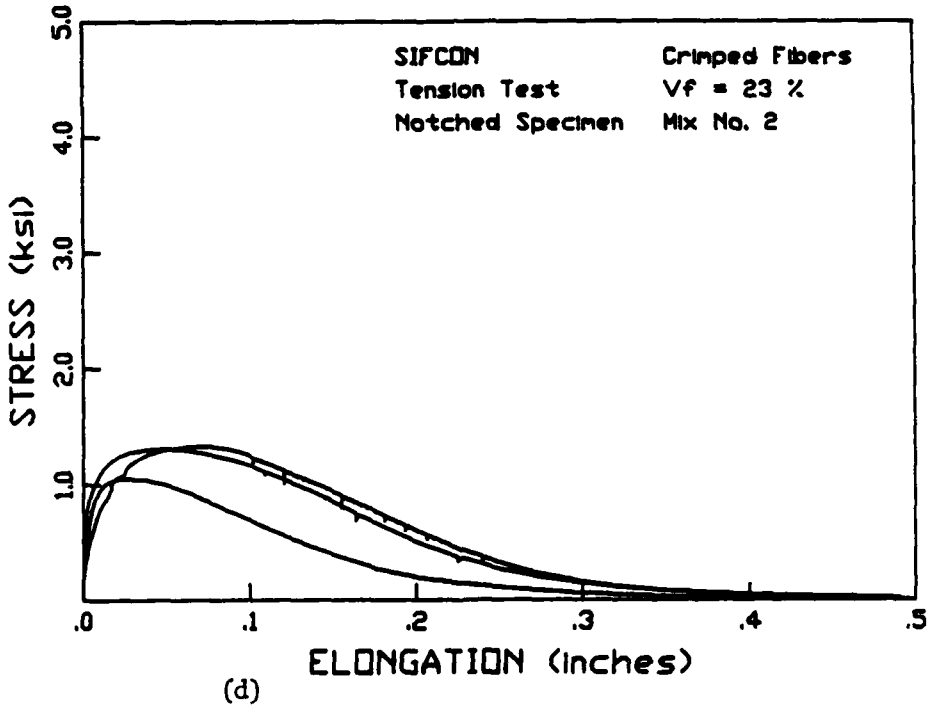

(d)

Figure 32. Stress-elongation response
c. Deformed fibers. Mix Two.
d. Crimped fibers. Mix Two.

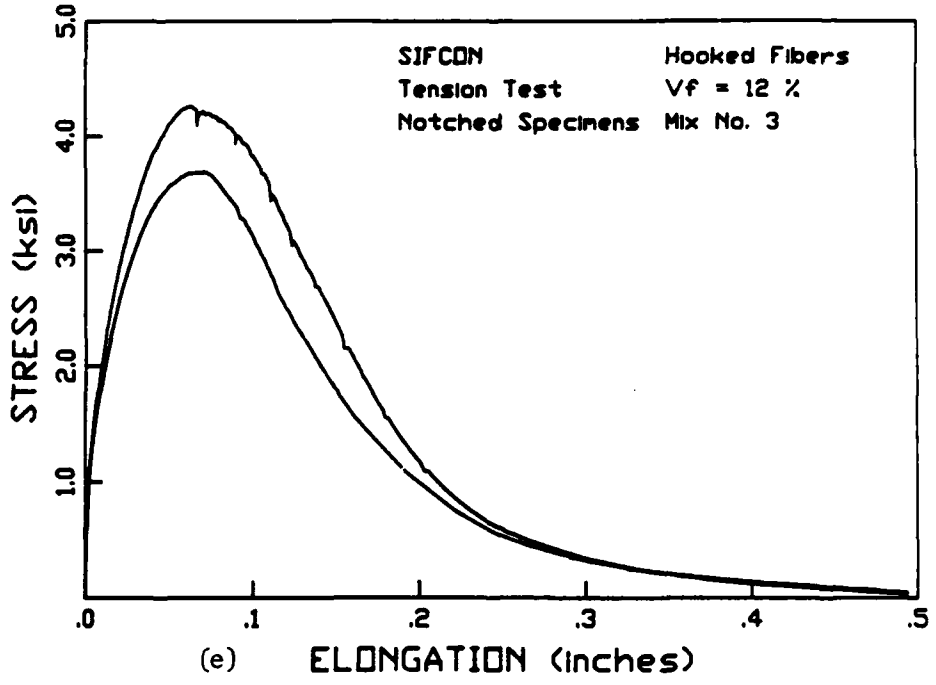

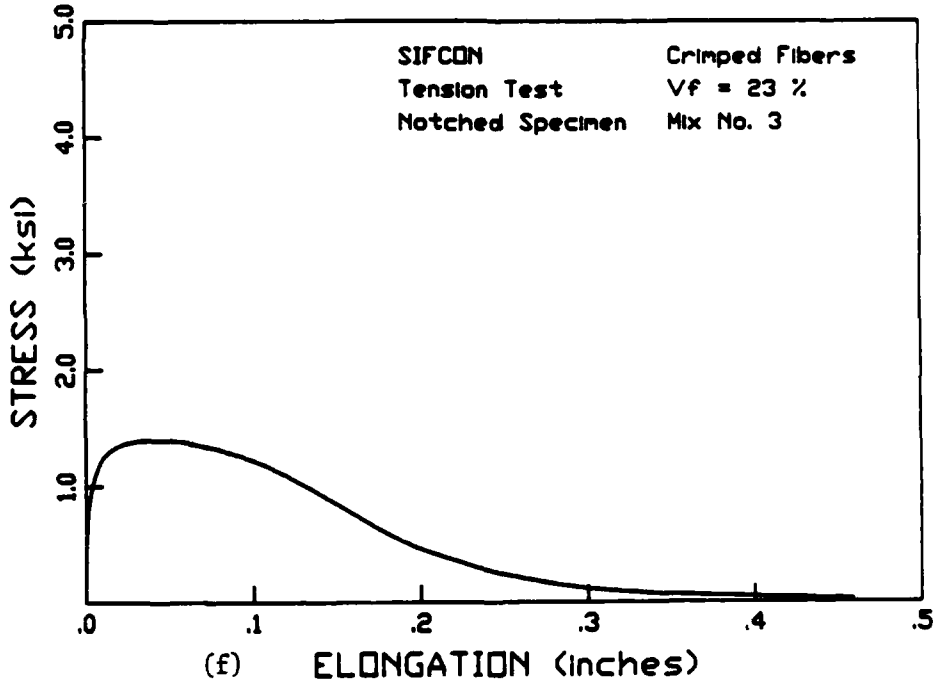

Figure 32. Stress-elongation response
e. Hooked fibers. Mix Three.
f. Crimped fibers. Mix Three.

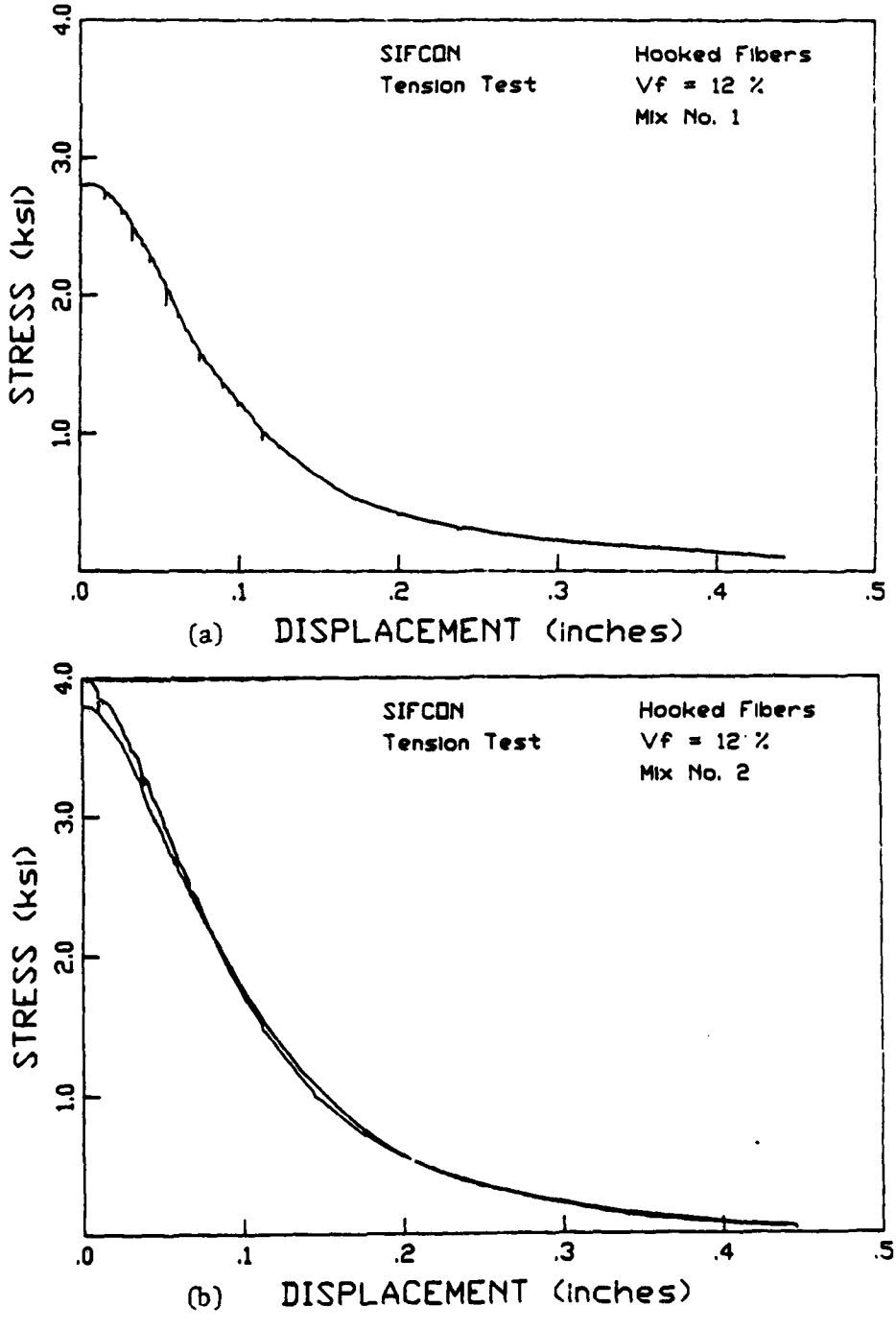

Figure 33. Stress-displacement response.
a. Hooked fibers. Mix One.
b. Hooked fibers. Mix Two.

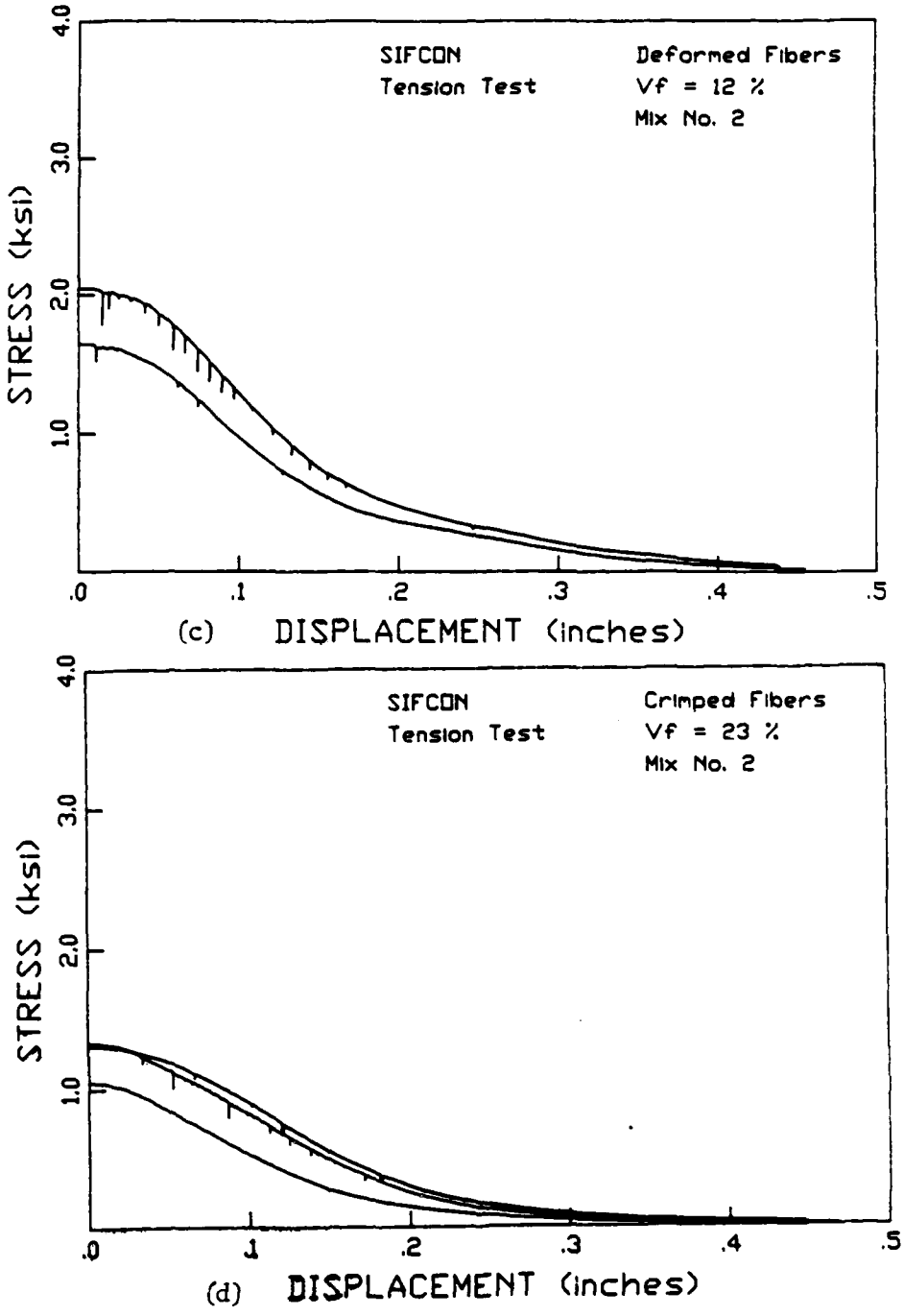

Figure 33. Stress-displacement response
c. Deformed fibers. Mix Two.
d. Crimped fibers. Mix Two.

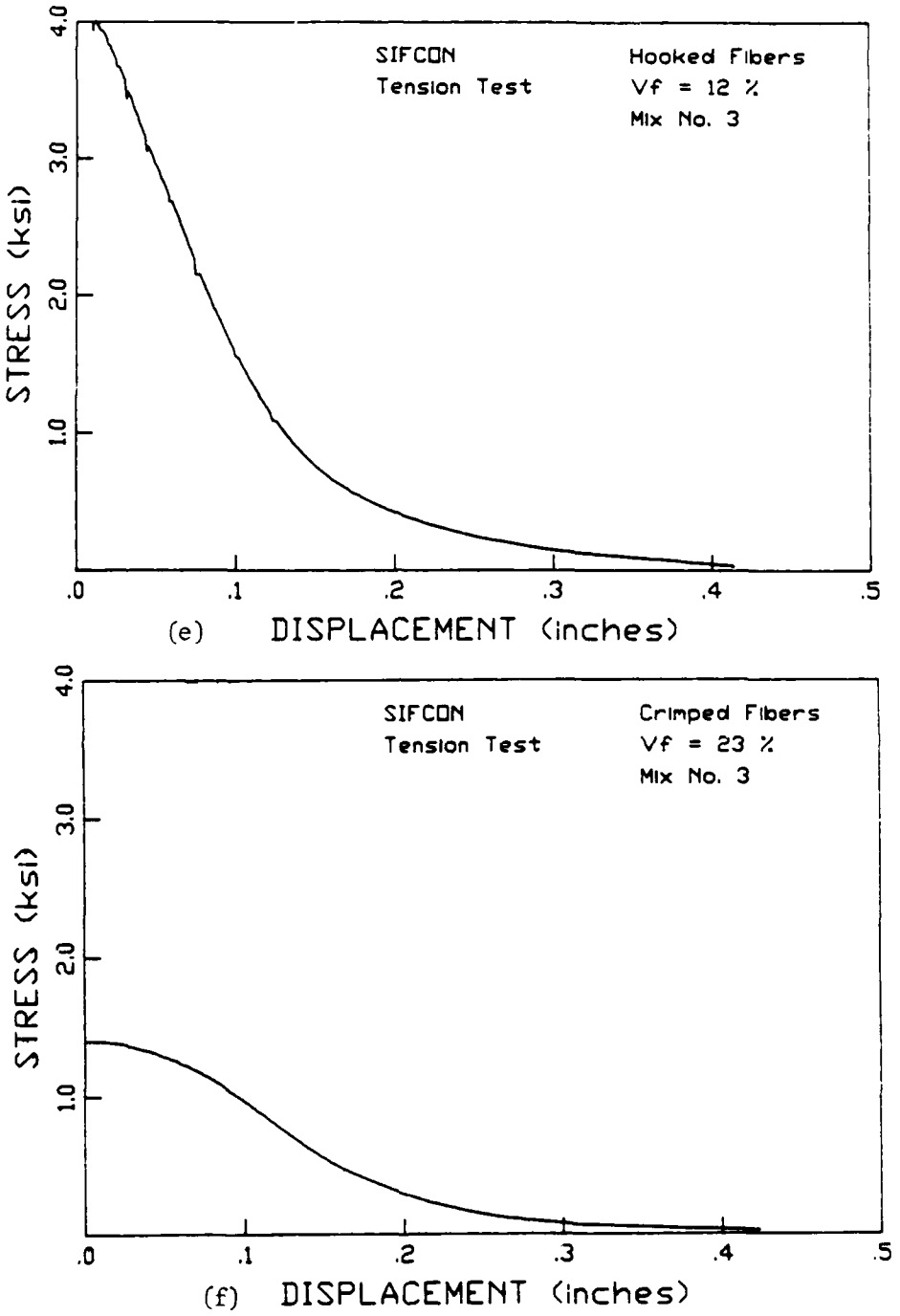

Figure 33. Stress-displacement response
e. Hooked fibers. Mix Three.
f. Crimped fibers. Mix Three.

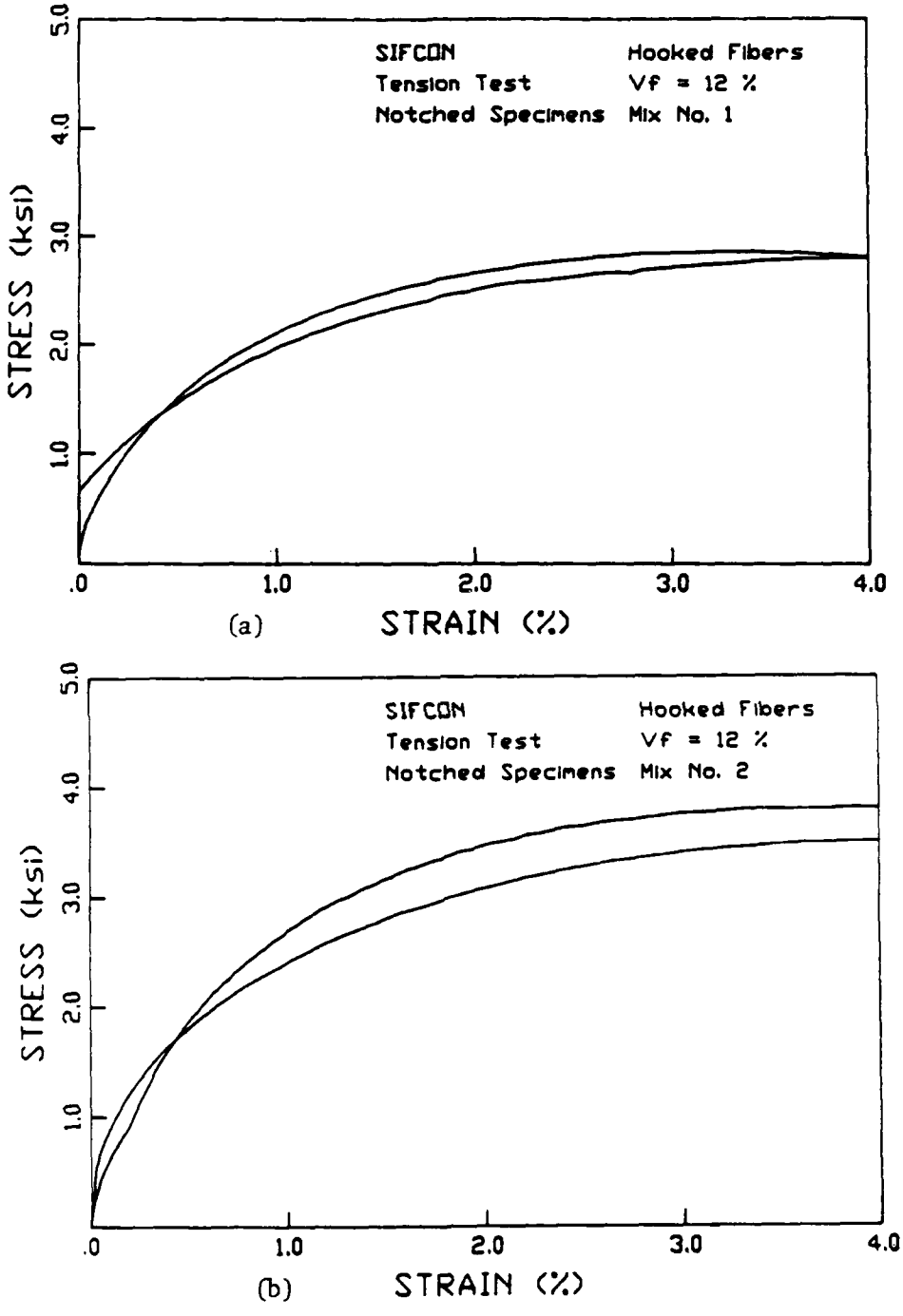

Figure 34. Stress-strain response.
a. Hooked fibers. Mix One.
b. Hooked fibers. Mix Two.

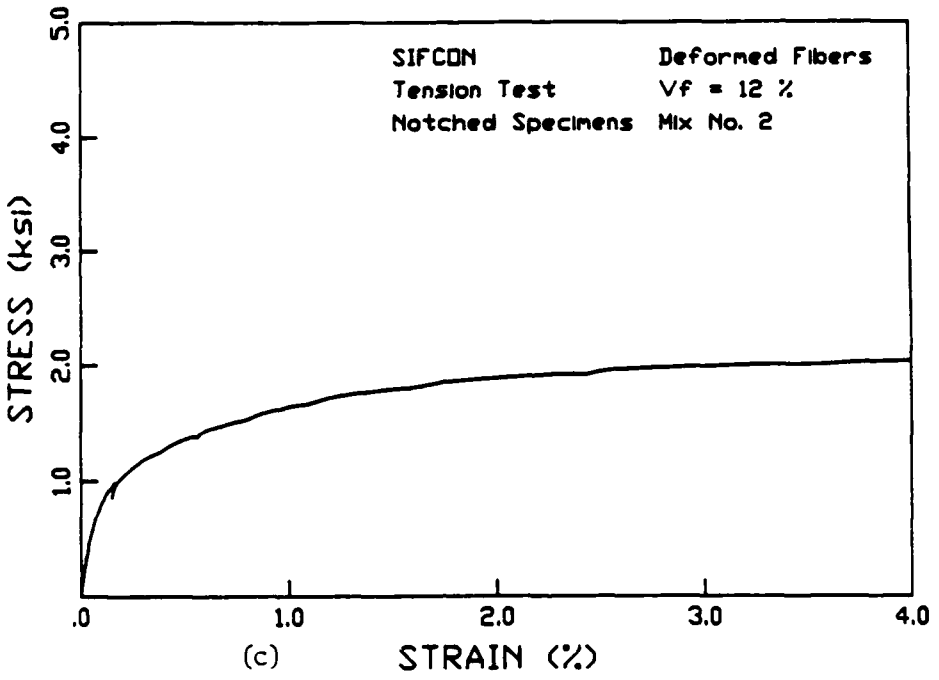

(c)

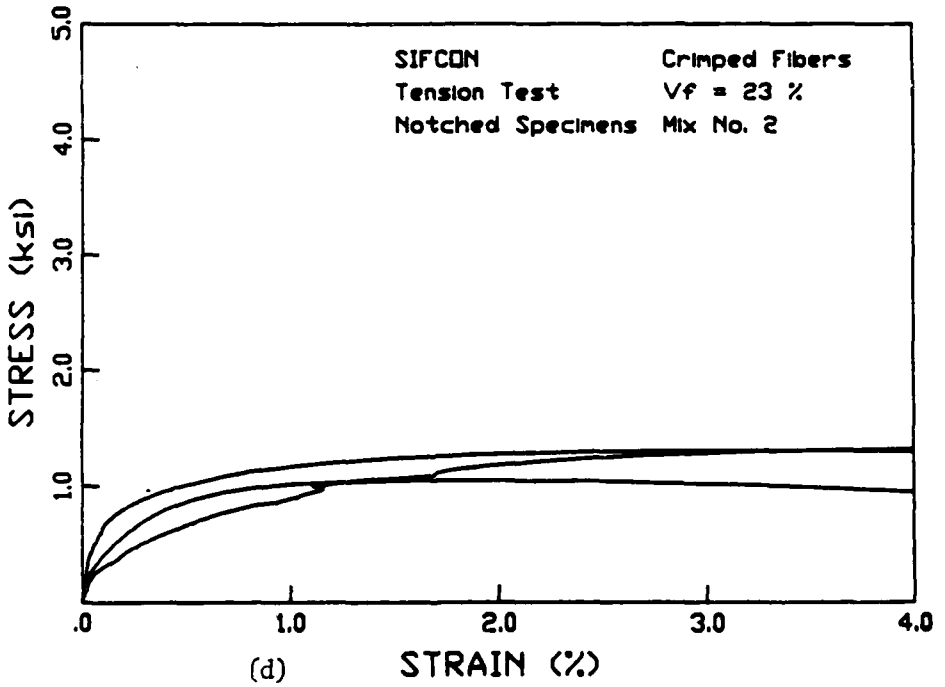

(d)

Figure 34. Stress-strain response
c. Deformed fibers. Mix Two.
d. Crimped fibers. Mix Two.

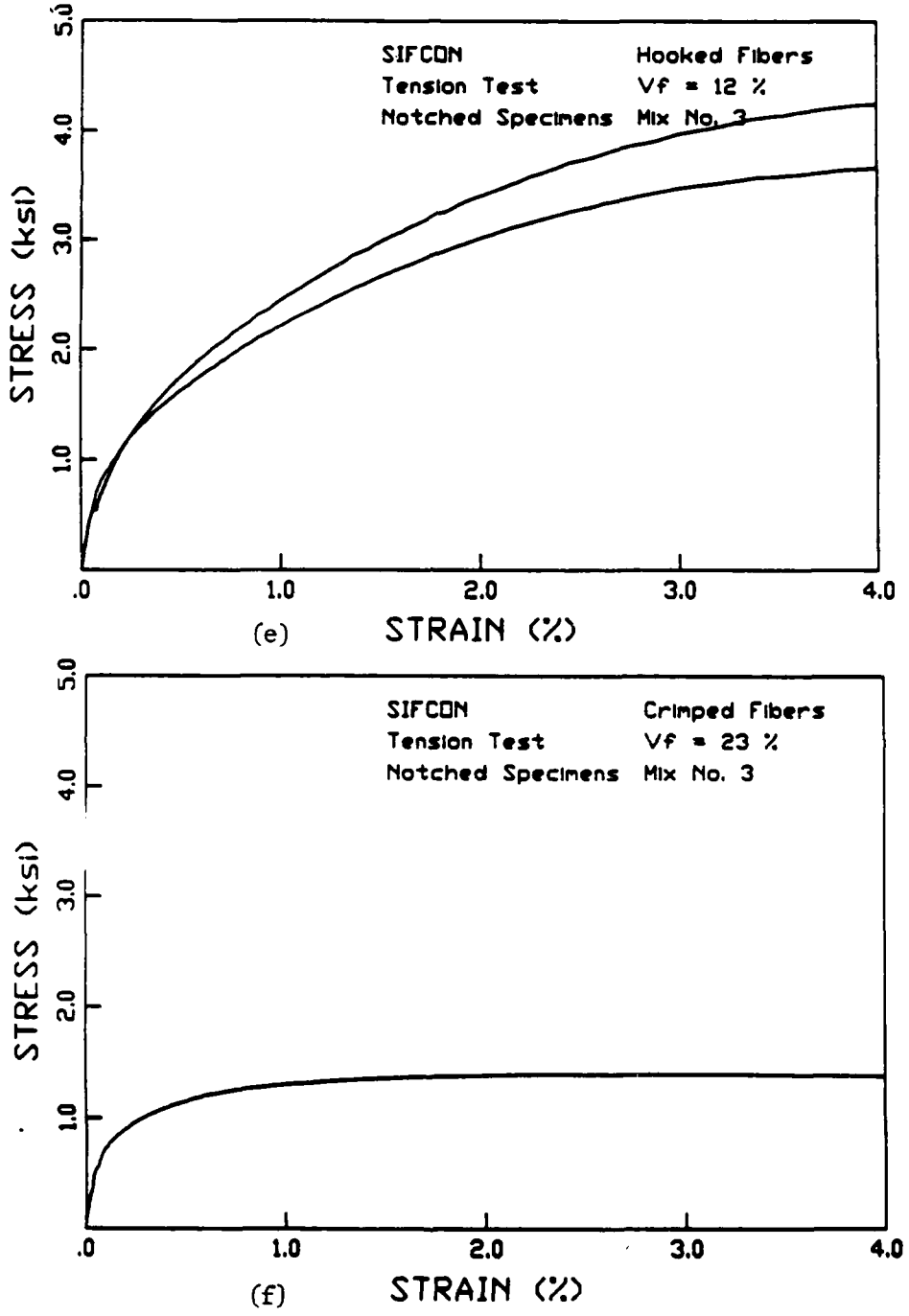

Figure 34. Stress-strain response
e. Hooked fibers. Mix Three.
f. Crimped fibers. Mix Three.

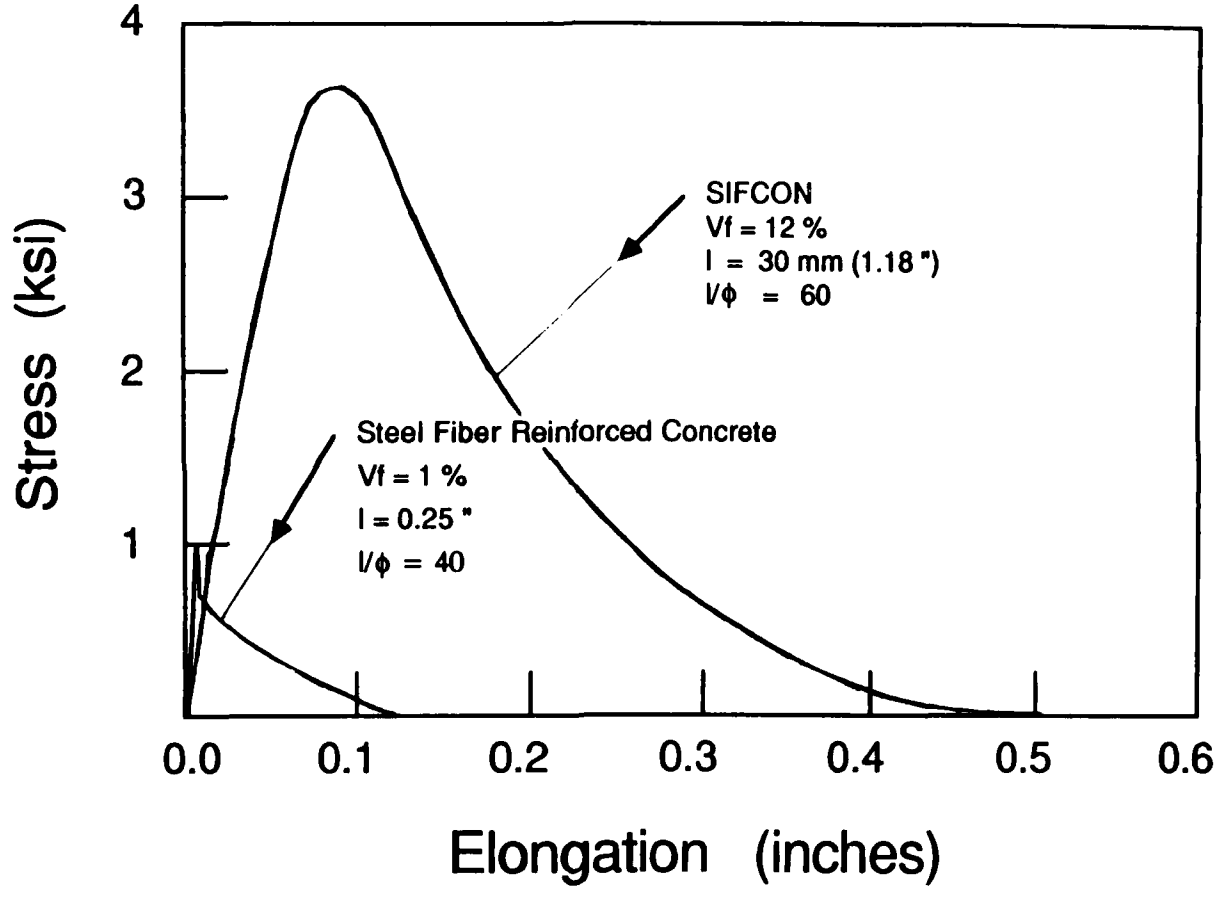

Figure 35. Stress-elongation response comparison of SIFCON to ordinary fiber-reinforced concrete.

tremendous ductility after matrix cracking.

3.6.2 Effect of Fiber

The results of the tests are summarized in tabular form in Table 7. The most noticeable affect of differing fibers is that crimped (Xorex II) fibers yield only one-third the tensile strength of hooked (Dramix) fibers of the same matrix (3.9 k/in^2 compared to 1.2 k/in^2). Crimped fibers also showed a more gradual decline in the descending branch of the stress-strain curve than did either hooked or deformed fibers.

Only two stress-strain curves were obtained for composites made with deformed (Surecrete) fibers, so few conclusions may be drawn concerning the behavior of composites made with these fibers. The only matrix type with recorded stress-displacement curves for all three fibers types is Mix Two. Composites made with Mix Two show an average tensile strength of 4 k/in^2 with hooked fibers, 1.8 k/in^2 with deformed fibers and 1.2 k/in^2 with crimped fibers. The lower strength of composites made with deformed fibers as compared to those made with hooked fibers is surprising. In Section 2, prism specimens made with hooked fibers showed about the same strength as specimens made with deformed fibers (about 3 k/in^2). Since more tensile specimens with deformed fibers were tested in Section 2, the poorer performance of deformed fiber composites observed in present tests may be due merely to an inadequate sampling of tested specimens.

3.6.3 Testing Difficulties

3.6.3.1 Grip Construction. The first few series of tensile stress-displacement tests were run using the grips constructed for the tensile stress-strain tests of Section 2. These grips prevented the development of any end moments in the specimens during testing but also led to nonuniform section failure in the specimens and subsequent bending in the specimens. Thus, several specimens were lost in this manner. To correct this problem, new grips were built which prevented specimen end rotation. These grips are shown in Figure 31. The new grips functioned well and did prevent the specimen bending present in the older testing system.

3.6.3.2 Insufficient Notch Depth. Specimens were notched 1/4 inch on all sides at midlength leading to a 30% reduction in cross-sectional area. However, this notch depth proved to be insufficient to guarentee failure in the notched region. While most specimens did fail in the notched area, close to 35% did not. This was the greatest test difficulty and was the major reason for the incompleteness of test data.

3.6.3.3 Software Problems. The data acquisition system utilized in the testing process stores test data in a binary format on 8-in floppy diskettes. Occasionally dust or unknown disk operating system errors occur and prevent the recording of data. Although this is not a common problem, data acquisition system errors caused the loss of test data for five of the thirty-six specimens tested in this program. However, direct plots of the load-elongation response on the X-Y recorder of the Instron testing machine are available for these specimens and can be digitized if needed.

Table 7. Average tension tests results.

Series ID.	Fiber Volume (%)	Maximum Stress (ksi)	Eq u. Strain at Max. Stress (%)	Inflection Point		Equivalent Surface Energy (kip-in / in ^{2})
				Stress (ksi)	Displ. past peak stress (inches)	
TPD1R	12.0	2.81	4.0	1.8	0.065	0.450
TPD2R	12.8	3.85	4.1	2.2	0.075	0.574
TPS2R	12.8	1.72	5.5	1.1	0.10	0.328
TPX2R	23.0	1.25	2.0	0.75	0.12	0.168
TPD3R	12.6	3.85	5.0	2.3	0.075	0.574
TPX3R	22.7	1.42	2.0	0.90	0.12	0.250

3.7 CONCLUSIONS

The following conclusions may be drawn from the stress-elongation tests of SIFCON specimens:

3.7.1 The stress-elongation response of SIFCON can be divided into two parts: an ascending part up to the peak stress and a descending part from the peak stress to complete separation. While the ascending part may be translated into an average stress-strain curve, the descending part describes the opening of a single crack and represents a stress-crack opening or stress-displacement response.

3.7.2 The ascending part of the stress-elongation response is briefly linear up to a point which may represent the onset of first crack propagation along the notched edges of the critical section. Then it becomes highly nonlinear up to the peak stress; this suggests slow crack growth behavior until a through matrix crack develops across the notched section. It is not clear from this part of the study if the propagation of the main crack was accompanied by multiple cracking or microcracking (process zone) within the gauge length on either side of the crack.

3.7.3 The shape of the stress-displacement (descending branch) curve of SIFCON is different from that of ordinary fiber-reinforced concrete which shows an exponentially decaying response (1,2). With SIFCON the curve has an inflection point quite similar to the descending branch under compressive loading. This difference in behavior may be due to the significant effect of fiber interlock in SIFCON. However like ordinary FRC, the maximum crack-opening is equal to about half the fiber length.

3.7.4 Compared to conventional steel-fiber-reinforced concrete which shows direct tensile strengths up to 800 lb/in^2, SIFCON developed tensile strengths of up to 4000 lb/in^2. The higher performance of SIFCON is attributable to the optimum combination of various fiber parameters.

3.7.5 In this part of the study, composites made with hooked fibers showed substantially higher strength and surface energy than composites made with deformed or crimped fibers.

3.7.6 The surface energy of SIFCON can be of the order of 600 $lb\text{-}in/in^2$. Such a high value is about ten times the average surface energy reported for conventional fiber reinforced concrete (3), and three to four orders of magnitude the surface energy of plain concrete. Additional and complete investigation of the fracture properties of SIFCON, with particular emphasis on its fracture energy, is recommended.

4.0 Constitutive Models for SIFCON

4.1 INTRODUCTION

Several studies have described equations to model the stress-strain characteristics of ordinary fiber reinforced concrete (Refs. 15-24). Fanella and Naaman proposed a series of equations which model the complete stress-strain curve of fiber-reinforced mortar in compression [3]. By examining the relationships between the various input variables (fiber dimensions, fiber-reinforcing index, matrix strength, and the fiber volume fraction) they derived a series of equations to predict the key points of the compressive stress-strain curve. These parameters included the maximum stress, the post peak inflection point on the descending branch of the stress-strain curve, and the stress level after a prespecified maximum elongation. Visalvanich and Naaman proposed a model of the tensile stress-displacement behavior of ordinary fiber-reinforced concrete using a third-degree polynomial. The polynomial began with the point of maximum post peak stress and descended to zero stress at a crack opening of one-half the fiber length (complete specimen separation and fiber pullout). The ascending branch of the curve was assumed to be linear up to the cracking strength of the composite, taken equal to that of the unreinforced matrix. Other studies have described equations to model the stress-strain behavior of plain concrete which may be readily applied to the modeling of fiber concretes (Refs. 15-17, 20-23).

4.2 OBJECTIVE AND SCOPE

The objective of this section is to develop analytical relationships to describe the complete stress-strain or stress-displacement curve of high-strength SIFCON in both compression and tension. Rational equations are proposed to calculate the quantities necessary to describe the stress-strain curve. Input parameters include known or easily measured quantities: fiber type, fiber volume fraction, fiber dimension, and composite ultimate strength.

4.3 STRESS-STRAIN CURVE OF SIFCON IN COMPRESSION

SIFCON may be successfully modelled using many of the same controlling variables and descriptive equations as ordinary fiber-reinforced concrete. The ascending branch of the stress-strain curve of SIFCON in compression is similar to that of other concrete materials and may be successfully modeled using the equations used to describe those materials. However, the descending branch of SIFCON's compressive and tensile stress-strain curves presents some difficulties. SIFCON composites tend to have a slowly decaying shape in the post peak stress-strain response characterized by a Naperian-based power function in appearance rather than the quickly decaying polynomial function used to model ordinary fiber concrete. To model this behavior, Absi and Naaman have proposed an equation with the Naperian-based function included to model the post peak stress-strain response of SIFCON

in compression.

4.3.1 Ascending Branch

To model the ascending branch of SIFCON's stress-strain curve, an equation of the following form was chosen:

$$f = f_o [1 - (1 - \varepsilon / \varepsilon_o)^A] \quad (1)$$

where

f	=	Compressive Stress
f_o	=	Maximum Compressive Stress
ε	=	Strain
ε_o	=	Strain at Maximum Stress
A	=	A parameter to be calculated

A similar equation was used in Reference 22 to model the ascending branch of concrete in compression. If Eq.1 is differentiated once, the following equation is obtained:

$$(\delta f / \delta \varepsilon) = (A f_o/\varepsilon_o) \left[1 - \varepsilon/\varepsilon_o \right]^{A-1} \quad (2)$$

Since one raised to any power is one, at $\varepsilon = 0$:

$$(\delta f / \delta \varepsilon)_{\varepsilon=0} = (A f_o/\varepsilon_o) \left[1\right]^{A-1} = A f_o/\varepsilon_o = E \quad (3)$$

where E is the initial tangent modulus of elasticity.

Thus $$A = E \varepsilon_o / f_o \quad (4)$$

E, ε_o, and f_o must now be determined. If available testing systems are accurate enough, all three of these parameters may be determined from the stress-strain curve of tested series of SIFCON specimens. If such systems are not available, the maximum stress may be readily determined by uniaxial compression tests and the values of ε_o and E calculated from the following equations:

E, the initial tangent modulus, may be calculated from the law of mixtures:

$$E = \lambda_1 V_f E_{\text{fibers}} + (1 - V_f) E_{\text{slurry}} \quad (5)$$

where

V_f = Volume Fraction of fibers

λ_1 = Factor generally assumed equal to 1 for compressive loading

The following values are recommended for steel fibers and plain slurry:

$E_{fibers} = 30 \times 10^6$ lb/in^2
$E_{slurry} = 1 \times 10^6$ lb/in^2

The strain at peak stress, ε_o, must be determined from a more empirical analysis. The ε_o is a function of fiber type, f_o, and $V_f \ell / \phi$ (the fiber reinforcing index).

where

ℓ = fiber length

ϕ = fiber diameter

A study of the relationship between ε_o and f_o disclosed that the strain at maximum stress is rather insensitive to varying values of the maximum stress, so a relationship was sought between ε_o and $V_f \ell / \phi$. An analysis of the data obtained in Section 1, has led to the following values of ε_0 (Table 8), assuming $V_f \ell / \phi = 7.0$ (the approximate reinforcing index of the experimental tests):

Table 8. ε_o Strain at maximum stress for $V_f \, l/\phi = 7$.

Fiber Align. to Axis	Hooked	Deformed	Crimped
Parallel	0.011	0.011	0.009
Normal	0.020	0.020	0.018

The following relationship was sought:

$$\varepsilon_o = \varepsilon_{initial} + K_1 V_f \ell / \phi \qquad (6)$$

Using test data, data from other researchers, and an equation derived by Fanella and Naaman

for ordinary fiber-reinforced concrete, the following parameters were calculated:

$\varepsilon_{initial} = 0.005$

$K_1 = 0.00076$ for fibers aligned parallel to loaded axis.
$K_1 = 0.0020$ for fibers aligned normal to loaded axis.

Thus, given the ultimate compressive strength of a SIFCON composite, the fiber type used, and the reinforcing index, the parameters ε_o and E may be estimated from Eqs. 5 and 6 and the parameter A calculated from Eq. 4. Then the ascending branch of the compressive stress-strain curve modeled from Eq. 1.

4.3.2 Descending Branch

To model the descending branch of SIFCON's compressive stress-strain curve, an equation with a Naperian-based exponential term was chosen. Figure 36 illustrates the variables given in this equation (Eq. 7):

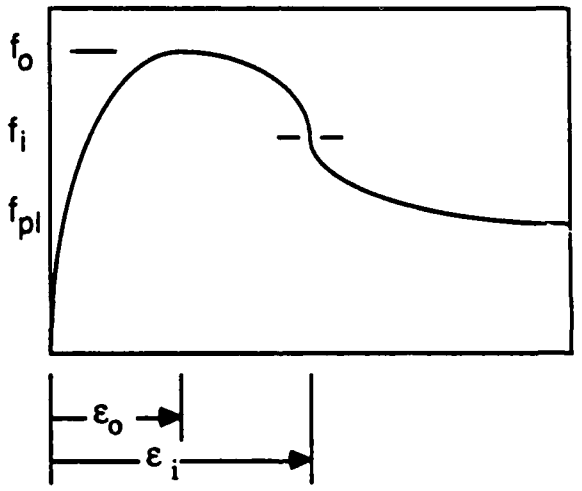

Figure 36. Stress-strain curve variables.

$$f = (f_o - f_{pi}) \, Exp[-b(\varepsilon - \varepsilon_o)^m] + f_{pl} \quad (7)$$

$$m = \{1 + \ln[(f_i - f_{pl}) / f_o - f_{pl})]\}^{-1} \quad (8)$$

$$b = [(m - 1)/m] (\varepsilon_i - \varepsilon_o)^{-m} \quad (9)$$

where

f_{pl} = Post peak Plateau Stress
f_o = Peak Stress
f_i = Stress at Post peak Inflection Point
ε_o = Strain at Peak Stress
ε_i = Strain at Post peak Inflection Point
b,m = Controlling parameters to be determined

Input data must include the peak stress, the fiber type, and the fiber reinforcing index. The plateau stress may or may not be known.

Case 1: Plateau Stress Known. A relationship is sought between the plateau stress, the peak (ultimate) stress, and the stress at the inflection point. Noting that the inflection stress must always lie between the peak stress and the plateau stress, the following relationship may be stated:

$$f_i = \lambda (f_{pl} + f_o) \quad (10)$$

where

$$f_{pl} / (f_{pl} + f_o) < \lambda < f_o / (f_{pl} + f_o)$$
$$0 < \lambda < 1$$

A simple average of the tested series yields $\lambda = 0.501$ with a standard deviation of 0.02. For simplicity, use:

$$f_i = (f_{pl} + f_o) / 2 \quad (11)$$

then

$$m = 1 / \{ 1 + \ln [1 / 2] \} \approx 3.26 \quad (12)$$

To determine the value of the inflection strain, a relationship was sought between the inflection strain, the strain at maximum stress, and the ratio of the plateau stress to the maximum stress. Figure 37 shows the experimental data for these parameters in graphical form.

To model this behavior, an equation of the following form is sought:

$$\varepsilon_i = \varepsilon_o + K_2 f_{pl} / f_o \quad (13)$$

Using a least sqares regression fit of data, the following values are determined for K_2:

$K_2 = 0.017$ for fibers aligned parallel to loaded axis.
$K_2 = 0.030$ for fibers aligned normal to loaded axis.

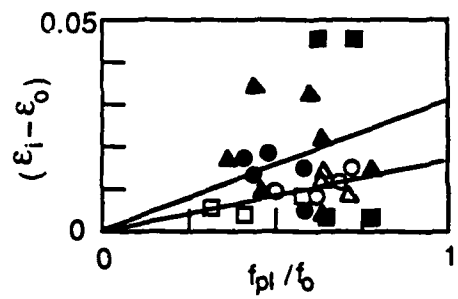

Fiber Type	Alignment	
	Parallel	Normal
Hooked	△	▲
Deformed	○	●
Crimped	□	■

Figure 37. Relationship between inflection strain and plateau stress.

Case 2: Plateau Stress Unknown. To determine the magnitude of the plateau stress, a relationship is sought between the plateau stress, the ultimate strength, and the fiber reinforcing index. This relationship is chosen to be of the form:

$$f_{pl} = V_f \ell / \phi \, (K_{31} + K_{32} \sqrt{f_o}) \qquad (14)$$

Using an approximate least squares regression analysis leads to the following values of K_{31} and K_{32}:

$K_{31} = 50$ lb/in^2 for crimped fibers aligned parallel to loaded axis.
$K_{31} = 350$ lb/in^2 for crimped fibers aligned normal to loaded axis.
$K_{31} = 200$ lb/in^2 for hooked and deformed fibers aligned parallel or normal to loaded axis.

$K_{32} = 8.0$ for all fibers and alignments.

where the ultimate strength, f_o, is given in units of lb/in^2.

Thus, given the ultimate strength of the SIFCON composite, the fiber type used, and the reinforcing index, controlling parameters may be calculated from the above equations and the descending branch of the compressive stress-strain curve modeled from Eq. 7.

4.3.3 Examples

Figures 38a and 38b show typical fits of the equations derived for the compressive stress-strain curve of SIFCON. The first graph (Figure 38a) is more of an ideal case, showing the characteristic shape of SIFCON clearly. The fit can be seen to be quite close. Figure 38b shows a more difficult fit. Although only roughly shaped like the actual stress-strain curve, the equation is as accurate as can be expected.

4.4 STRESS-STRAIN CURVE OF SIFCON IN TENSION

The ascending branch of SIFCON's tensile stress-strain curve may be modeled using the same equations as those for compression.

$$f = f_{ot} \left[1 - (1 - \varepsilon / \varepsilon_{ot})^D \right] \tag{15}$$

$$D = E \varepsilon_{ot} / f_{ot} \tag{16}$$

where f_{ot} is the ultimate tensile strength of the composite. The initial tangent modulus, E, may be calculated from the law of mixtures, with due account for the efficiency of fiber reinforcement and the bond stress versus slip modulus:

$$E = \lambda_1 V_f E_{fibers} + (1 - V_f) E_{slurry} \tag{17}$$

as stated in the case of SIFCON in compression. A value of λ_1 equal 1/30 may be taken as a first approximation for SIFCON in tension with fibers parallel to the loading axis, while a value of zero should be used for fibers normal to the loading axis.

To determine the strain at the point of maximum stress, the following relationship was sought:

$$\varepsilon_{ot} = \varepsilon_{slurry} + K_4 V_f \ell / \phi \tag{18}$$

By averaging test data, the following parameters were calculated:

$\varepsilon_{slurry} = 0.0005$

$K_4 = 0.00097$ for deformed fibers aligned parallel to loading axis.
$K_4 = 0.00174$ for hooked fibers aligned parallel to loading axis.

To determine the ultimate tensile strength of SIFCON, a relationship was sought between the tensile strength of the composite due to the addition of fibers and the compressive post peak plateau stress. This relationship was sought since the compressive plateau stress represents a shear mode of failure as the two specimen halves slide across one another after development of the shear failure plane, and since shear strength and tensile strength are generally directly related. This yielded the following approximation:

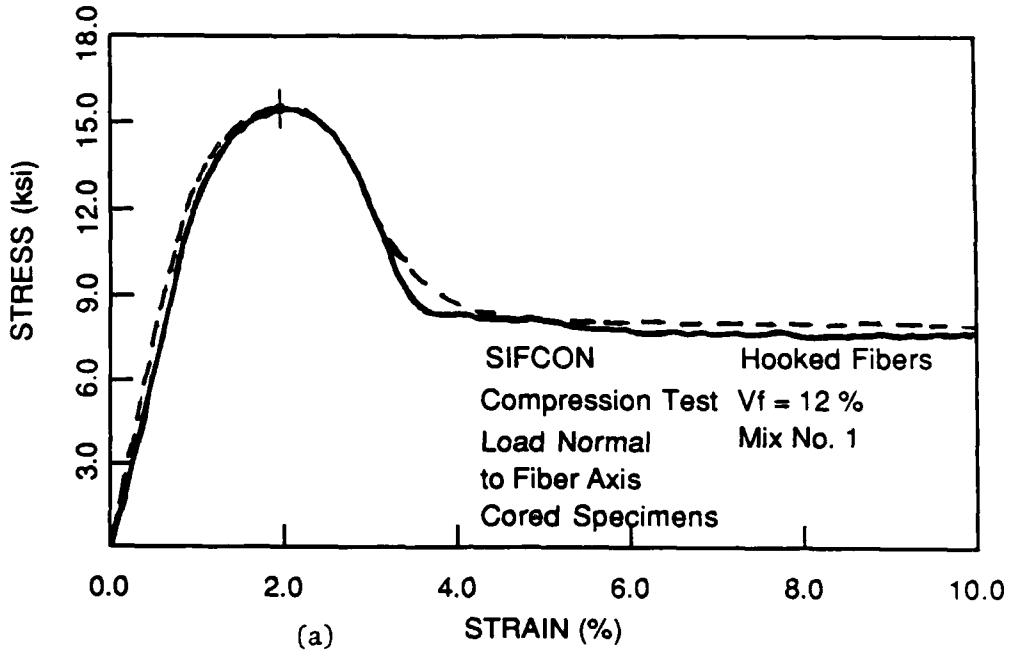

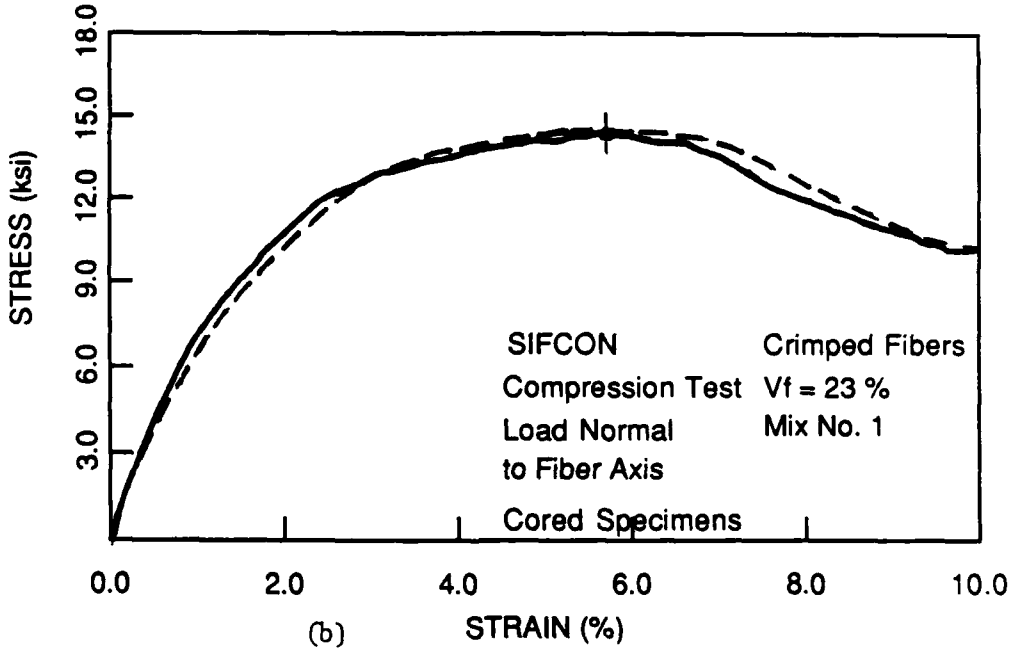

Figure 38. Comparison between predicted and observed stress-strain curves.
a. Showing a typical fit.
b. Showing a difficult fit.

$$f_{ot} = \alpha f_{pl} \approx (1/3)\, f_{pl} \qquad (19\,a)$$

or

$$f_{ot} = (1/3) V_f \ell/\phi\,(200 + 8\,\sqrt{f_o}) \quad \text{in lb/in}^2 \qquad (19\,b)$$

assuming f_{ot} is larger than the cracking strength of the unreinforced slurry matrix.

Thus, given the ultimate compressive strength of a SIFCON composite, the fiber type used, and the reinforcing index, the compressive plateau stress may be calculated from Eq. 14 and the parameters D, E, ε_{ot}, and f_{ot} may be estimated from Eqs. 16, 17, 18, and 19. Then the ascending branch of the tensile stress-strain curve can be modeled from Eq. 15.

4.5 STRESS-DISPLACEMENT CURVE OF SIFCON IN TENSION

4.5.1 Background

The post peak, stress-displacement curve of ordinary fiber-reinforced concrete in tension has been successfully modelled by several authors (Refs. 8, 9, 12, 16, 17, 24). The equations which these authors propose to model the tensile stress-displacement curve have two common properties: (1) a stress-displacement curve with a single curvature shape (this accurately reflects the behavior of ordinary fiber concrete) and (2) complete loss of load sustaining capacity by the time the crack displacement reaches a distance of one-half the reinforcing fiber length.

Visalvanich and Naaman proposed a third degree polynomial to model the post peak stress-displacement relationship of fiber reinforced concrete in tension:

$$\sigma / \sigma_{pc} = [\,0.1\,(2\delta / \ell) + 1][(2\delta / \ell) - 1]^2 \qquad (20)$$

Based on the work of Kaadi (Ref. 16), Nammur and Naaman developed the following equation to model the tensile post peak, stress-displacement relationship of fiber-reinforced concrete at different strain rates.

$$\sigma / \sigma_{pc} = \{\,1 - (2\delta / \ell) / v\}\, \mathrm{Exp}[\,-A\,(2\delta / \ell)\gamma] \qquad (21)$$

$$\sigma_{pc} = [\,(\alpha\tau)_{st}\,(\varepsilon / \varepsilon_{st})^{0.05}\,]\,(V_f\,\ell / \phi)$$

$$v = (\varepsilon / \varepsilon_{st})^{-0.07}$$

$$A = 2.53\,[\,\ln\,(\varepsilon / \varepsilon_{st})^{-0.09}] \quad \text{for } \varepsilon \neq \varepsilon_{st}$$

$$A = 3.38 \quad \text{for } \varepsilon = \varepsilon_{st} \text{ (static condition)}$$

$$\gamma = 1.2 - 0.05 \ln\,(\varepsilon / \varepsilon_{st})$$

In the above model, complete loss of load-sustaining capacity at a crack displacement of half the fiber length occurs only at the static strain rate. Higher strain rates lead to a complete loss of load capacity at smaller crack displacements.

4.5.2 Proposed Relationships

Equations 20 and 21 exhibit a single curvature shape which is characteristic of the stress-displacement curve of ordinary fiber-reinforced concrete. However, the stress-displacement curve of SIFCON has a different shape with a double curvature. While the equations derived for fiber reinforced concrete can be used as a first approximation for the behavior of SIFCON, a more accurate representation of the double curvature may be modelled by equations which exhibit double curvature. To model this behavior, a fourth degree polynomial may be used. In that case, however, the general formula for the calculation of the five unknown equation constants is extremely complex. Another more accurate equation of the form used successfully by Absi and Naaman to model the descending branch of the compressive stress-strain curve of fiber reinforced concrete and SIFCON may instead be used to model the tensile stress-displacement curve. Thus an equation of the following form is sought:

$$f = a\,[\mathrm{Exp}\,(-b\,(\delta)^{m}) - c\,(\delta)^{n}] \tag{22}$$

Where a,b,m, and c are four constants to be evaluated from four boundary conditions of the curve:

$$(f)_{\delta = o} = f_{ot} \tag{22 a}$$

$$(f)_{\delta = \ell/2} = 0 \tag{22 b}$$

$$(df / d\delta)^2_{\delta = \delta it} = 0 \tag{22 c}$$

$$(f)_{\delta = \delta it} = f_{it} \tag{22 d}$$

Where δ_{it} is the crack opening at the inflection point. This leads to the following constants:

$$a = f_{ot} \tag{23 a}$$

$$c = 2\,\mathrm{Exp}\,(-b\,(\ell/2)^{m})/\ell \tag{23 b}$$

$$b = (m-1)/[m\,(\delta_{it})^{m}] \tag{23 c}$$

$$m = 1/\{1 + \ln[\,f_{it}/f_{ot} + c\,\delta_{it}]\} \tag{23 d}$$

The first term in Eq. 22 provides the characteristic double curvature shape of a Naperian-based function, while the second term in Eq. 22 is a correction term to bring the stress to zero at a displacement of half the fiber length. The exponent in the second term is arbitrary but a value of one is recommended. Any value greater than n = 2 will greatly complicate the calculation of the constant c which is determined from the third boundary condition listed above (Eq. 22 c).

The stress and crack opening at the inflection point must be determined from the results of the experimental tests. To calculate the inflection stress, the following relationship was sought:

$$f_{it} = \rho f_{ot} \tag{24}$$

where f_{ot} is assumed larger than the strength of the unreinforced matrix.

From a simple averaging of test data, the ratio ρ was found to equal 0.60.

$$\rho = 0.60$$

To calculate the inflection point displacement, the following relationship was sought between the inflection displacement and the reinforcing index:

$$\delta_{it} / (\ell / 2) = K_5 V_f \ell / \phi \tag{25}$$

or more conveniently:

$$\delta_{it} = K_5 V_f \ell^2 / \phi \tag{26}$$

From test data, the following values are found for the parameter K_5:

$K_5 = 0.017$ for crimped fibers.
$K_5 = 0.010$ for hooked or deformed fibers.

Given the compressive strength, fiber type, fiber length, and fiber reinforcing index, it is now possible to approximate the stress-crack displacement behavior of SIFCON in tension. The proposed equations to model the stress-displacement behavior are summarized below:

$$f = f_{ot} [\text{Exp} (-b (\delta)^m) - c (\delta)] \tag{27 a}$$

$$c = 2 \text{Exp} [-b (\ell / 2)^m] / \ell \tag{27 b}$$

$$b = (m - 1) / [m (\delta_{it})^m] \tag{27 c}$$

$$m = 1 / \{1 + \ln[f_{it} / f_{ot} + c \delta_{it}]\} \tag{27 d}$$

where

f	=	Tensile Stress
f_{ot}	=	Maximum Tensile Stress (See Eq. 19 b)
f_{it}	=	Tensile Stress at inflection point (See Eq. 24)
c,b,m	=	Constants to be calculated
δ	=	Tensile crack displacement

δ_{it} = Crack displacement at inflection point (See Eq. 26)

ℓ = Fiber length

Equations 27a, 27b, and 27d are three independent equations with three unknowns. Thus they can be solved. However a closed form solution cannot be found. The values of m, c, and b can vary over a wide range. For instance:

For δ_{it} = 0.1, V_f = 12%, $\ell/2$ = 0.5 in, and f_{ot} = 2.5 lb/in^2, the solution of the above equations leads to: m = 2.044, b = 54.28, and c = 3.8 x 10^{-6}. If only the value of δ_{it} is changed to 0.2 in, the solution would yield: m = 1.84, b = 8.82, and c = 0.17.

4.5.3 Examples of Curve Fitting in Tension

Figures 39a and 39b show the typical fit of the equations derived for the tensile stress-strain and stress displacement curves of SIFCON in tension. Figure 39a shows the stress-strain relationship and Figure 39b shows the stress-displacement relationship. While the equation fit is not exact, it does closely follow the general shape of the experimental stress-displacement curves. The fit is very good for all practical purposes.

4.6 ANALYTICALLY GENERATED CURVES IN COMPRESSION AND TENSION

Figures 40 and 41 show typical families of curves which are generated for some of the common fiber-reinforcing cases. Figure 40 shows analytically generated compressive stress-strain curves for two values of the reinforcing index (2.4 and 7.2), assuming deformed fibers with axis normal to the loading direction. Figure 41a shows typical curves modeling the tensile stress-strain response of SIFCON with various values of the parameter D (which is proportional to the modulus of elasticity of the composite). Figure 41 shows the curves used to model the tensile stress-displacement response. Here a value of 3 k/in^2 was asssumed for the maximum tensile strength of the composite f_{ot}.

These figures give some idea of the behavior of the modeling equations and their sensitivity to variable input parameters. While the mathematical form of these equations seems quite representative of the behavior of the composite, the prediction equations of the parameters obtained from the data may need extensive reevaluation. These prediction equations should be considered approximations only, until further data and analysis allow for a better tuning of the parameters for improved accuracy and reliability.

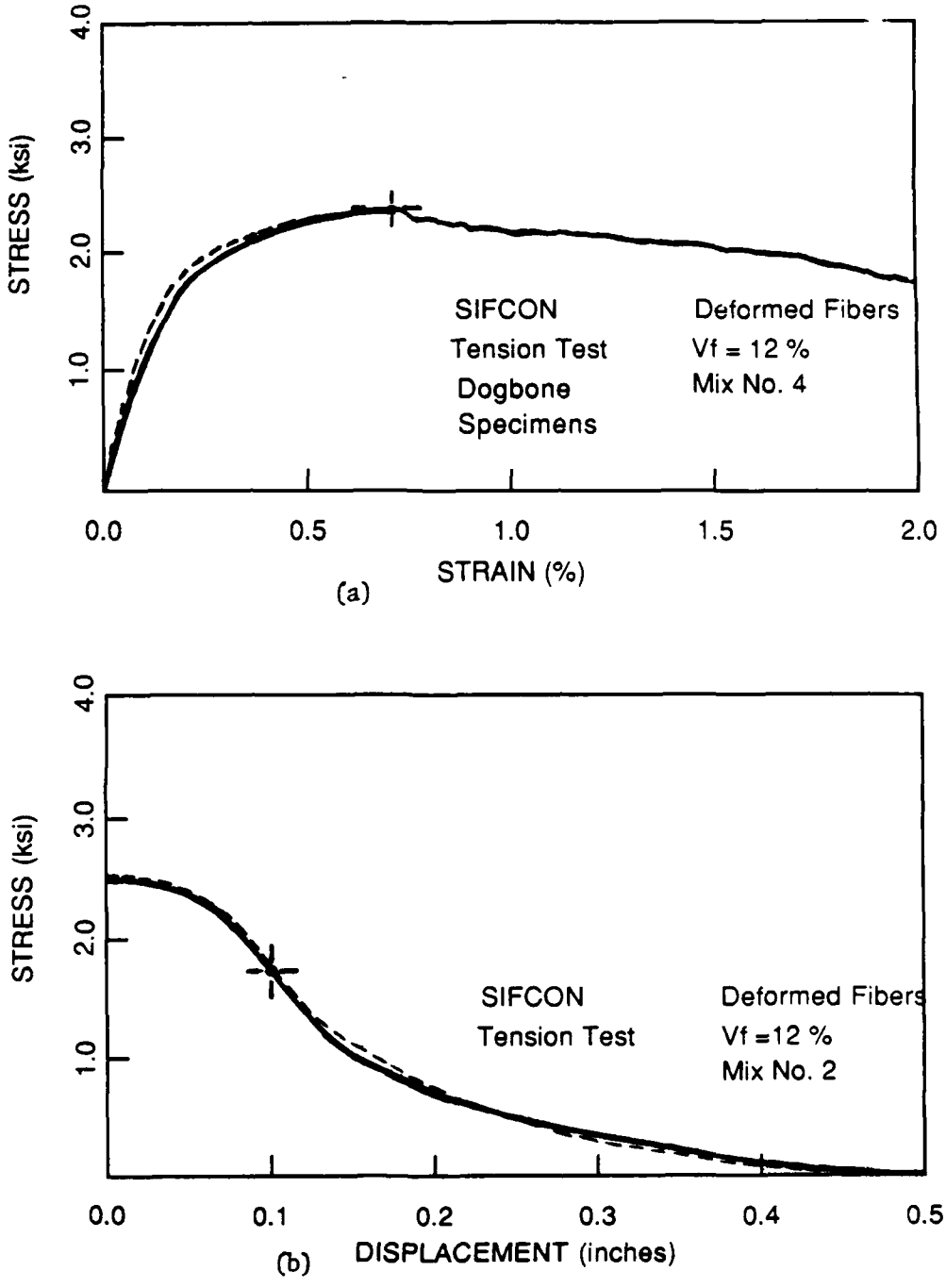

Figure 39. Comparison between predicted and observed stress-displ. curves.
a. Stress-strain.
b. Stress-displacement.

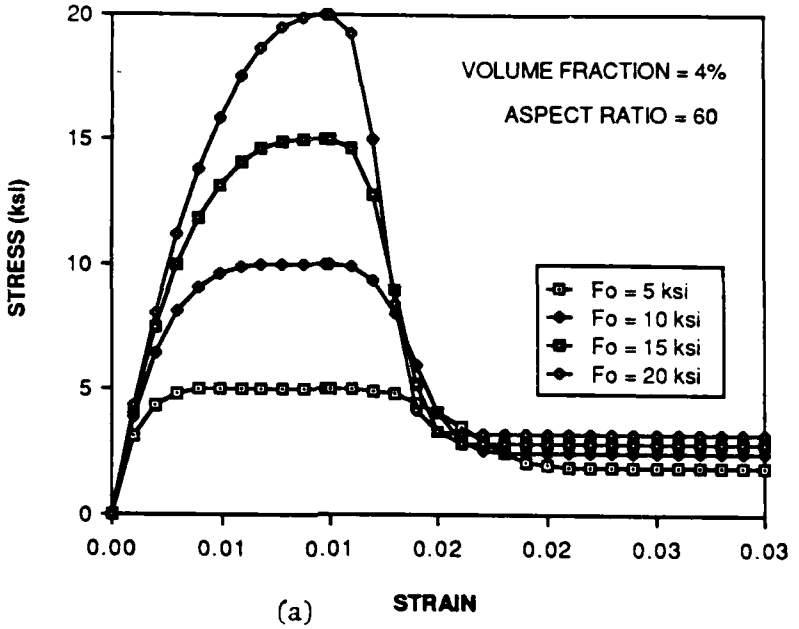

(a)

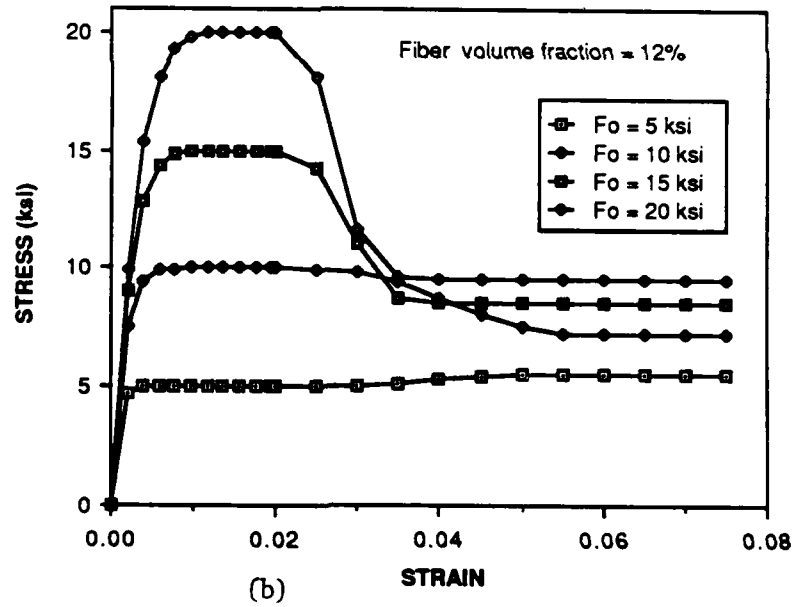

(b)

Figure 40. Analytically generated stress-strain curves of SIFCON in compression .
a. Reinforcing index of 2.4.
b. Reinforcing index of 7.2.

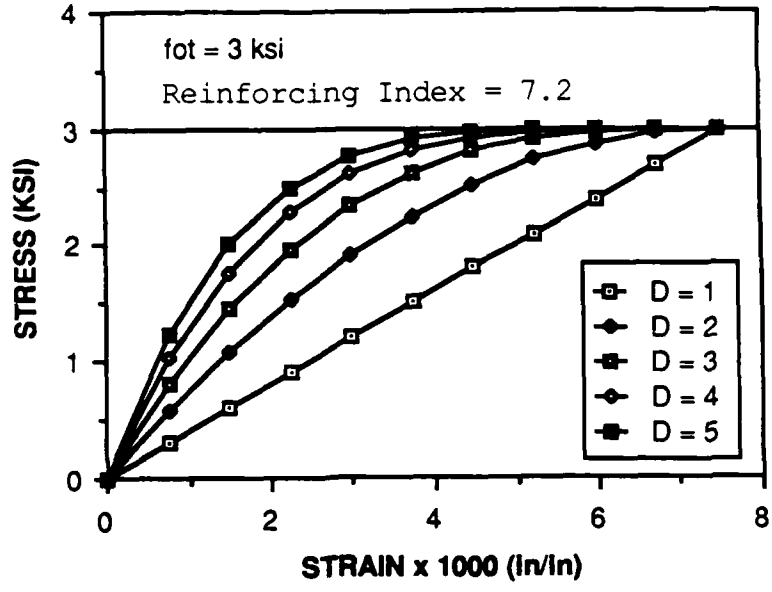

(a)

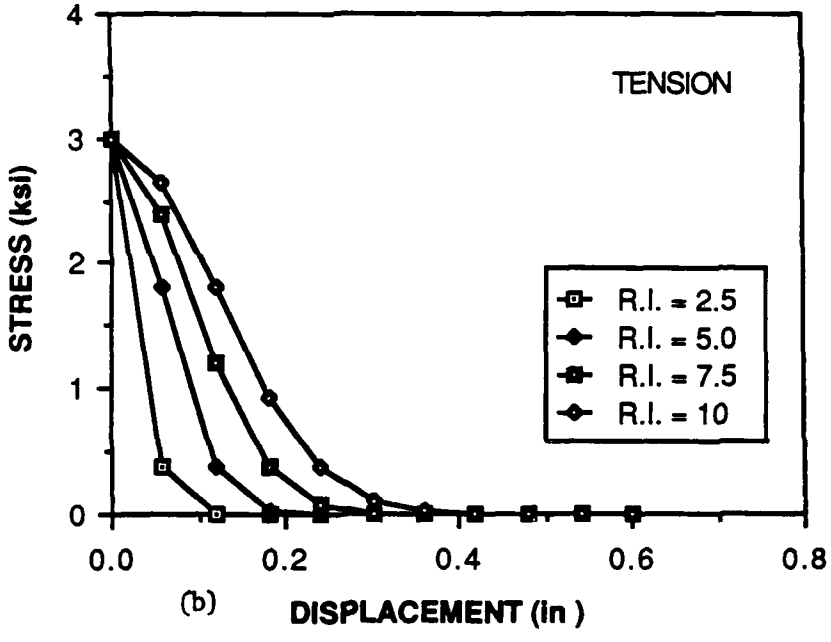

(b)

Figure 41. Analytically generated SIFCON response in tension for f_{ot} = 3 k/in^2.
a. Stress-strain (ascending branch) for different values of the parameter D.
b. Stress-displacement (descending branch) for different reinforcing indexes.

REFERENCES

1. Balaguru, P., and Kendzulak, J., "Flexural Behavior of Slurry Infiltrated Fiber Concrete (SIFCON) Made Using Condensed Silica Fume," ACI Special Publication SP 91-60, American Concrete Institute, Detroit, 1986, pp. 1216-1229.

2. Lankard, D.R., and Lease, D.H., "Highly Reinforced Precast Monolithic Refractories," Bulletin American Ceramic Society, Vol. 61, No.7, 1982, pp. 728-732.

3. Lankard, D.R., and Newell, J.K., "Preparation of Highly Reinforced Steel Fiber Reinforced Concrete Composites," ACI Special Publication, SP-81, American Concrete Institute, Detroit, 1984, pp. 286-306.

4. Lankard, D.R., "Slurry Infiltrated Fiber Concrete (SIFCON): Properties and Applications," in Very High Strength Cement Based Composites, J.F. Young, Editor, Materials Research Society, Vol. 42, Pittsburgh, 1985, pp. 227-286.

5. "Summary Report on Preparation and Properties of Slurry Infiltrated Fiber Concrete (SIFCON) prepared with four Bekaert Steel Fibers," Reported by Lankard Materials Laboratory, Inc., Columbus, Ohio. February, 1985.

6. Schneider, B., Mondragon, R., and Kirst, J., "Task Report NMERI, TAB-69 (8.36-01)", New Mexico Engineering Research Institute, Albuquerque, NM, June 1984, 83 pp.

7. Otter, D.E., and Naaman, A.E., "Steel Fiber Reinforced Concrete Under Static and Cyclic Compressive Loading," Proceedings of the Third International Symposium on Developments in Fiber Reinforced Cements and Concretes, Sheffield, England, July, 1986.

8. Fanella, D.A. and Naaman, A.E., "Stress-Strain Properties of Fiber Reinforced Mortar in Compression," Journal of the American Concrete Institute, Vol. 79, No. 4, July-August, 1985.

9. Absi, E., and Naaman, A.E., "Rheological Model of Fiber Concrete," Proceedings of the Third International Symposium on Developments in Fiber Reinforced Cements and Concretes, Sheffield, England, July, 1986, in French.

10. Baggott, R., and Sarandily, A., "Very High Strength Steel Fiber Reinforced Autoclave Mortars," Proceedings of RILEM Third International Symposium on Developments in Fiber Reinforced Cement and Concrete, Sheffield, July 1986.

11. Novokshchenov, Vladimir, "Cracking in Hot Climates," Concrete International Design and Construction, August, 1986, Vol.8, No.8, pp. 27-33.

12. Visalvanich, K. and Naaman, A.E., "A Fracture Model for Fiber Reinforced

Concrete," Journal of the American Concrete Institute, Vol. 80, No.2, Mar.-Apr. 1983, pp. 128-138.

13. Nammur, G.G., and Naaman, A.E., "Strain Rate Effects on the Tensile Properties of Fiber Reinforced Concrete," in Cement Based Composites - Strain Rate Effects on Fracture, S. Mindess, Editor, Materials Research Society, Pittsburgh, PA, 1986.

14. Naaman, A.E., "Fiber Reinforced Concrete Under Dynamic Loading," Special Publication SP-81, American Concrete Institute, Detroit, 1984, pp. 375 - 386.

15. Desayi, P. and Krishnan, S., "Equation for Stress-Strain Curve of Concrete," Journal of the American Concrete Institute, Proc. V. 61, March 1964, pp. 345-350.

16. Kaadi, G.W.,"Behavior of Fiber Reinforced Concrete Under High Rates of Tensile Loading," M.S. Thesis, University of Illinois, Chicago, 1981.

17. Popovics, S., "A Review of Stress-Strain Relationships for Concrete," Journal of the American Concrete Institute, Proc. 67, March 1970, pp. 243-248.

18. Saenz, L. P., Discussion of Reference [12], Journal of the American Concrete Institute, Proc. Vol. 61, No. 9, Sept. 1964, pp. 1229-1236.

19. Salse, E.A.B. and Fintel, M., "Strength, Stiffness and Ductility of Slender Shear Walls," Fifth World Conference on Earthquake Engineering, Rome 1973, Session 3A.

20. Sangha, C.M. and Dhir, R.K., "Strength and Complete Stress-Strain Relationships for Concrete Tested in Uniaxial Compression under Different Test Conditions," Matériaux et Construction, RILEM, Vol. 5, No. 30, 1972.

21. Sargin, M.,"Stress-Strain Relationship for Concrete and the Analysis of Structural Concrete Sections," Study No. 4, Solid Mechanics Division, University of Waterloo, Waterloo, Ontario, Canada, 1971, 167 pp.

22. Shah, S.P., Fafitis, A., and Arnold, R., "Cyclic Loading of Spirally Reinforced Concrete," ASCE Journal of the Structural Division, Vol. 109, No.7, July 1983, pp. 1695-1710.

23. Smith, G.M. and Young, L.E., "Ultimate Flexural Analysis Based on Stress-Strain Curve of Cylinders," Journal of the American Concrete Institute, Proc. Vol. 63, Dec. 1956, pp. 597-609.

24. Turner, P. W. and Barnard, P. R., "Stiff Constant Strain Rate Testing Machine," The Engineer (London), Vol. 214, No. 5557, July 1962, pp. 146-148.

APPENDIX A

UNREINFORCED MATRIX TESTS

A.1 Determination of Slurry Strength

As part of the experimental program, it was desired to obtain the ultimate strength of the plain unreinforced slurry matrix. To determine these strengths, 3x6-in plain, unreinforced cylinders of slurry were cast and cured in the same manner as the reinforced specimens. First, plain slurry cylinder specimens were poured into 3x6-in Plexiglas molds left to set overnight and unmolded 24 h later. The cylinders were then immersed into 70°F (21°C) water for 7 days. After 7 days, the cylinders were removed from the water and left to cure in the laboratory environment (70°F, 70% relative humidity). After two months of laboratory curing, the cylinders were tested in uniaxial compression at a constant stroke rate of 0.0005 in/s (83 μstrains/s).

Unfortunately, large visible shrinkage cracks developed during laboratory curing, and this significantly reduced specimen strengths. These cracks were probably caused by differential shrinkage during the period of exposure to the air. The outer layer of slurry shrinks more than the inner core during shelf curing periods, causing a differential shrinkage of outer layer and inner core. This causes shrinkage cracks to appear on the surface of the specimen. These cracks extended deep into the cylinders.

The results of the tests are shown in Table A1. Since the slurries are designed to be very high strength ($\geq$ 10,000 lb/in^2) the effect of shrinkage cracking was obviously to greatly reduce the strength of the cylinders. The resultant data are very inconsistent.

In an attempt to correct this difficulty, 2x2-in mortar cubes were cast and cured in the same manner as the 3x6-in cylinders. After 2 wk of laboratory environment curing, these cubes were tested in uniaxial compression to determine the matrix strength. The results are shown in Table A2. Tables A1 and A2 show that the strengths obtained from the cube tests are more consistent than those of the cylinder tests and yield matrix strengths closer to the predicted values.

Based on the results of these cube tests, the 2x2-in cube strengths of plain unreinforced mortar for Mixes One through Four examined in this study may be estimated to be 12.1 k/in^2, 10.3 k/in^2, 10.9 k/in^2, and 12.8 k/in^2 respectively.

Table A1. 3x6-in cylinder plain slurry strengths (lb/in^2).

Cylinder Number	Mix No.			
	1	2	3	4
1	9400	4100	4200	6500
2	6100	2300	5800	2400
3	9100	8770	4380	4000
4	5900	4200	7500	3700

Table A2. 2x2-in plain slurry cubes strengths (lb/in^2).

Cylinder Number	Mix No.			
	1	2	3	4
1	11275	10750	10625	14375
2	11275	10500	10000	13125
3	13250	10000	11000	10625
4	12750	9750	12000	13250
5	N.A.	9875	10875	N.A.
6	N.A.	10750	N.A.	N.A.
Average	12138	10271	10900	12844
Stand. Dev.	1025	450	726	1582

APPENDIX B

TWELVE-INCH COMPRESSION CYLINDERS

B.1 Effect of Specimen Size on Failure Mode

Tests of SIFCON cylinders in compression consistently yielded the same mode of shear failure. The SIFCON cylinder would separate into two halves which would then slide across each other. The angle of this failure crack would usually be of the ratio of 2-to-1. Since the ordinary specimens were 6 in high and 3 in wide and the failure plane would usually include one of the cylinder end surfaces, doubts arose as to whether the angled shear splitting plane was the true mode of failure in compression or whether the failure mode was due to the confining influence of the end platens.

To resolve this issue, four 3x12-in SIFCON cylinders were poured and tested in uniaxial compression. The results are shown in Chapter One of this report which includes a photograph of the tested specimens. All four cylinders failed at their midlength in the usual splitting mode of compression failure. Therefore, it is believed that this diagonal splitting of the specimen into halves is in fact the true mode of compression cylinder failure and occurs regardless of the effects of end platen confinement.

B.2 Effect of Lateral Confinement by Plattens on Compression Cylinder Tests

The failure mode of SIFCON compression cylinders is the development of a single diagonal shearing plane in the specimen. After the formation of this shearing plane, stress-displacement behavior is characterized by a relatively constant plateau stress over large displacements. This plateau stress is a measure of the shear strength of the interface between the two specimen halves as they slide across each other.

The completion of compression cylinder tests and subsequent release of the tested cylinder was always accompanied by some elastic strain recovery and an audible "bang" as one-half the tested specimen would jump laterally in its tested position. This indicated the presence of substantial lateral shear stress confinement at the point where the steel testing platen touched the SIFCON specimen.

To quantitatively investigate the effect of this lateral confinement, two series of cylinders with Mix One and crimped or hooked fibers were cast, tested with reduced confining stress, and compared to cylinders of the same composition with ordinary test confinement. The confining stress was reduced by placing oiled sheets of plastic on the ends of the experimental series cylinders during testing in the universal loading machine.

The comparison is shown graphically in Figures B1 and B2. The figures show that the effect of lateral confinement is indeed significant. The presence of lateral end-confinement shear stress appears to increase the observed ultimate strength of the SIFCON cylinders slightly. However, the most noticeable effect is in the post peak stress-strain response. In this region

the plateau stress is reduced by 1 to 2 k/in^2 for the cylinders with reduced lateral end confinement. This response is exactly as expected. With less lateral end confinement, movement of specimen halves across one another is easier and less load is required to compress the failed cylinder specimen.

To accurately measure the effect of this phenomenon requires the use of more sophisticated testing equipment than were used in this study. Such tests are recommended in future investigations.

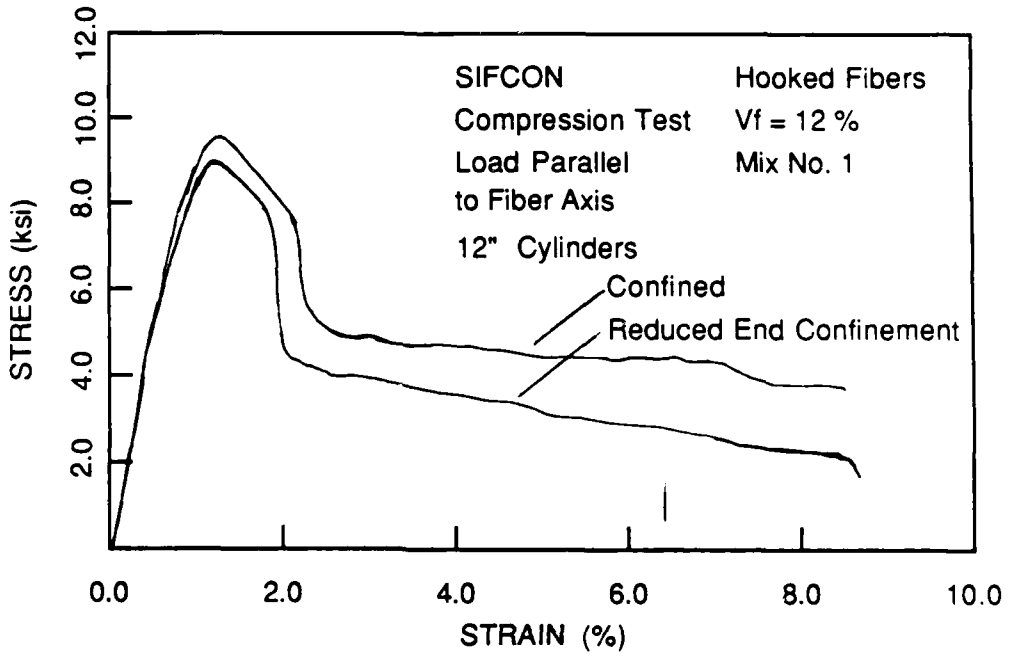

Figure B1. Effect of Platten Confinement on Test Results using Hooked Fibers.

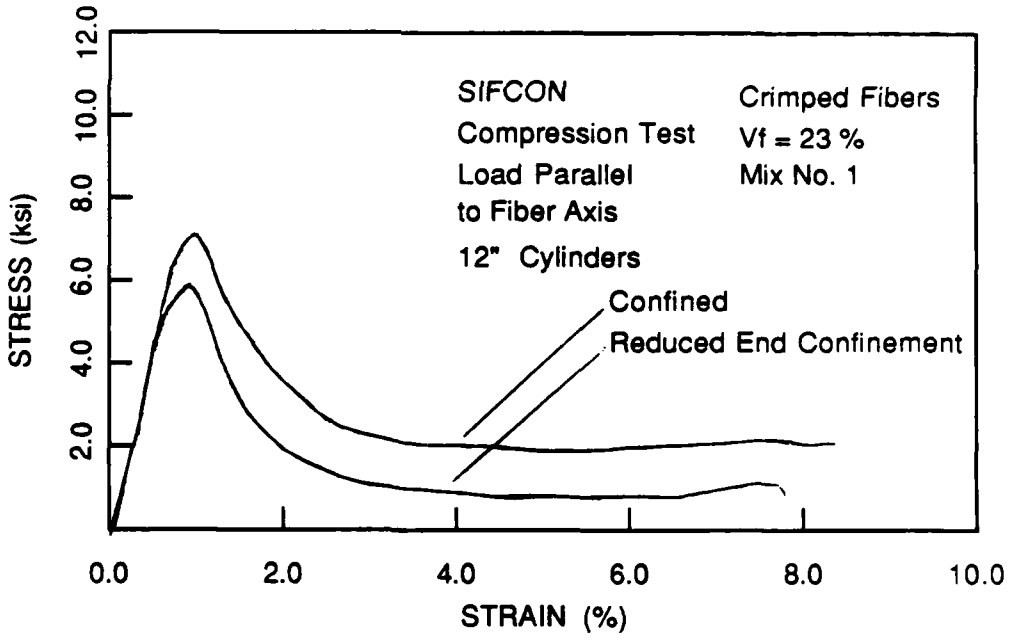

Figure B2. Effect of Platten Confinement on Test Results using Crimped Fibers.

APPENDIX C

PHYSICAL SPECIMEN DATA

Table C1. Compression cylinders load parallel to fiber axis.

Series Code	Spec.	Vf (%)	Weight (lbs)	Series Code	Spec.	Vf (%)	Weight (lbs)
CPX1	A	22.80	4.99	CPX3	A	22.17	4.86
	B	22.88	5.07		B	23.00	4.85
	C	22.92	5.06		C	22.17	4.87
	D	22.94	5.10		D	22.15	4.85
CPD1	A	12.89	4.00	CPD3	A	11.89	3.87
	B	12.80	4.02		B	11.92	3.86
	C	12.91	3.98		C	12.03	3.91
	D	12.93	4.12		D	11.80	3.83
CPS1	A	12.72	3.75	CPS3	A	12.89	3.92
	B	12.76	4.04		B	12.56	3.85
	C	12.78	4.14		C	12.05	3.82
	D	12.72	4.12		D	11.31	3.77
CPX2	A	22.88	4.95				
	B	23.00	5.00	—	—	—	—
	C	23.00	4.98				
	D	23.51	5.02				
CPD2	A	12.08	3.97	CPD4	A	12.58	4.10
	B	12.00	3.80		B	12.23	4.00
	C	12.01	3.85		C	11.99	3.96
	D	11.98	3.84		D	11.90	3.95
CPS2	A	12.36	3.96	CPS4	A	12.60	4.07
	B	12.51	4.02		B	11.86	3.97
	C	12.50	3.97		C	12.40	4.03
	D	12.38	3.88		D	11.85	4.01

Cylinder: 3" x 6"
Volume: 42.4 in^3

Table C2. Compression cylinders load normal to fiber axis (cored specimens).

Series Code	Spec.	Vf (%)	Weight (lbs)	Series Code	Spec.	Vf (%)	Weight (lbs)
CNX1B	A	22.79	4.53	CNX3B	A	22.67	4.38
	B		4.50		B		-
	C		4.48		C		-
	D		4.51		D		-
CND1B	A	12.05	3.41	CND3B	A	11.84	-
	B		3.38		B		-
	C		3.29		C		-
	D		3.36		D		-
CNS1B	A	12.13	3.43	CNS3B	A	12.00	3.42
	B		3.44		B		-
	C		3.36		C		-
	D		3.38		D		-
CNX2B	A	22.66	4.30	—	—	—	—
	B		-				
	C		-				
	D		-				
CND2B	A	11.62	3.41	CND4B	A	12.12	3.40
	B		3.43		B		3.40
	C		3.37		C		3.38
	D		3.32		D		3.40
CNS2B	A	12.05	-	CNS4B	A	12.02	3.40
	B		-		B		3.38
	C		-		C		3.37
	D		-		D		3.42

Cylinders: 2.75" x 6"
Volume: 35.6 in^3

Table C3. Compression cylinders load normal to fiber axis (molded specimens).

Series Code	Spec.	Vf (%)	Weight (lbs)	Series Code	Spec.	Vf (%)	Weight (lbs)
CNX1M	A	21.10	4.63	CNS2M	A	10.00	3.77
	B	22.00	4.77		B	9.90	3.69
	C	21.50	4.72		C	10.25	3.83
	D	22.00	4.76		D	9.95	3.72
CND1M	A	10.56	3.98				
	B	10.30	3.94	—	—	—	—
	C	9.90	3.91				
	D	9.90	3.91				
CNS1M	A	10.08	3.80	CNX3M	A	21.04	4.83
	B	9.81	3.70		B	21.13	4.91
	C	9.83	3.71		C	21.50	4.98
	D	9.85	3.72		D	21.70	5.04
CNX2M	A	21.20	4.82	CND3M	A	9.65	3.80
	B	21.40	4.92		B	9.65	3.79
	C	21.70	4.95		C	10.56	3.89
	D	21.04	4.76		D	10.40	3.85
CND2M	A	9.60	3.73	CNS3M	A	10.20	3.87
	B	10.50	3.83		B	10.23	3.88
	C	10.00	3.81		C	9.98	3.79
	D	10.10	3.81		D	10.05	3.83

Cylinders: 3" x 6"
Volume: 42.4 cubic inches

Table C4. Twelve-in-long compression cylinders.

Series Code	Spec.	Vf (%)	Weight (lbs)	Series Code	Spec.	Vf (%)	Weight (lbs)
CLD1M	A	11.23	-	CLS1M	A	22.50	-
	B	11.23	-		B	22.50	-
	C	11.43	-		C	21.74	-

Table C5. Tension prisms (notched specimens).

Series Code	Spec.	Vf (%)	Weight (lbs)	Series Code	Spec.	Vf (%)	Weight (lbs)
TPX1R	A	23.00	19.30	TPS2R	A	12.79	14.46
	B		18.58		B		13.83
	C		19.04		C		14.48
	D		19.42		D		14.03
TPD1R	A	12.00	14.56	—	—	—	—
	B		15.36				
	C		15.52				
	D		-				
TPS1R	A	11.76	15.62	TPX3R	A	22.72	18.81
	B		14.77		B		19.12
	C		-		C		18.86
	D		15.50		D		18.83
TPX2R	A	23.00	19.21	TPD3R	A	12.60	15.17
	B		19.24		B		15.01
	C		19.11		C		14.86
	D		18.86		D		14.84
TPD2R	A	12.78	15.08	TPS3R	A	10.78	14.57
	B		15.00		B		14.38
	C		15.10		C		14.83
	D		15.02		D		14.42

Table C6. Tension prisms (dogbone specimens).

Series Code	Spec.	Vf (%)	Weight (lbs)	Series Code	Spec.	Vf (%)	Weight (lbs)
TPD1D	A	11.72	12.53	TPD4D	A	12.10	12.97
	B		12.37		B		12.80
	C		12.60		C		12.43
	D		12.60				12.60
TPS1D	A	12.64	12.93	TPS4D	A	13.77	12.93
	B		12.72		B		13.16
	C		12.90		C		13.24
	D		12.46		D		-

Fiber Packing Table

Fiber Tradename	Supplier	length	diameter	l / ϕ	Fiber Volume Fraction		
					No Vibr.	Mod. Vibr.[a]	Heavy Vibr.[b]
Xorex II	RibTec	1.5 "	0.035 "	40	-	16	-
		1 "	0.035 "	30	20	23	-
Dramix	Bekaert	50 mm	0.5 mm	100	3	5	-
		30 mm	0.5 mm	60	10	12	16
Surecrete	Surecrete	30 mm	0.5 mm	60	9	12	17
Fibercon	Mitchell Fibercon Inc.	0.75 "	0.01" x 0.022 "	40	-	17	-

[a] 10-min vibration on a vibration table satisfying testing standard ASTM C-138, C-192 at 3600 r/m (maximum table capacity).

[b] 1-h vibration on a vibration table satisfying testing standard ASTM C-138, C-192.

APPENDIX E

ADDITIONAL FIGURES OF STRESS-STRAIN CURVES IN COMPRESSION

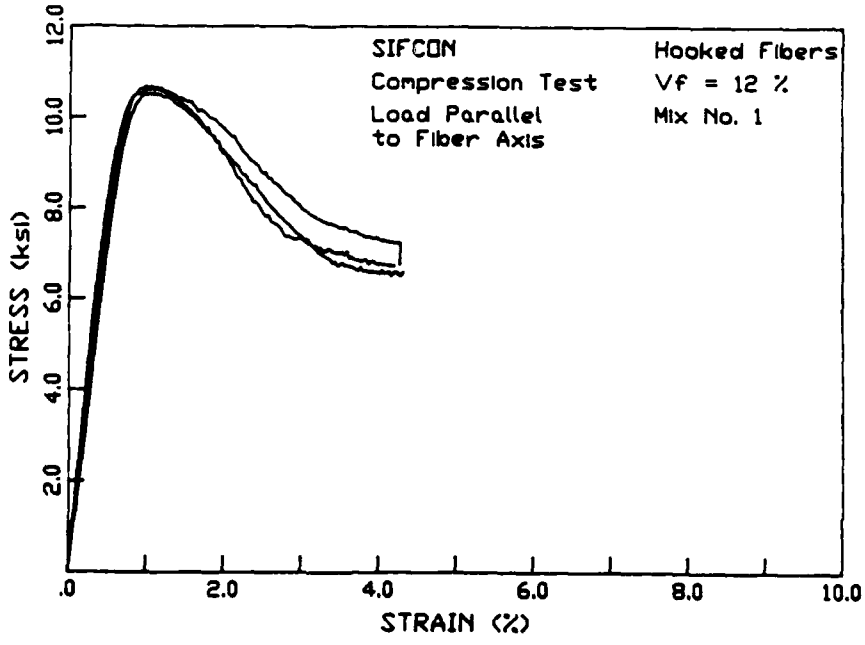
SIFCON
Compression Test
Load Parallel
to Fiber Axis
Hooked Fibers
Vf = 12 %
Mix No. 1
STRESS (ksi)
12.0
10.0
8.0
6.0
4.0
2.0
.0
2.0
4.0
6.0
8.0
10.0
STRAIN (%)

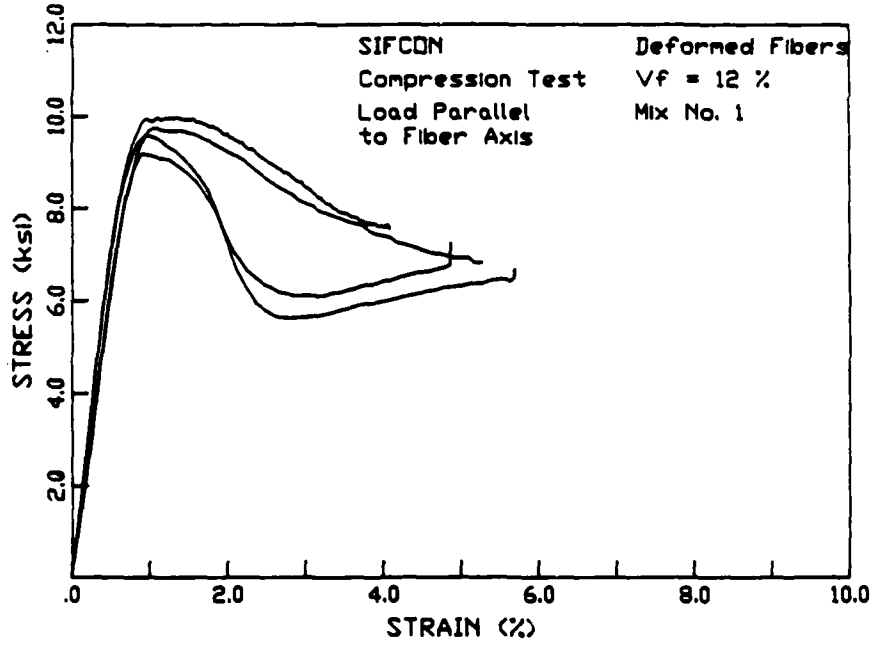
SIFCON
Compression Test
Load Parallel
to Fiber Axis
Deformed Fibers
Vf = 12 %
Mix No. 1
STRESS (ksi)
12.0
10.0
8.0
6.0
4.0
2.0
.0
2.0
4.0
6.0
8.0
10.0
STRAIN (%)

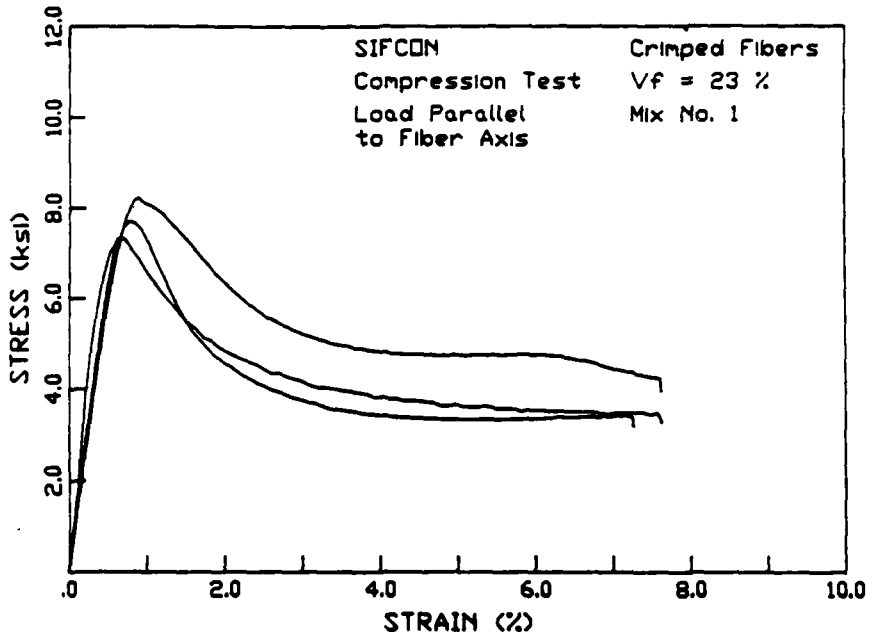
SIFCON
Compression Test
Load Parallel
to Fiber Axis
Crimped Fibers
Vf = 23 %
Mix No. 1
STRESS (ksi)
12.0
10.0
8.0
6.0
4.0
2.0
.0
2.0
4.0
6.0
8.0
10.0
STRAIN (%)

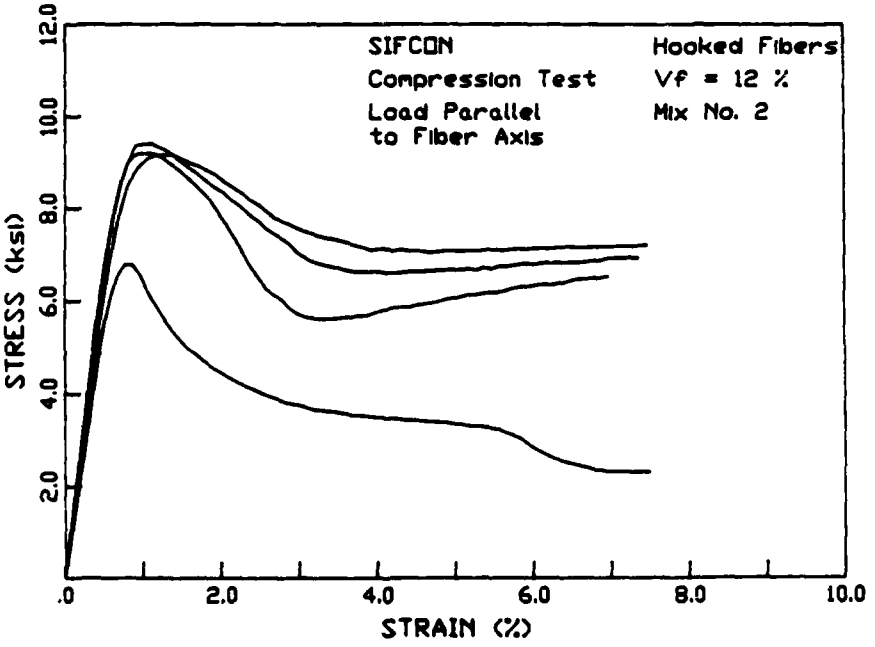
SIFCON
Compression Test
Load Parallel
to Fiber Axis
Hooked Fibers
Vf = 12 %
Mix No. 2
STRESS (ksi)
12.0
10.0
8.0
6.0
4.0
2.0
.0
2.0
4.0
6.0
8.0
10.0
STRAIN (%)

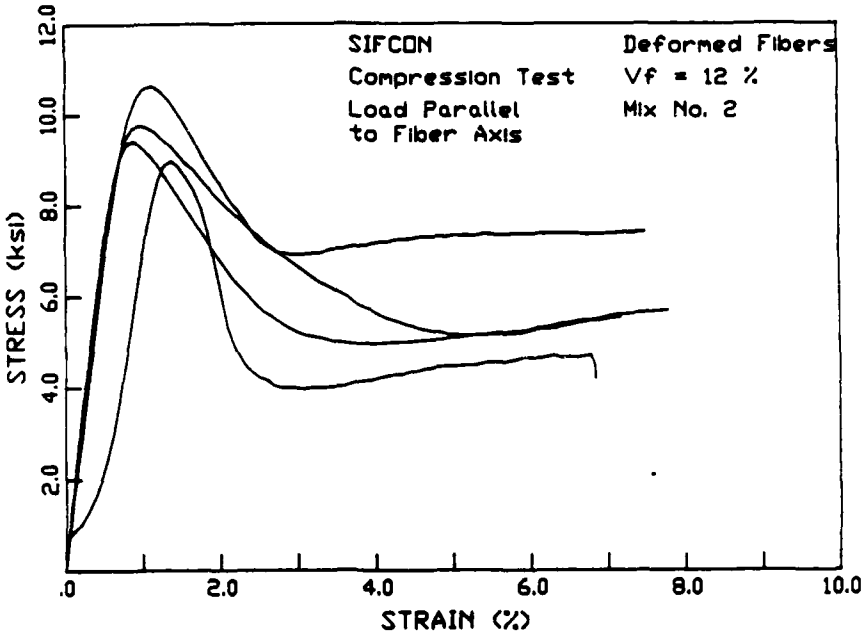
SIFCON
Compression Test
Load Parallel
to Fiber Axis
Deformed Fibers
Vf = 12 %
Mix No. 2
STRESS (ksi)
12.0
10.0
8.0
6.0
4.0
2.0
.0
2.0
4.0
6.0
8.0
10.0
STRAIN (%)

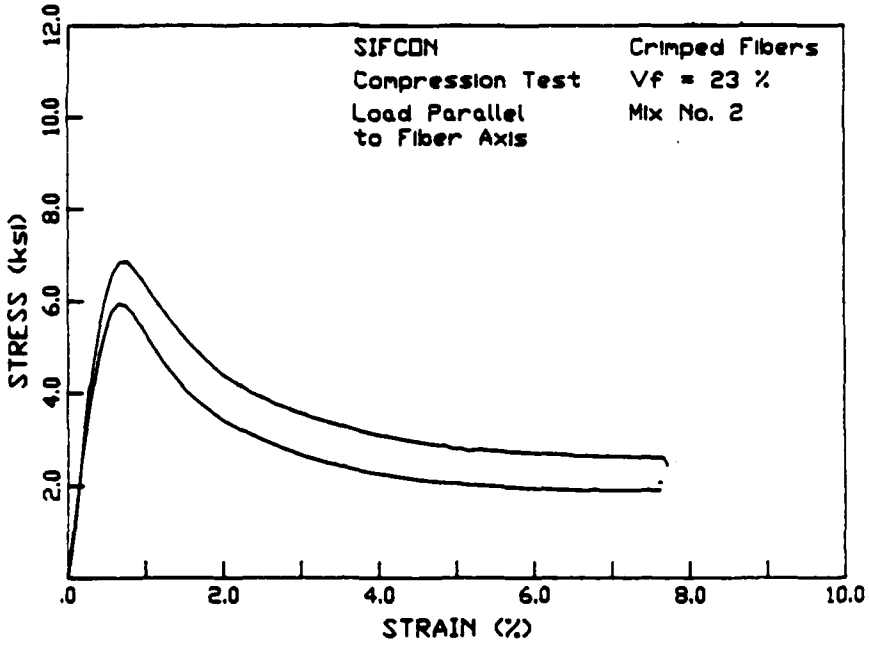
SIFCON
Compression Test
Load Parallel
to Fiber Axis
Crimped Fibers
Vf = 23 %
Mix No. 2
STRESS (ksi)
12.0
10.0
8.0
6.0
4.0
2.0
.0
2.0
4.0
6.0
8.0
10.0
STRAIN (%)

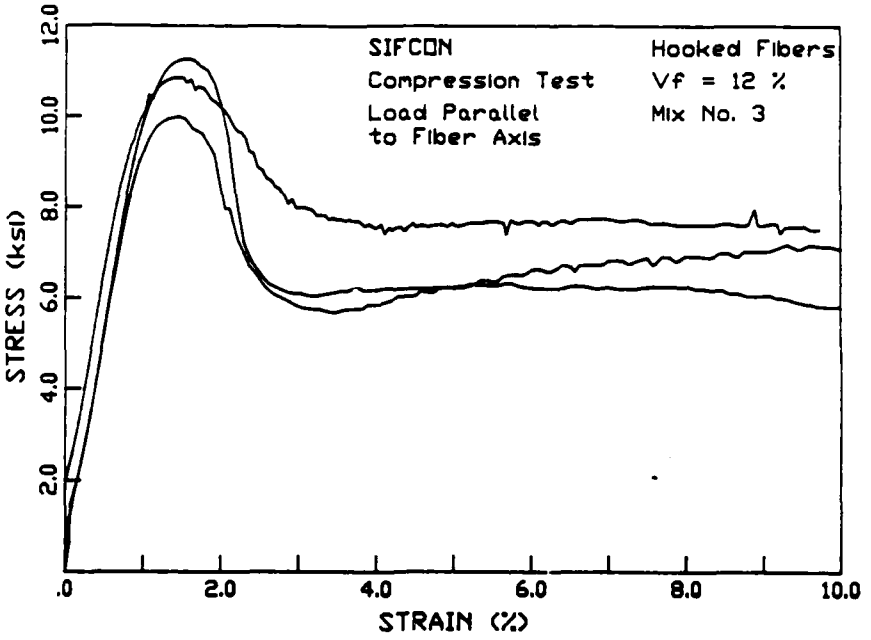
SIFCON
Compression Test
Load Parallel
to Fiber Axis
Hooked Fibers
Vf = 12 %
Mix No. 3
STRESS (ksi)
12.0
10.0
8.0
6.0
4.0
2.0
.0
2.0
4.0
6.0
8.0
10.0
STRAIN (%)

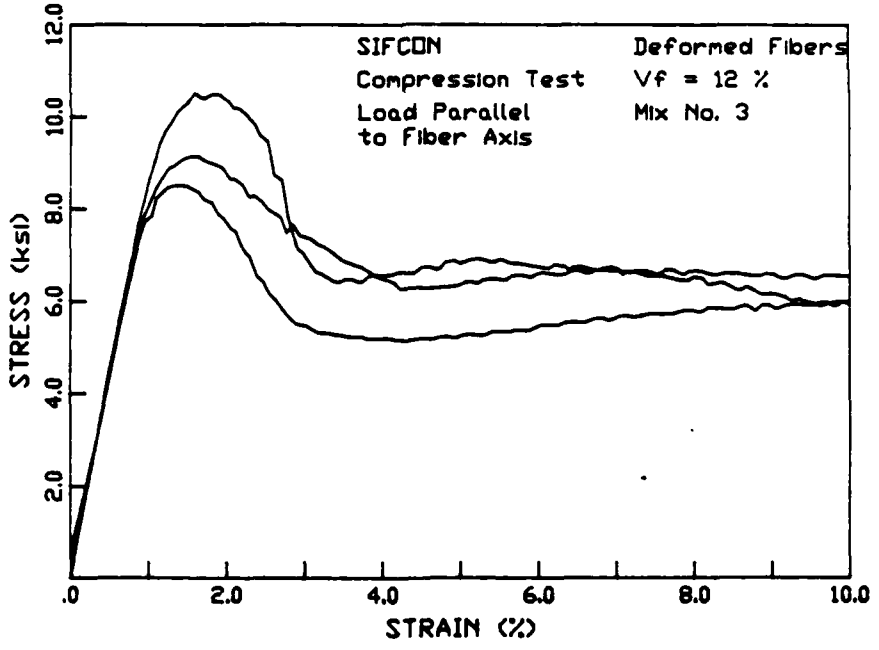
SIFCON
Compression Test
Load Parallel
to Fiber Axis
Deformed Fibers
Vf = 12 %
Mix No. 3
STRESS (ksi)
12.0
10.0
8.0
6.0
4.0
2.0
.0
2.0
4.0
6.0
8.0
10.0
STRAIN (%)

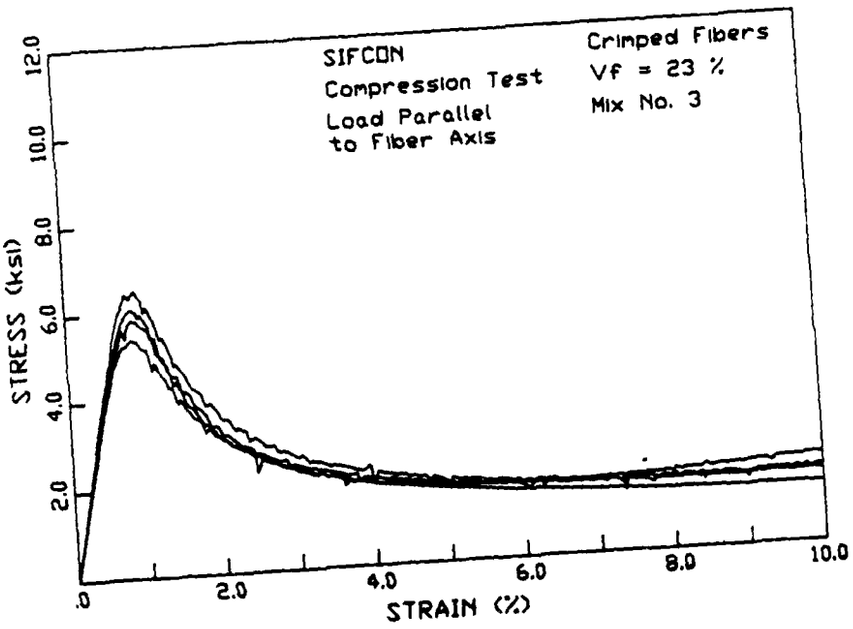
SIFCON
Compression Test
Load Parallel
to Fiber Axis
Crimped Fibers
Vf = 23 %
Mix No. 3
STRESS (ksi)
12.0
10.0
8.0
6.0
4.0
2.0
0
2.0
4.0
6.0
8.0
10.0
STRAIN (%)

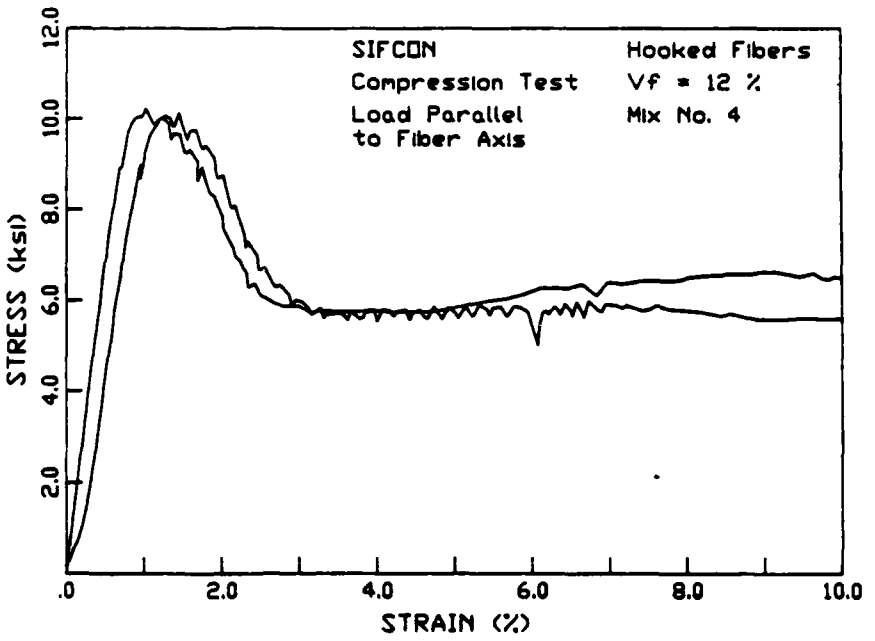
SIFCON
Compression Test
Load Parallel
to Fiber Axis
Hooked Fibers
Vf = 12 %
Mix No. 4
STRESS (ksi)
STRAIN (%)
2.0
4.0
6.0
8.0
10.0
12.0
.0
2.0
4.0
6.0
8.0
10.0

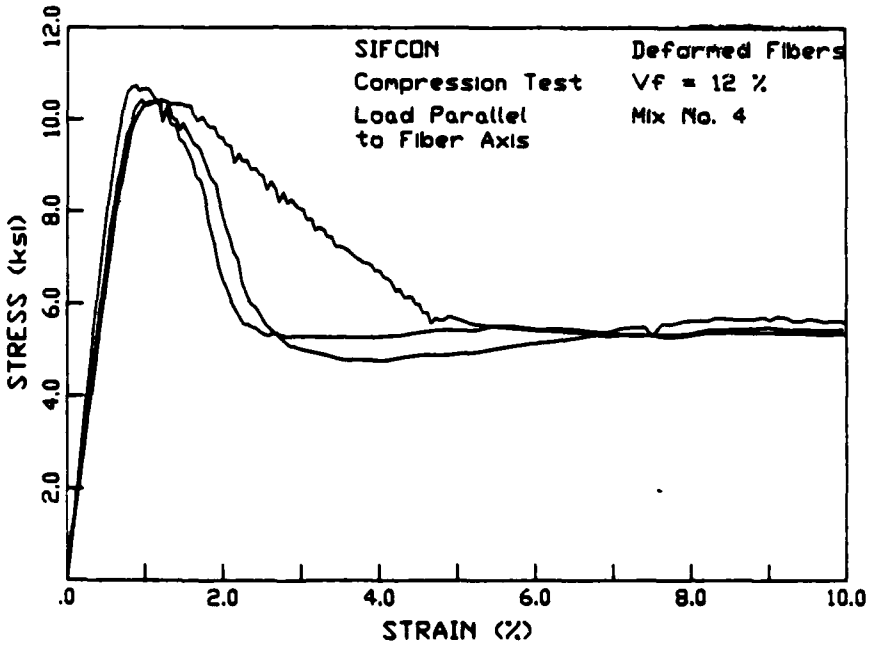
SIFCON
Compression Test
Load Parallel
to Fiber Axis
Deformed Fibers
Vf = 12 %
Mix No. 4
STRESS (ksi)
STRAIN (%)
2.0
4.0
6.0
8.0
10.0
12.0
.0
2.0
4.0
6.0
8.0
10.0

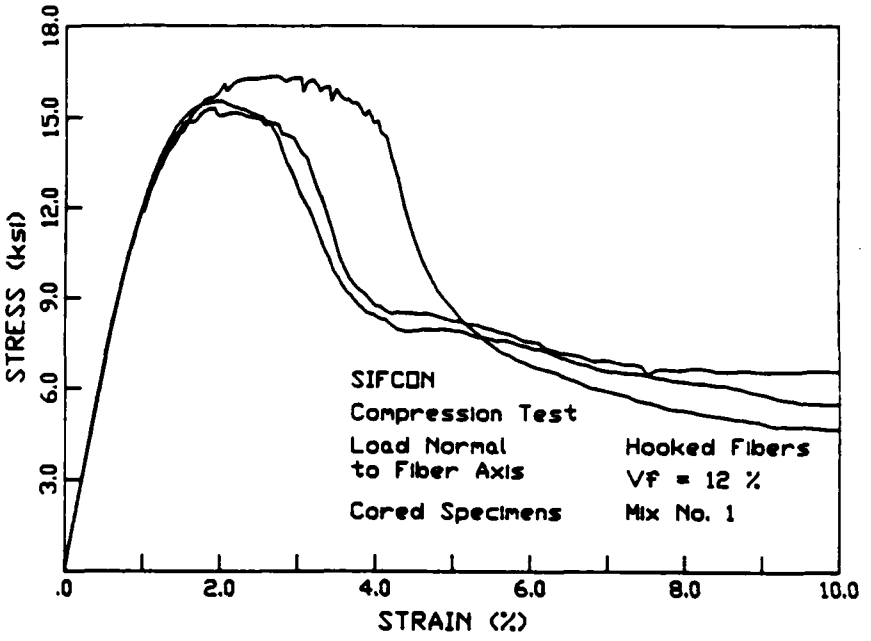
STRESS (ksi)
18.0
15.0
12.0
9.0
6.0
3.0
.0
2.0
4.0
6.0
8.0
10.0
STRAIN (%)
SIFCON
Compression Test
Load Normal
to Fiber Axis
Cored Specimens
Hooked Fibers
Vf = 12 %
Mix No. 1

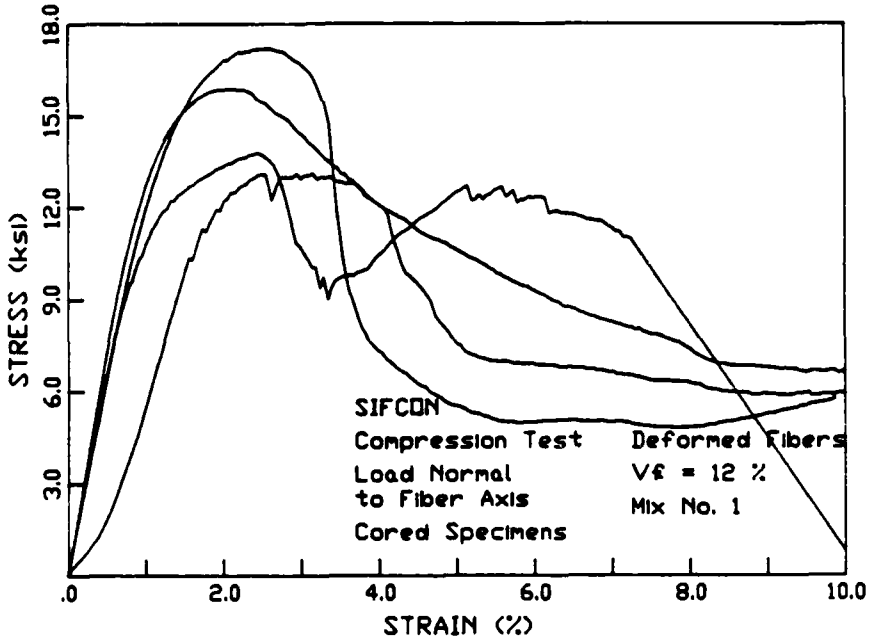
STRESS (ksi)
18.0
15.0
12.0
9.0
6.0
3.0
.0
2.0
4.0
6.0
8.0
10.0
STRAIN (%)
SIFCON
Compression Test
Load Normal
to Fiber Axis
Cored Specimens
Deformed Fibers
Vf = 12 %
Mix No. 1

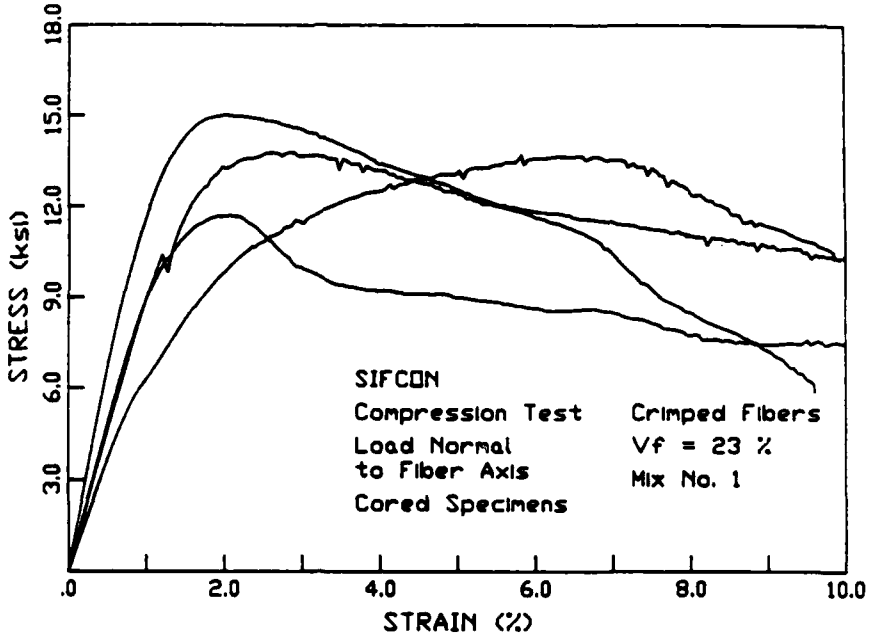
STRESS (ksi)
3.0
6.0
9.0
12.0
15.0
18.0
.0
2.0
4.0
6.0
8.0
10.0
STRAIN (%)
SIFCON
Compression Test
Load Normal
to Fiber Axis
Cored Specimens
Crimped Fibers
Vf = 23 %
Mix No. 1

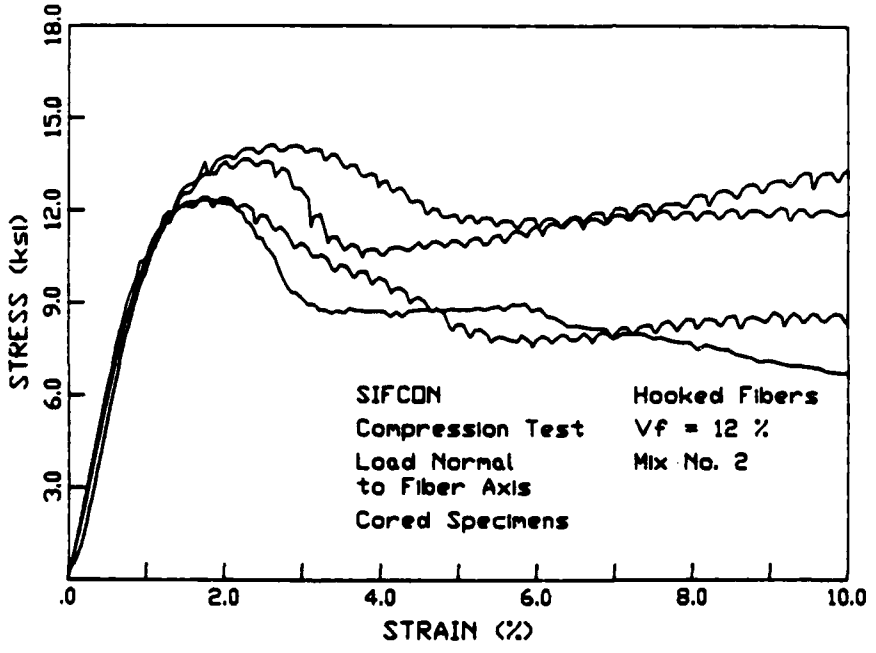
STRESS (ksi)
3.0
6.0
9.0
12.0
15.0
18.0
.0
2.0
4.0
6.0
8.0
10.0
STRAIN (%)
SIFCON
Compression Test
Load Normal
to Fiber Axis
Cored Specimens
Hooked Fibers
Vf = 12 %
Mix No. 2

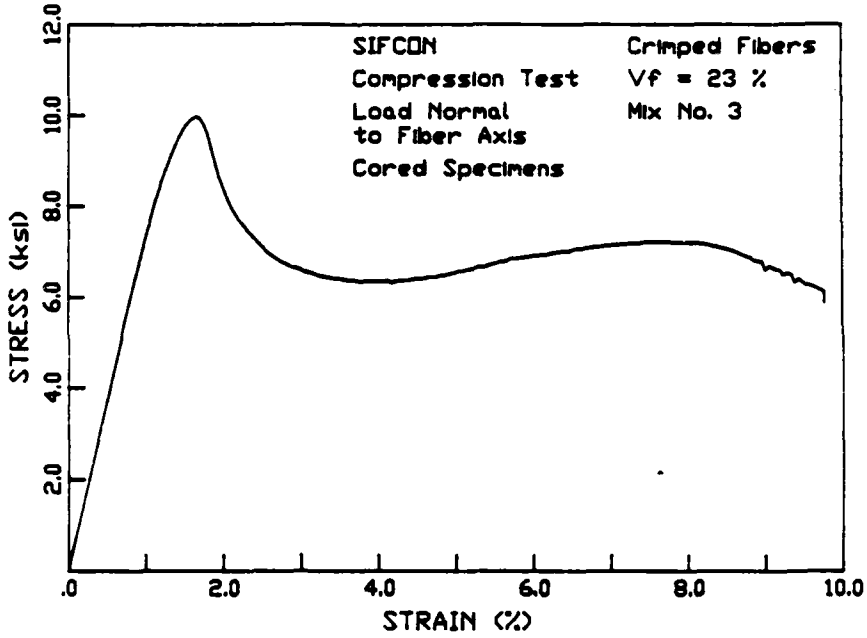
SIFCON
Compression Test
Load Normal
to Fiber Axis
Cored Specimens
Crimped Fibers
Vf = 23 %
Mix No. 3
STRESS (ksi)
12.0
10.0
8.0
6.0
4.0
2.0
.0
2.0
4.0
6.0
8.0
10.0
STRAIN (%)

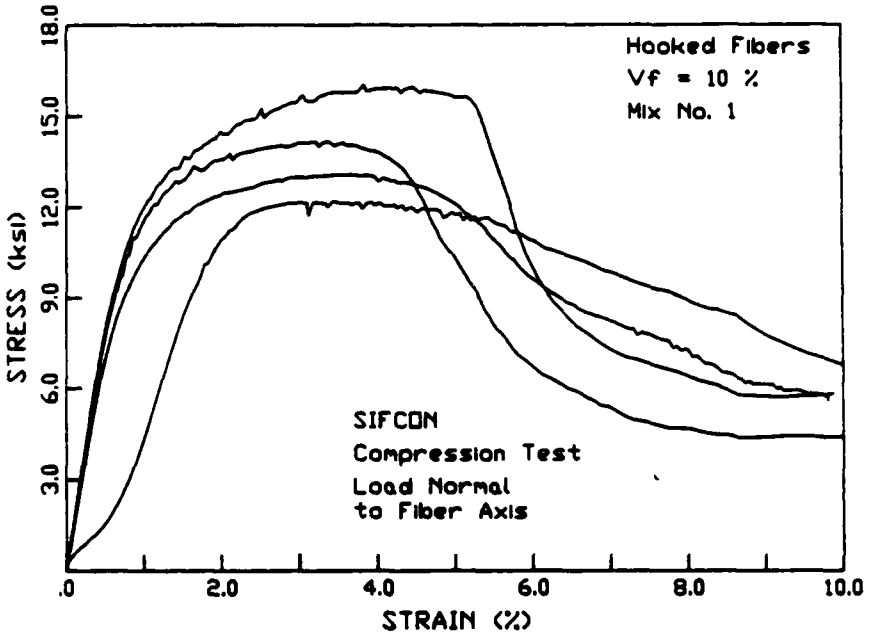
Hooked Fibers
Vf = 10 %
Mix No. 1
SIFCON
Compression Test
Load Normal
to Fiber Axis
STRESS (ksi)
3.0
6.0
9.0
12.0
15.0
18.0
.0
2.0
4.0
6.0
8.0
10.0
STRAIN (%)

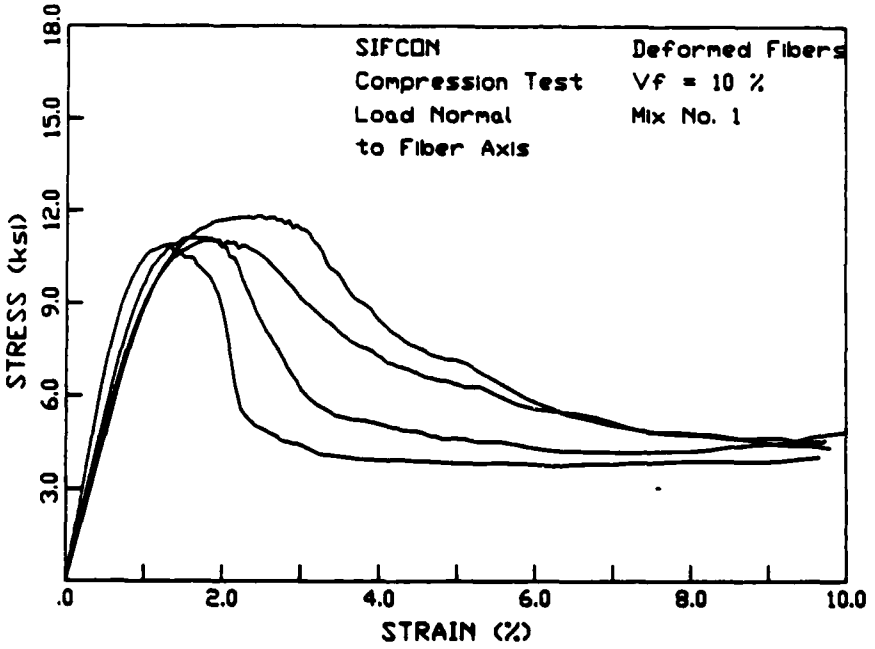
SIFCON
Compression Test
Load Normal
to Fiber Axis
Deformed Fibers
Vf = 10 %
Mix No. 1
STRESS (ksi)
3.0
6.0
9.0
12.0
15.0
18.0
.0
2.0
4.0
6.0
8.0
10.0
STRAIN (%)

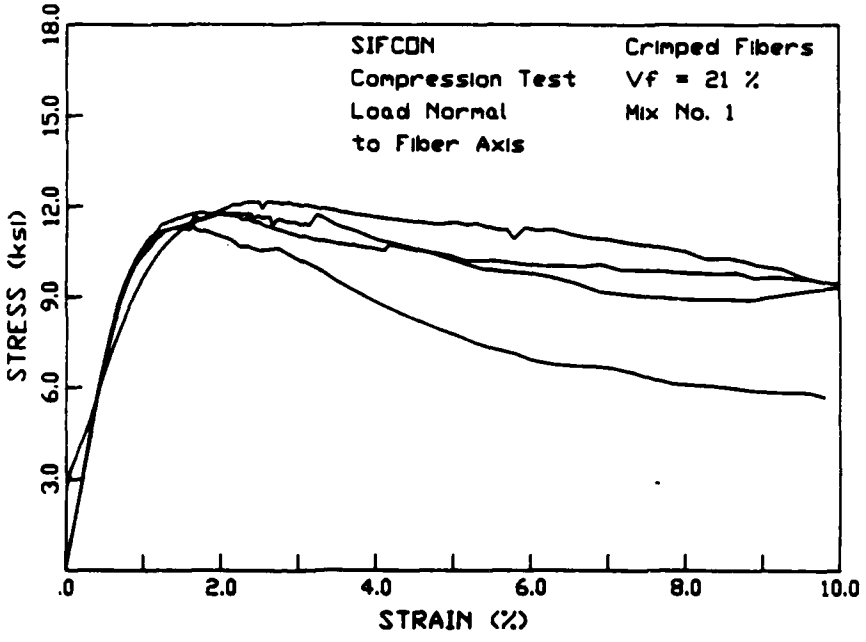
SIFCON
Compression Test
Load Normal
to Fiber Axis
Crimped Fibers
Vf = 21 %
Mix No. 1
STRESS (ksi)
18.0
15.0
12.0
9.0
6.0
3.0
.0
2.0
4.0
6.0
8.0
10.0
STRAIN (%)

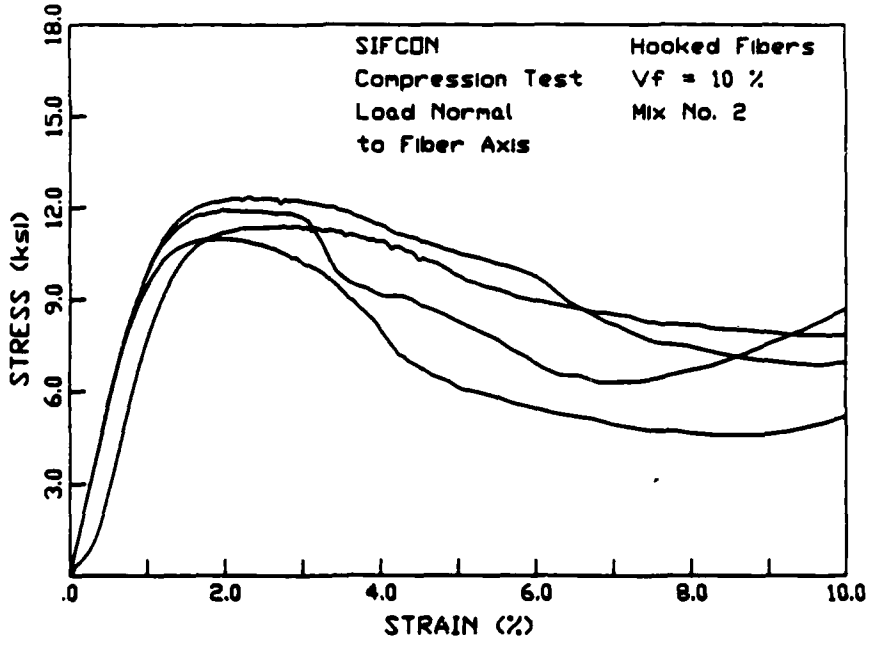
SIFCON
Compression Test
Load Normal
to Fiber Axis
Hooked Fibers
Vf = 10 %
Mix No. 2
STRESS (ksi)
18.0
15.0
12.0
9.0
6.0
3.0
.0
2.0
4.0
6.0
8.0
10.0
STRAIN (%)

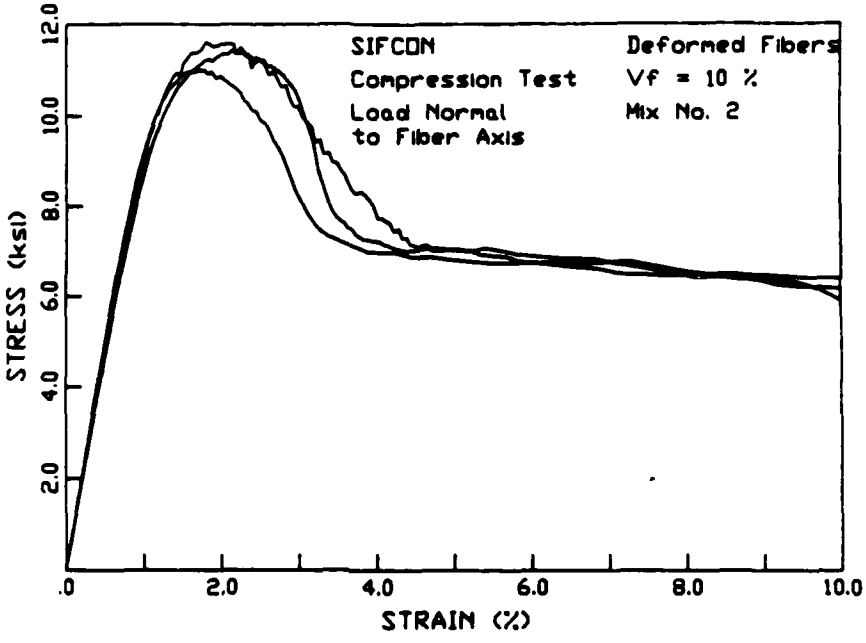
SIFCON
Compression Test
Load Normal
to Fiber Axis
Deformed Fibers
Vf = 10 %
Mix No. 2
STRESS (ksi)
12.0
10.0
8.0
6.0
4.0
2.0
.0
2.0
4.0
6.0
8.0
10.0
STRAIN (%)

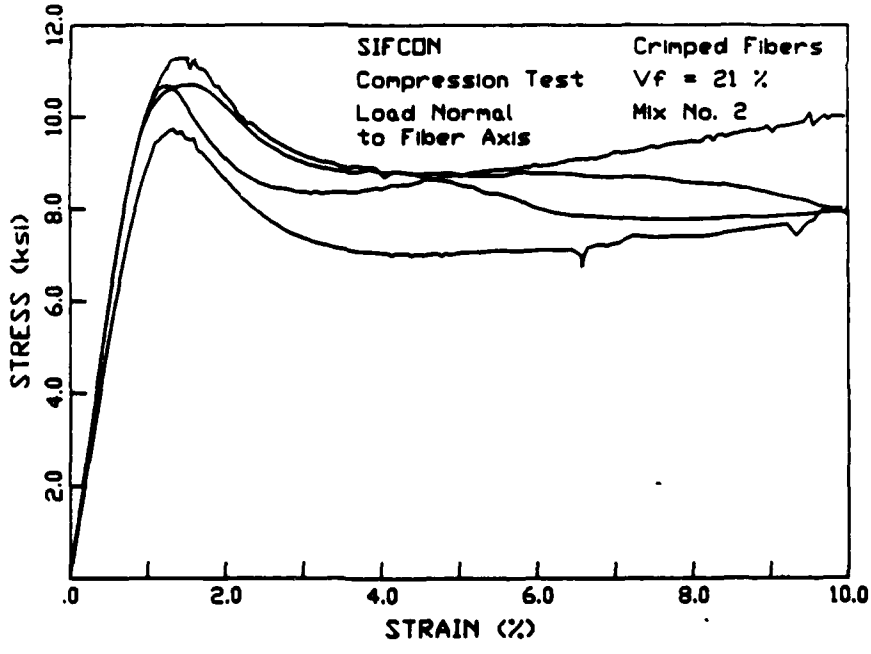
SIFCON
Compression Test
Load Normal
to Fiber Axis
Crimped Fibers
Vf = 21 %
Mix No. 2
STRESS (ksi)
12.0
10.0
8.0
6.0
4.0
2.0
.0
2.0
4.0
6.0
8.0
10.0
STRAIN (%)

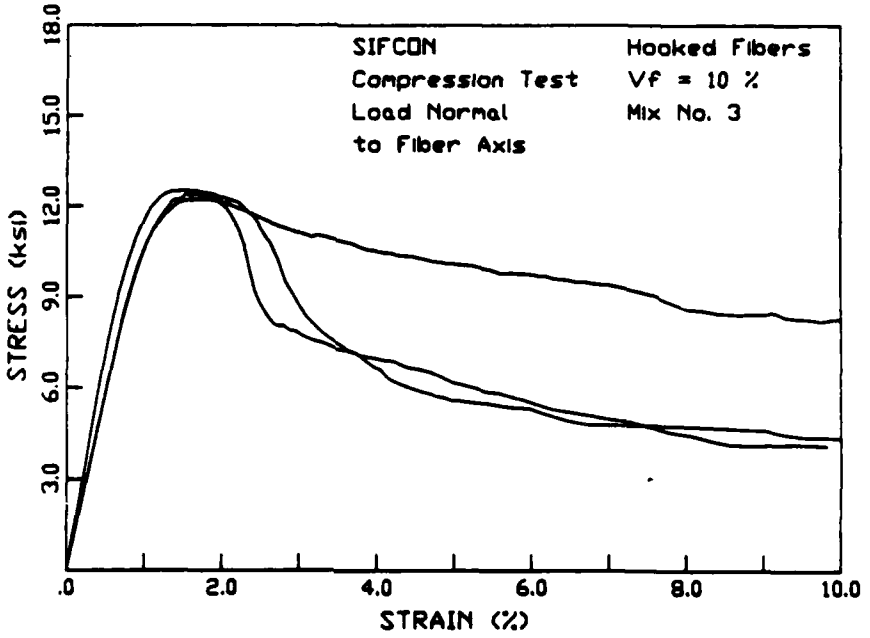
SIFCON
Compression Test
Load Normal
to Fiber Axis
Hooked Fibers
Vf = 10 %
Mix No. 3
STRESS (ksi)
18.0
15.0
12.0
9.0
6.0
3.0
.0
2.0
4.0
6.0
8.0
10.0
STRAIN (%)

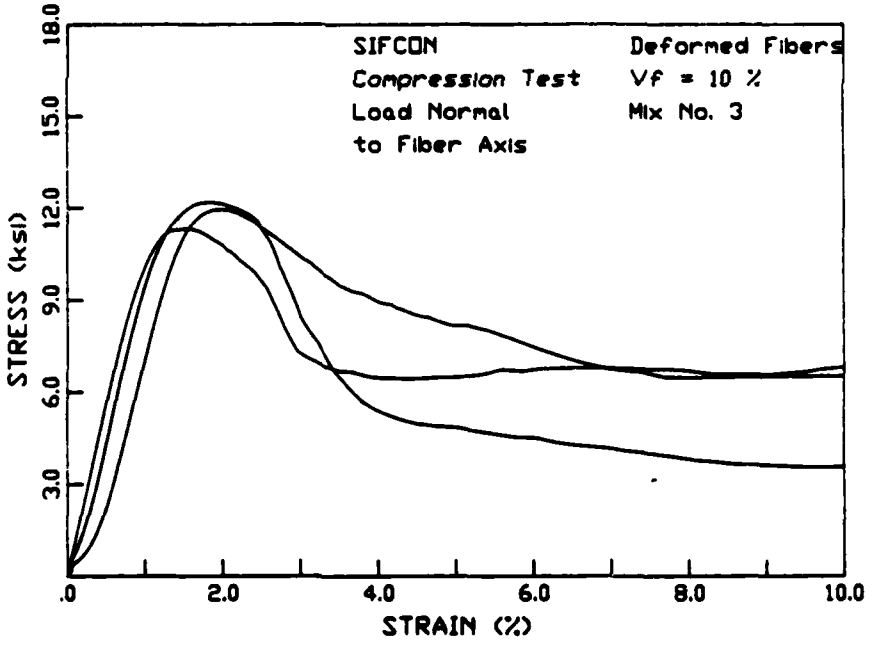
SIFCON
Compression Test
Load Normal
to Fiber Axis
Deformed Fibers
Vf = 10 %
Mix No. 3
STRESS (ksi)
18.0
15.0
12.0
9.0
6.0
3.0
.0
2.0
4.0
6.0
8.0
10.0
STRAIN (%)

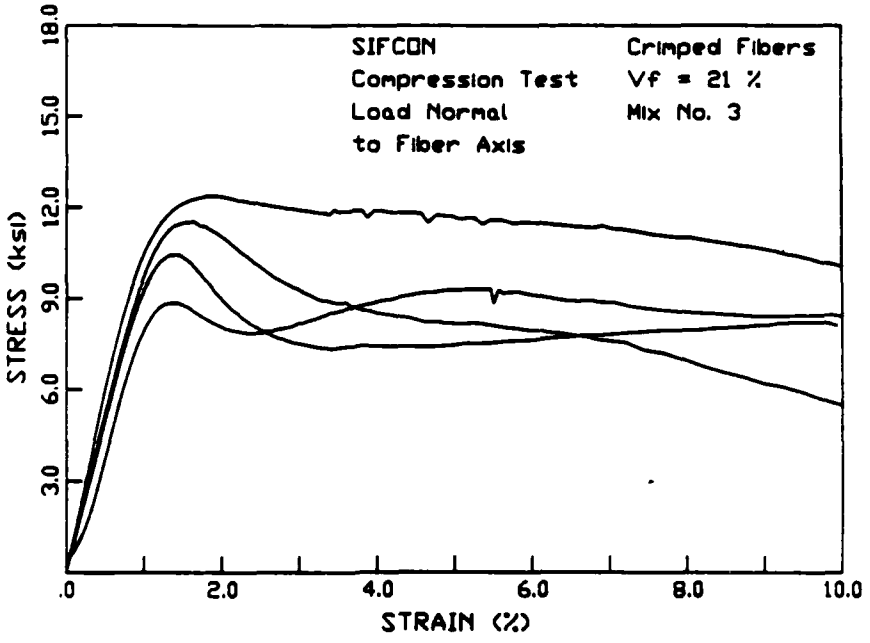
SIFCON
Compression Test
Load Normal
to Fiber Axis
Crimped Fibers
Vf = 21 %
Mix No. 3
STRESS (ksi)
18.0
15.0
12.0
9.0
6.0
3.0
.0
2.0
4.0
6.0
8.0
10.0
STRAIN (%)

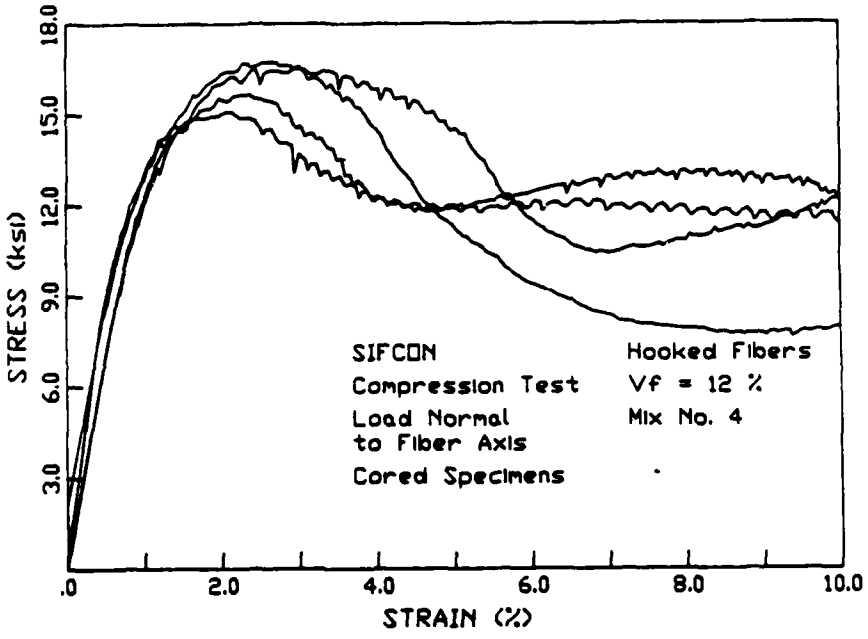
STRESS (ksi)
18.0
15.0
12.0
9.0
6.0
3.0
.0
2.0
4.0
6.0
8.0
10.0
STRAIN (%)
SIFCON
Compression Test
Load Normal
to Fiber Axis
Cored Specimens
Hooked Fibers
Vf = 12 %
Mix No. 4

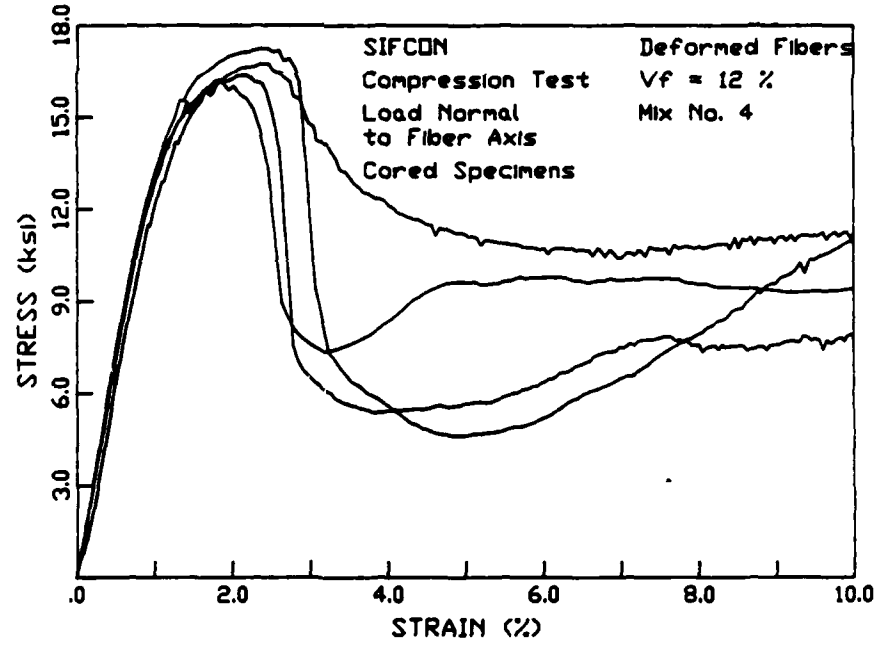
STRESS (ksi)
18.0
15.0
12.0
9.0
6.0
3.0
.0
2.0
4.0
6.0
8.0
10.0
STRAIN (%)
SIFCON
Compression Test
Load Normal
to Fiber Axis
Cored Specimens
Deformed Fibers
Vf = 12 %
Mix No. 4

APPENDIX F

COMPRESSIVE STRENGTH COMPARISON BETWEEN CORED AND POURED SPECIMENS

F.1 Background

Previous testing of SIFCON has revealed that there is a considerable difference in the recorded uniaxial compressive strength of specimens which are poured and those which are cored from slabs. The difference is caused by a phenomenon called edge effects, whereby the steel fibers do not align themselves randomly near the edge of the mold but, instead, tend to align themselves along the surface of the mold. This effect causes lesser strength to be observed in specimens which are poured than in those which are cored. As is customary in construction work, compressive strength tests are performed as a quality control check. Since coring requires special equipment that is much more expensive than pouring in molds, it is beneficial to establish a correlation between cored and poured specimens. The real strength of SIFCON in compression could hence be ecomomically obtained from standard cylinder specimens poured and tested according to ASTM recommendations.

F.2 Objective and Scope

The main objective of the work described in this Appendix is to compare the compressive strength of SIFCON specimens which are cored to those which are poured, and develop a simple relationship to allow prediction of cored specimen compressive strength from poured specimen compressive strength and vice-versa.

F.3 Experimental Program

The experimental program of this Appendix has been integrated in the overall experimental program of this report. Specifically, it consists of 11 series each of cored and poured compressive test specimens. These are described in the last part of Figure 3 and apply to specimens where the fiber axis is primarily normal to the loading axis of the cylindrical specimens. Edge effects would not be present if the fibers were parallell to the loading axis. The experimental variables are described in Figure 3 and include three types of fibers and four types of matrices. The fibers and the matrices are described in Tables 1 and 2. Figure 3 also gives the identification code for each series of tests. The notation code is explained in detail in Figure 2 of the Executive Summary at the beginning of this report. Poured specimens were 3x6-in cylinders, while cored specimens were 2.75x6 in. At first, cored specimens were capped with a thin layer of "Cyclap" a high strength sulfur compound. However, as the capping started "shattering and exploding" beyond stresses of about 12 k/in^2 the capping was eliminated. It seems that SIFCON 's deformation characteristics are such that it can easily adapt to small differences in end face parllellism and roughness. Its stress-strain response in compression goes far in the nonelastic plastic range of behavior, thus the need for capping is not as important as in plain concrete. As mentioned in Section 1,

poured specimens were tested without capping. This is because they were poured in special molds that allowed perfectly flat and parallel end surfaces.

All the specimens were tested according to the test procedure described in Section 1, except that some specimens were tested in compression up to 5% total strain instead ot 10%. Compressive strength results are summarized in Table F1 of this Appendix, while Table F2 provides a comparison between the average strength of poured and cored specimens for the eleven series of tests. The three phases mentioned in Table F2 refer to three different test periods. These were necessary since in many instances cored specimens were damaged during coring and the corresponding series had to be prepared again.

It can be observed from Table F2 that the ratio of compressive strength of cored specimens to that of poured specimens varied between 1.06 and 1.52, with an average of 1.28. As expected cored specimens led to compressive strengths consistently higher than poured specimens

An attempt was made to see if a correlation can be obtained between the compressive strength of cored and poured specimens that can reflect strengths levels of the order of 10 to 20 k/in^2. The results are shown in Figure F1 where the average strength of each series of cored specimens is plotted against the average strength of the identical series of poured specimens. A least square fit line was obtained from the average data and led to the following equation plotted in Figure F1:

$$f'_{cc} = 1.35\ f'_{cp} - 0.77 \qquad (k/in^2) \qquad (F1)$$

where f'_{cc} and f'_{cp} are the compressive strengths of cored and poured specimens respectively.

It should be noted that the above relationship holds for a range of compressive strengths between 10 and 20 k/in^2. As can be observed from Figure F1, the correlation is poor, hence an average ratio of 1.28 may be used in practice to predict the compressive strength of cored SIFCON specimens from poured specimens.

It should be noted however that the above relationship applies only for the sizes of fibers and molds used in this investigation. It is believed that different sizes will lead to different relationships.

Figures F2 and F3 show typical comparisons between the stress-strain curves in compression of cored versus poured SIFCON specimens for two types of fibers used. Additional curves are shown in Figures F4 to F8 for various cored specimens prepared with different matrices.

F.4 Conclusion

Based on the results of the limited investigation described in this Appendix, it is recommended that the compressive strength of cored SIFCON specimens be predicted from that of identical but poured specimens using an average ratio of 1.28, that is:

$$f'_{cc} = 1.28\ f'_{cp} \qquad \text{(F2)}$$

Table F1. Cored SIFCON test results.

SERIES	No.	fc' (k/in^2)	SERIES AVG. fc'(k/in^2)
CNH2B	1	14.1	13.2
	2	16.4	
	3	9.2	
	4	----	
CND2B	1	15.2	15.8
	2	15.5	
	3	16.4	
	4	16.0	
CNS2B	1	16.8	17.2
	2	18.1	
	3	16.8	
	4	----	
CNH3B	1	13.0	12.7
	2	15.7	
	3	12.0	
	4	10.0	
CND3B	1	15.7	15.6
	2	14.7	
	3	16.5	
	4	15.6	
CNS3B	1	15.9	16.7
	2	17.4	
	3	----	
	4	----	
CND4B	1	18.2	18.8
	2	20.5	
	3	17.4	
	4	19.1	
CNS4B	1	15.8	16.3
	2	16.8	
	3	16.	
	4	16.7	

Table F2. Comparison of cored and poured test series.

SERIES	AVG. f'c POURED (k/in^2)	AVG. f'c CORED (k/in^2)			RATIO Cored/Poured
		PHASE 1	PHASE 2	PHASE 3	
CNH1	11.7	13.4	----		1.15
CND1	13.6	15.4	----		1.13
CNS1	11.0	14.9	----		1.35
CNH2	10.5	----	13.2		1.26
CND2	11.5	13.1	15.8		1.26
CNS2	11.3	----	17.2		1.52
CNH3	10.7	10.0	12.7		1.06
CND3	12.2	----	15.6		1.28
CNS3	11.7	----	16.7		1.43
CCD4	12.6	16		18.8	1.38
CNS4	13.1	16.7		16.3	1.26

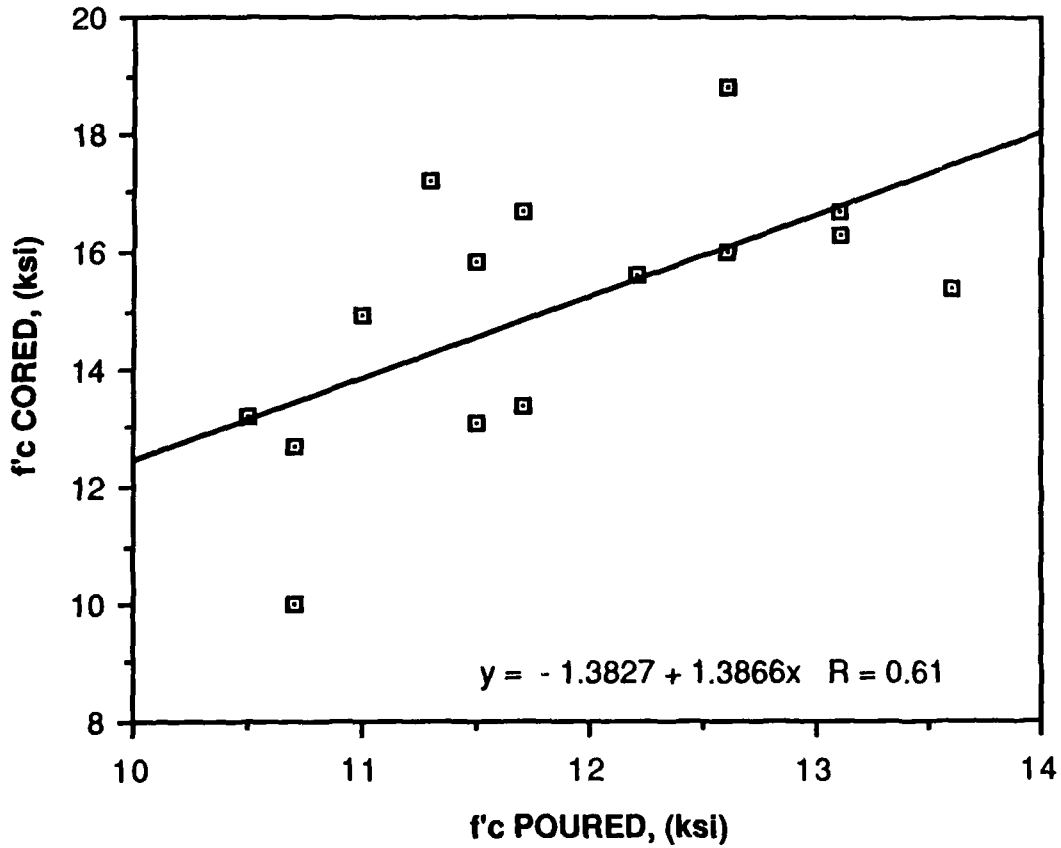

Fig. F1. Average compressive strength of cored vs. poured test series.

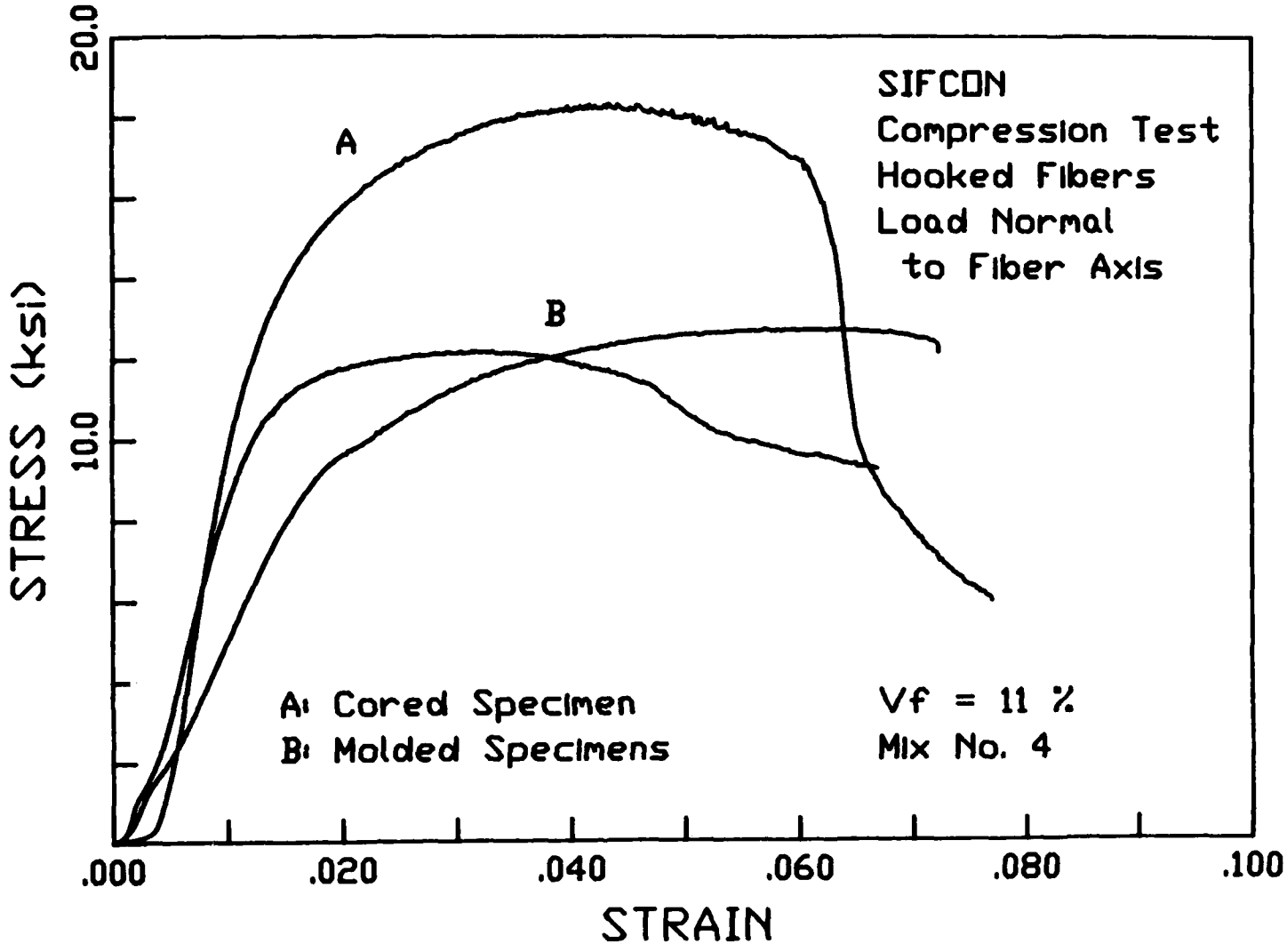

Fig. F2. Typical comparison between the stress-strain response in compression of cored versus poured specimens (hooked fibers).

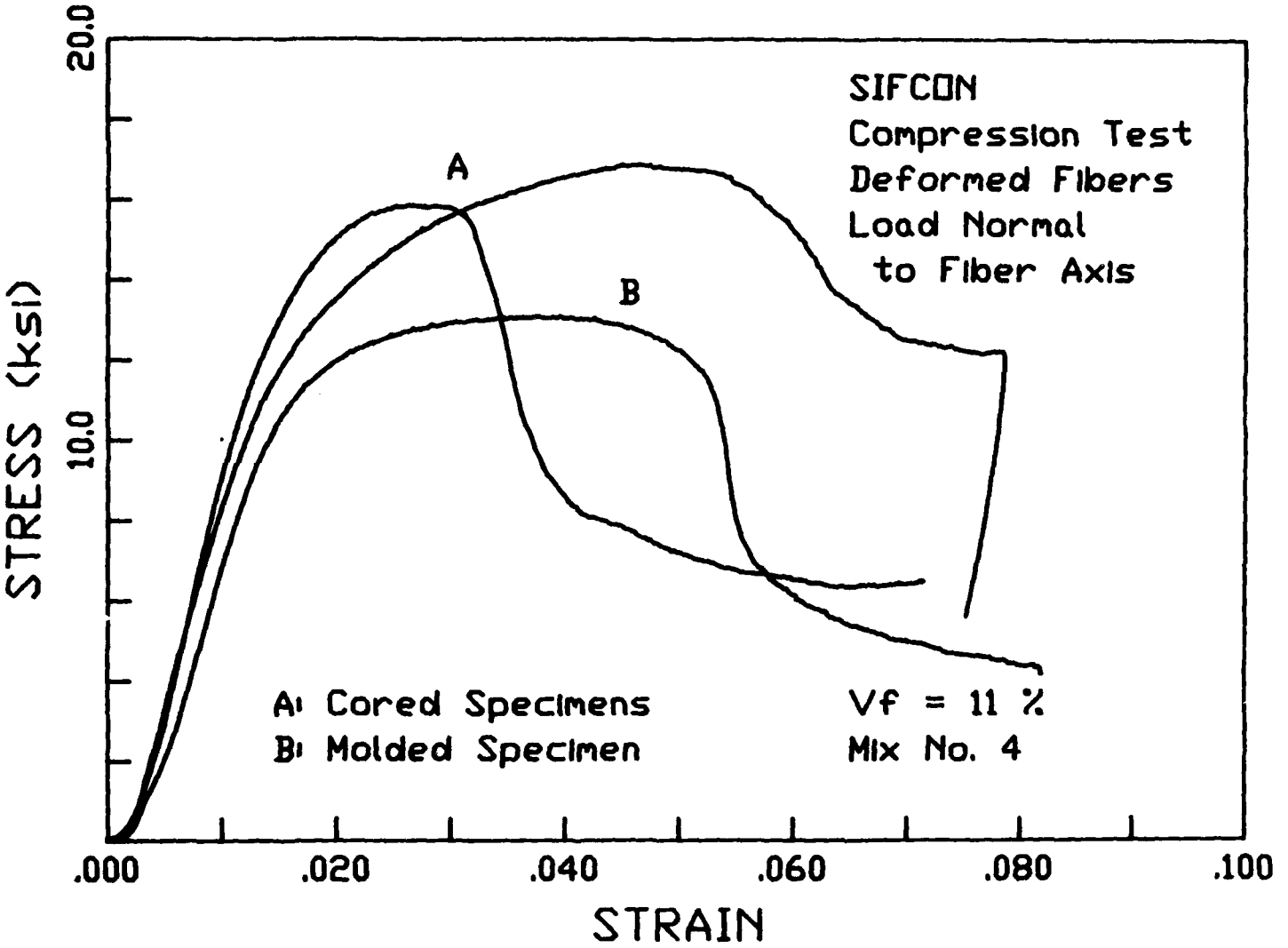

Fig. F3. Typical comparison between the stress-strain response in compression of cored versus poured specimens (deformed fibers).

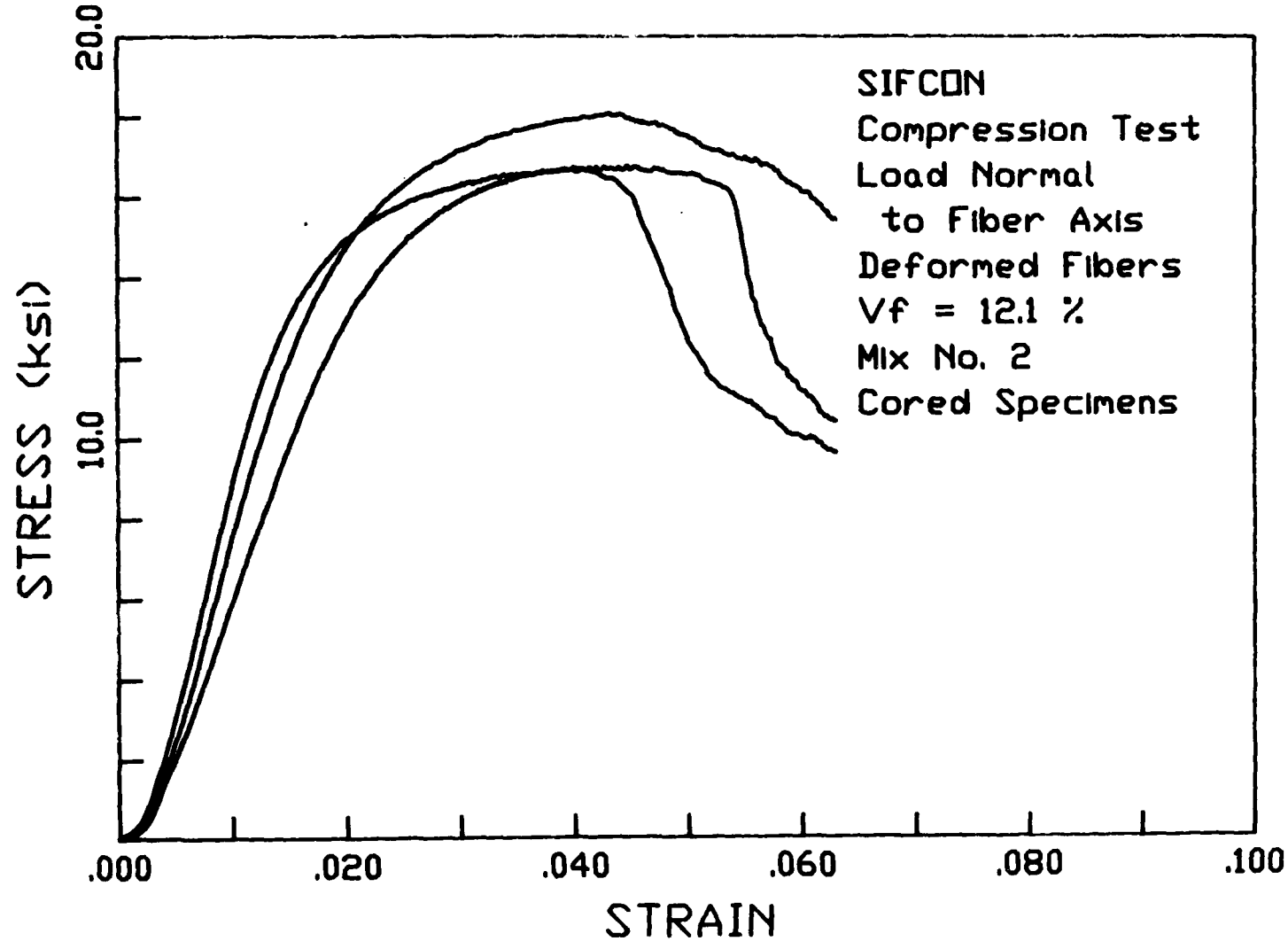
20.0
10.0
STRESS (ksi)
.000
.020
.040
.060
.080
.100
STRAIN
SIFCON
Compression Test
Load Normal
to Fiber Axis
Deformed Fibers
Vf = 12.1 %
Mix No. 2
Cored Specimens

Figure F4

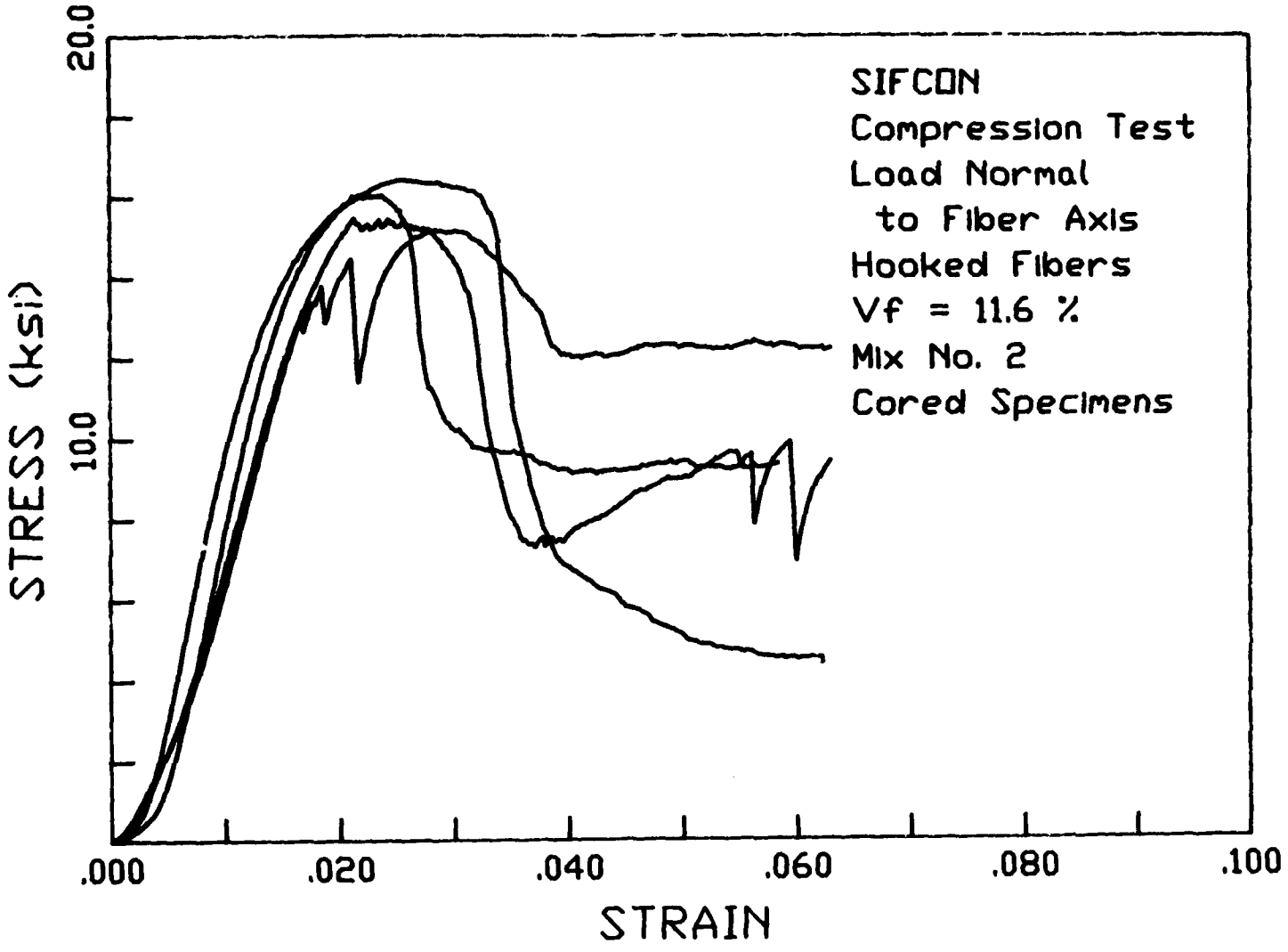
SIFCON
Compression Test
Load Normal
to Fiber Axis
Hooked Fibers
Vf = 11.6 %
Mix No. 2
Cored Specimens
STRESS (ksi)
20.0
10.0
.000
.020
.040
.060
.080
.100
STRAIN

Figure F5

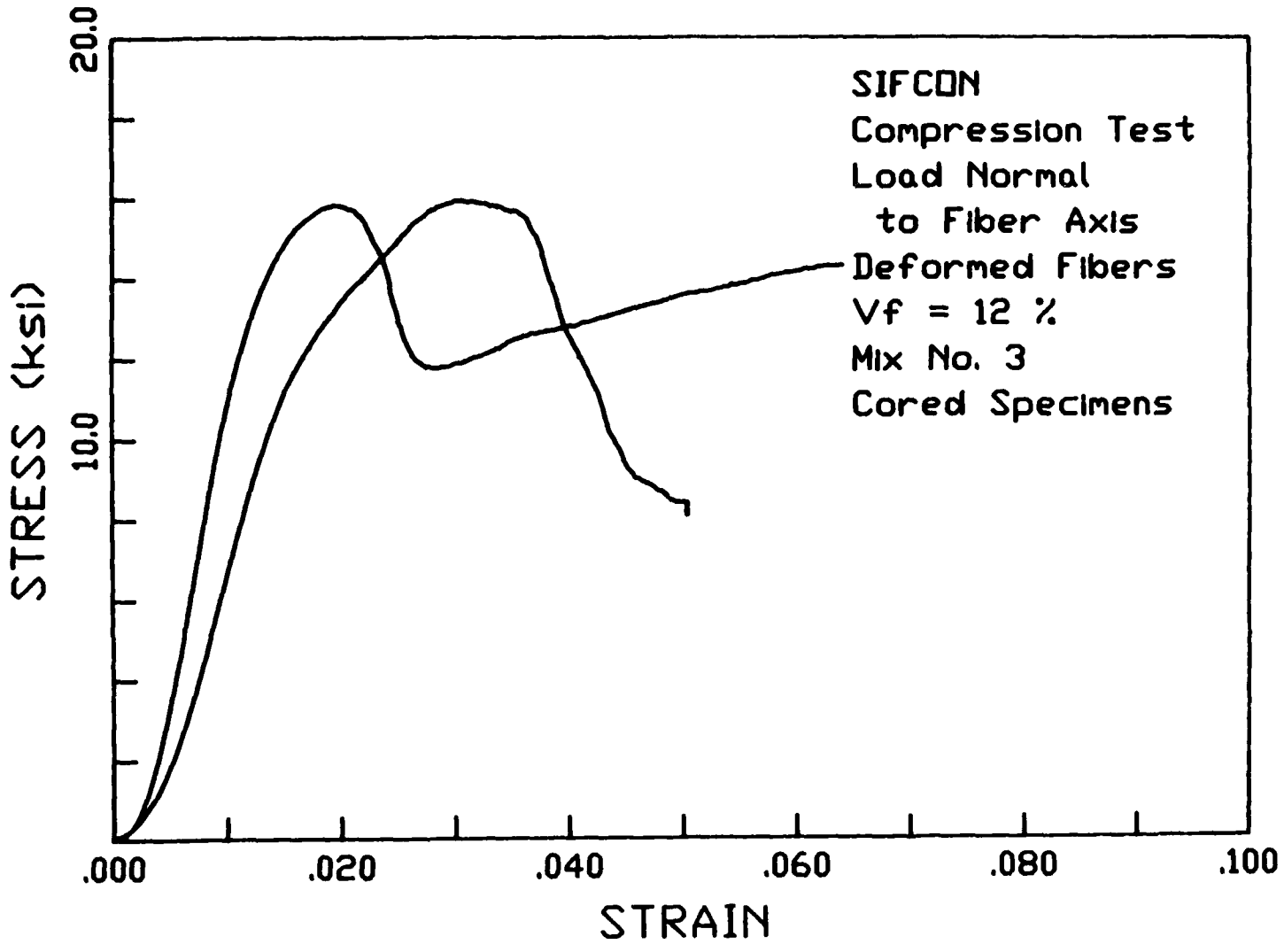
20.0
10.0
STRESS (ksi)
.000
.020
.040
.060
.080
.100
STRAIN
SIFCON
Compression Test
Load Normal
to Fiber Axis
Deformed Fibers
Vf = 12 %
Mix No. 3
Cored Specimens

Figure F6

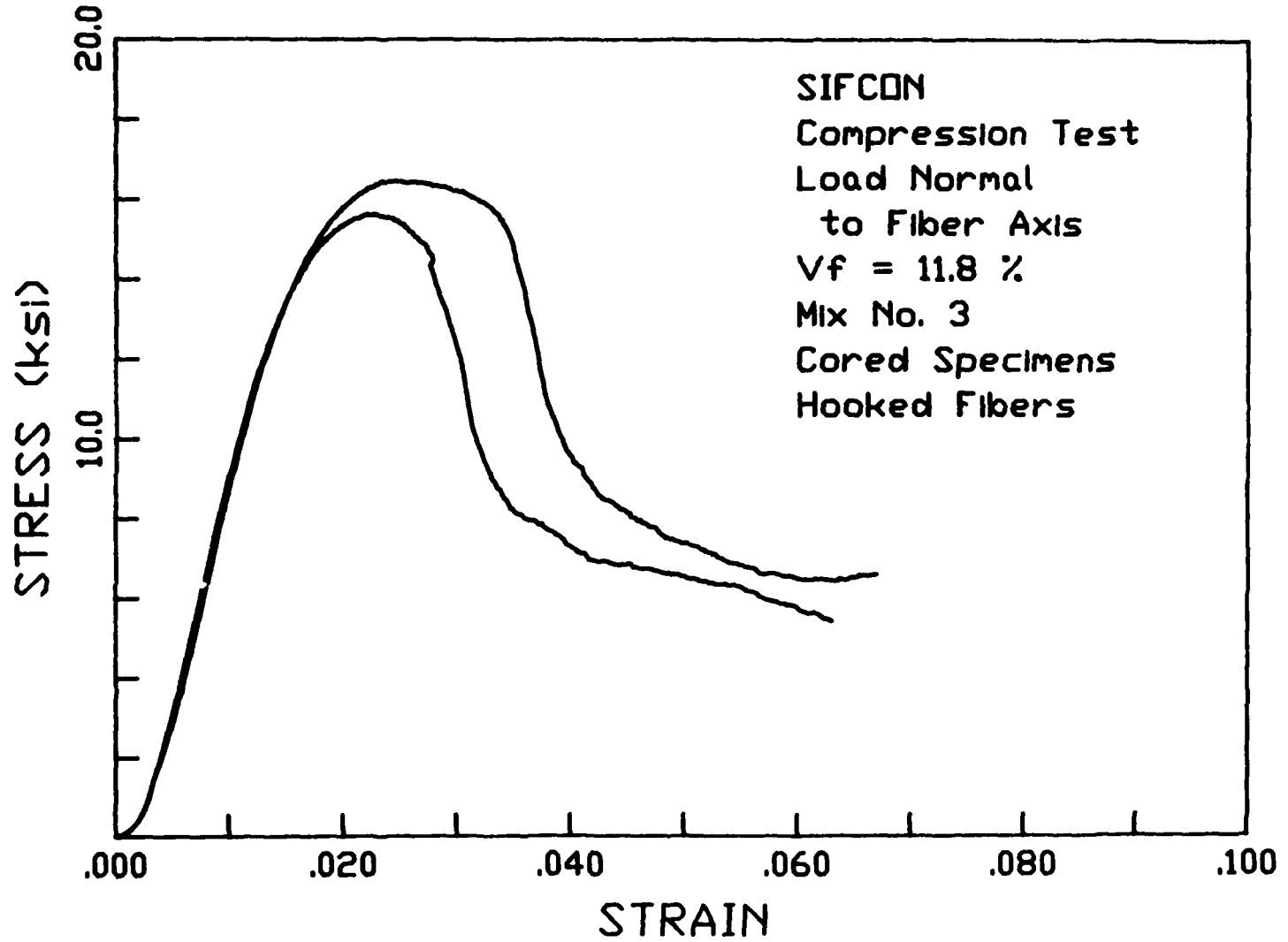
SIFCON
Compression Test
Load Normal
to Fiber Axis
Vf = 11.8 %
Mix No. 3
Cored Specimens
Hooked Fibers
STRESS (ksi)
20.0
10.0
.000
.020
.040
.060
.080
.100
STRAIN

Figure F7

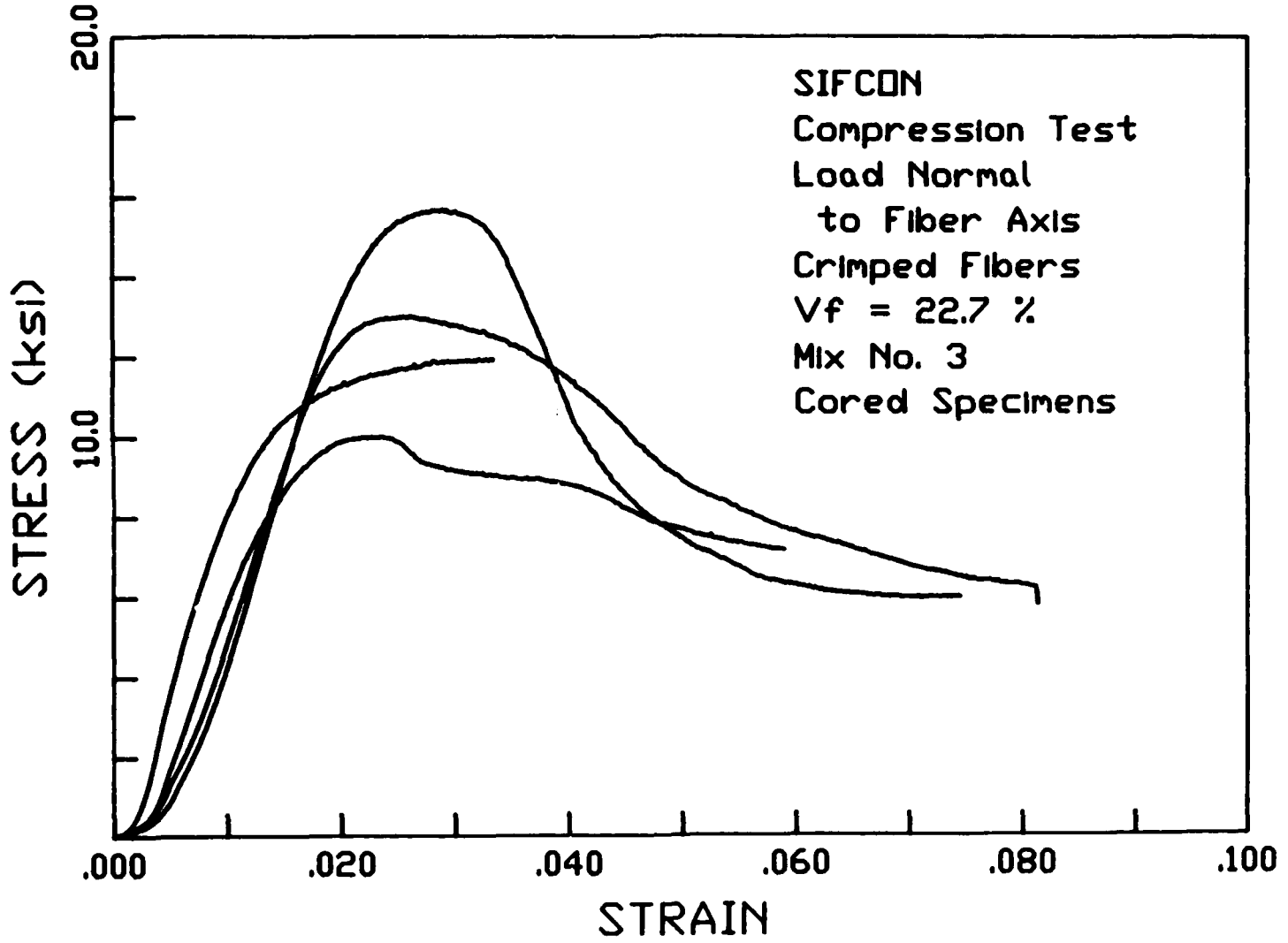
SIFCON
Compression Test
Load Normal
to Fiber Axis
Crimped Fibers
Vf = 22.7 %
Mix No. 3
Cored Specimens
STRESS (ksi)
20.0
10.0
.000
.020
.040
.060
.080
.100
STRAIN

Figure F8

DISTRIBUTION

AF Armament Dev & Test Cen
Eglin AFB, Fla.
AFIT/LDEE, WPAFB, Ohio.
Aeronautical Sys Div/DES/AES
WPAFB, Ohio.
AF Engr & Svcs Cen/RDCS
Tyndall AFB, Fla.
AFWL/NTEO/NTESR/SUL/HO, KAFB, N. Mex.
Applied Rsch Assoc, Albuq, N. Mex.
Applied Rsch Assoc, Raleigh, N.C.
Armaments Div/YQ, Eglin AFB, Fla.
Battelle Memorial Institute
Columbus, Ohio.
BDM Corporation, McLean, Va.
California Rsch & Tech Inc
Chatsworth, Calif.
Dept of the Army, Ch of Engr/DAEN
Washington, D.C.
Construction Engr Rsch Lab/CERL-SL
Champaign, Ill.
Def Adv Rsch Proj Agency
Arlington, Va.
DNA/STTI, Washington, D.C.
Fed Emerg Mngmnt Agency/NPI
Washington, D.C.
HQ USAFE Europe/DEXX, Apo, N.Y.
LANL, Los Alamos, N. Mex.
Naval Civil Engr Lab Naval
Construction Battalion Cen
Port Hueneme, Calif.
Naval Facilities Engr Cmd Hqs
Alexandria, Va.
Naval Weapons Cen, China Lake, Calif.
NMSU, Las Cruces, N. Mex.
Sandia Nat'l Lab, Albuq, N. Mex.
SRI Int'l, Menlo Park, Calif.
Science Appl Inc, San Landro, Calif.
SW Rsch Inst, San Antonio, Tex.
TRW Inc Sp & Def
Redondo Beach, Calif.
Univ of Colo., Boulder, Colo.
Univ of Minn., Minneapolis, Minn.
AUL/LSE, Maxwell AFB, Ala.
DTIC/FDAC, Alexandria, Va.
HQ AFCSA/SAMI, Washington, D.C.
AFELM, Rand Corp, Santa Monica, Calif.
UNM, Albuq, N. Mex.
USAF Academy, Colo. Springs, Colo.
US Army Engr WW Exper Station
Vicksburg, Miss.
US Army Nuc & Chem Agency
Springfield, Va.
Weidlinger Assoc Cons Engrs
Menlo Park, Calif.
Univ of Mich., Ann Arbor, Mich.
Official Record Copy
AFWL/NTESR/Capt Cheney